

---

Electronic Thesis and Dissertation Repository

---

4-3-2012 12:00 AM

## Optically Driven PH Gradient Generator Based on Self-Assembled Proton Pumps for Activating Hydrogel Microactuators

Khaled M. Al-Arife, *The University of Western Ontario*

Supervisor: Professor George Knopf, *The University of Western Ontario*

A thesis submitted in partial fulfillment of the requirements for the Doctor of Philosophy degree in Mechanical and Materials Engineering

© Khaled M. Al-Arife 2012

Follow this and additional works at: <https://ir.lib.uwo.ca/etd>

 Part of the [Mechanical Engineering Commons](#)

---

### Recommended Citation

Al-Arife, Khaled M., "Optically Driven PH Gradient Generator Based on Self-Assembled Proton Pumps for Activating Hydrogel Microactuators" (2012). *Electronic Thesis and Dissertation Repository*. 415.  
<https://ir.lib.uwo.ca/etd/415>

This Dissertation/Thesis is brought to you for free and open access by Scholarship@Western. It has been accepted for inclusion in Electronic Thesis and Dissertation Repository by an authorized administrator of Scholarship@Western. For more information, please contact [wlsadmin@uwo.ca](mailto:wlsadmin@uwo.ca).

OPTICALLY DRIVEN PH GRADIENT GENERATOR BASED ON SELF-  
ASSEMBLED PROTON PUMPS FOR ACTIVATING HYDROGEL  
MICROACTUATORS

(Spine title: Optically driven pH gradient generator based on self-assembled proton  
pumps)

(Thesis format: Monograph)

by

Khaled M. Al-Arife

Graduate Program in Engineering Science  
Department of Mechanical & Materials Engineering

A thesis submitted in partial fulfillment  
of the requirements for the degree of  
Doctor of Philosophy

School of Graduate and Postdoctoral Studies

The University of Western Ontario  
London, Ontario, Canada

© Khaled M. Al-Arife 2012

THE UNIVERSITY OF WESTERN ONTARIO  
SCHOOL OF GRADUATE AND POSTDOCTORAL STUDIES

**CERTIFICATE OF EXAMINATION**

Supervisor

\_\_\_\_\_  
Dr. George K. Knopf

Examiners

\_\_\_\_\_  
Dr. John Yeow

\_\_\_\_\_  
Dr. Jun Yang

\_\_\_\_\_  
Dr. Samuel Asokanthan

\_\_\_\_\_  
Dr. Robert Sobot

The thesis by

**Khaled M. Al-Arife**

entitled:

**Optically driven pH gradient generator based on self-assembled proton pumps for activating hydrogel microactuators**

is accepted in partial fulfillment of the  
requirements for the degree of  
Doctor of Philosophy

Date \_\_\_\_\_

\_\_\_\_\_  
Chair of the Thesis Examination Board

## ABSTRACT

This dissertation presents a new approach for developing a biologically inspired photo-electro-chemo-mechanical microactuator by exploiting the ion pumping characteristics of bacteriorhodopsin (bR) proton pumps and the pH sensitivity of smart hydrogels. The ultimate goal of this project is to prove the viability of integrating bR monolayer into novel actuation applications using molecular level architectures. To accomplish this, the bR proton pumps are molecularly labelled, organized, and directionally immobilized on Au-coated substrate, and then integrated with pH sensitive hydrogel. When responding to an incident light beams, the internal proton pumping mechanism is mathematically modeled for quantifying the processing of the photonic energy into electro-chemical potential. Experimental and theoretical findings indicate that the photo-electric response of the dry bR is attributed to charge displacement and recombination; whereas, the response of the aqueous bR measured is a real proton pumping mechanism. The photo-electric properties, light source conditions all have influence on the observed photo-electric response characteristics.

The presented technology is proven both experimentally and analytically through simulation. Experiments are conducted using acrylic acid (AA) monomer linked to 2-hydroxyethyl methacrylate (HEMA) monomer and the developed bR monolayer forming this hybrid microactuator. The light detecting part of the actuator is the bR monolayer. In this part the incident light beams are processed in the bR proton pumps through their photo-cycle to transport protons from the cytoplasmic side to the extracellular side of the bR protein. The bR monolayer is fabricated with molecular level recognition, labelling, and adsorption leading to a novel architecture able to transport protons through a porous substrate. Once protons are transported from one side to the other side of the membrane, the concentration of the hydrogen ions is changed. The change in the hydrogen ions concentration is expected theoretically and has been proved by monitoring pH changes in the ionic solution as pH gives direct indication on the hydrogen ions concentration. The change in the pH is exploited by integrating the light detecting part of the actuator to the pH-sensitive hydrogel which acts as the actuator shell that receives the pH changes and treat it as an input signal and then process it to undergo in an electric phase transition that

leads to volume transition and associated mechanical work. The generated mechanical work is exploited in microactuation techniques with interest in microfluidic valves to control the flow in the microchannels.

Based on the presented work the bR monolayer shows great potential for becoming a viable biomaterial for use in optical sensing and actuation. Many industrial and biomedical applications may benefit from the presented advances in generating higher performance micro-systems.

**KEYWORDS:** Optical driven microactuator, molecular self-assembly, bacteriorhodopsin (bR) monolayer, biotin labelling, pH gradient generator, biofunctionalized surface.

## **ACKNOWLEDGEMENTS**

I would like to acknowledge the many people who offered me help, guidance, and support throughout my academic career at the University of Western Ontario. Primary, among them was my thesis advisor, Dr. George Knopf. Dr. Knopf took me into his laboratory, had confidence on me to work on this project. It gives me a great honor to thank Dr. Knopf for his encouragement, guidance, support and patience. I would also like to thank Dr. Amrjeet Bassi for his guidance in the biochemical parts of the project.

I would also like to thank my mother Hamida. My mother was encouraging me to be successful in academia since I was in the elementary school. I would like to thank her. Also, I was hoping to have my father Mohamed sharing me my happiness of graduation. Unfortunate he passed away before seeing this day. I would like to thank him and say that, his encouragement and advices will go with me always.

I would also like to thank my wife Aisha and my daughters Hamida, Batol, and Roaa for their encouragement and patience.

I would like to extend my thanks to Dr. Buddy Ratner of University of Washington at Seattle, Dr. Janos Lanyi of University of California at Irvine, Dr. Ronald Siegel of University of Minnesota at Twin Cities, Dr. Richard Henderson of the Medical Research Council (UK), Dr. Stan Dunn of the University of Western Ontario, and Dr. Jayshri Sabarinathan of the University of Western Ontario for their helpful discussions.

I am also grateful to my brother Osama for his support, and my friends Dr. Mahmud Alujli, Osama Drbe, Ahmed Sloiman, Mohamed Obadi, Khaled Elbanan, and Souheil Afara they were great friends and the best company.

Finally, I would like thank the University of Western Ontario, and would say the knowledge that I learned in it will go with me always.

# TABLE OF CONTENTS

<b>Certificate of Examination .....</b>	<b>ii</b>
<b>Abstract.....</b>	<b>iii</b>
<b>Acknowledgements .....</b>	<b>v</b>
<b>Table of Contents .....</b>	<b>vi</b>
<b>List of Figures.....</b>	<b>xi</b>
<b>Nomenclature .....</b>	<b>xvi</b>
<b>CHAPTER 1</b>	
<b>Introduction.....</b>	<b>1</b>
1.1 The Problem.....	1
1.2 Optofluidics.....	2
1.3 Optical Actuation in Microfluidic Systems .....	4
1.4 Motivation of the Present Work.....	6
1.5 Objectives and Scope of this Work.....	8
1.6 Overview of the Thesis .....	11
<b>CHAPTER 2</b>	
<b>Review of Bacteriorhodopsin .....</b>	<b>14</b>
2.1 Photosensitive Proteins .....	14
2.2 General Structure of Purple Membrane and Bacteriorhodopsin.....	16
2.3 Photoelectrochemical Cycles of Bacteriorhodopsin .....	19
2.4 Photoelectric Properties of Bacteriorhodopsin .....	23
2.5 Applications of Bacteriorhodopsin .....	25
2.5.1 Photochromic applications .....	26
2.5.2 Photoelectric applications .....	26

## CHAPTER 3

<b>Production and Immobilization of Bacteriorhodopsin.....</b>	<b>28</b>
3.1 Introduction .....	28
3.2 Production of Bacteriorhodopsin (bR) Protein .....	28
3.2.1 Materials for fermentaion of Halobacterium salinarum growth media	30
3.2.2 Fermentation and growth media.....	31
3.2.3 Extraction and purification of bacteriorhodopsin (bR) .....	34
3.3 Review of Immobilization Methods .....	36
3.3.1 Electric field sedimentation (EFS) technique.....	37
3.3.2 Langmuir-Blodgett deposition (LB) technique .....	38
3.3.3 Electrostatic layer-by-layer adsorption (LBL) technique.....	39
3.3.4 Self-assembly of PMs using biotin labelling.....	40
3.4 Fabrication of Self- Assembled bR Monolayer .....	42
3.4.1 Biotin labeling of bacteriorhodopsin.....	42
3.4.2 Substrate preparation and activation .....	42
3.4.3 Adsorption of the ordered bR monolayer.....	43
3.5 Concluding Remarks.....	44

## Chapter 4

<b>Photoelectric Characteristics of the Self-Assembled bR Monolayer. ....</b>	<b>46</b>
4.1 Introduction.....	46
4.2 Phototransduction Process in Dried bR Films .....	48
4.2.1 Role of water molecules in proton pumping process .....	48
4.2.2 Dehydration effects on photochemical cycle and proton pumping.....	49
4.3 Surface Coverage of the Substrate with Biotinylated bR .....	51
4.4 Investigation of Photoelectric Response of the bR Monolayer .....	54
4.4.1 Exprimental setup .....	54
4.4.2 Photovoltaic response of bR monolayer to continuous light illumination .....	55
4.4.3 Photovoltaic response of bR monolayer to short light pulses .....	59
4.4.4 Discussion .....	62



4.5 Concluding Remarks.....	64
<b>CHAPTER 5</b>	
<b>pH-Gradient Generated by Self-Assembled bR Proton Pumps .....</b>	<b>65</b>
5.1 Introduction.....	65
5.2 The Approach.....	69
5.2.1 Embedded bR proton pumps .....	69
5.2.2 Self-assembled proton pumps on a porous substrate .....	70
5.3 Fabrication and Experimental Analysis .....	71
5.3.1 Preparation of the bio-functionalized porous substrate.....	71
5.3.2 Fabrication of the polydimethylsiloxane (PDMS) microfluidic chip ....	71
5.3.3 Surface coverage of the Au-PAA substrate with biotinylated bR.....	74
5.3.4 Photo-electro-chemical response based on pH- gradients.....	77
5.4 Molecular Mechanism for the Light Driven pH Gradient Generation .....	84
5.5 Monitoring Solution Acidity Using Phenolphthalein Dye.....	86
5.6 Concluding Remarks.....	88
<b>CHAPTER 6</b>	
<b>Smart Hydrogel Microactuator .....</b>	<b>89</b>
6.1 Introduction.....	89
6.2 Hydrogel Microactuators .....	89
6.2.1 Physics and chemistry of the pH-sensitive hydrogels .....	90
6.2.2 Synthesis techniques of hydrogels .....	92
6.3 pH-Sensitive Hydrogel Microvalve .....	93
6.3.1 Fabrication of pH-sensitive hydrogel.....	93
6.3.2 Fabrication of the microfluidic chip.....	94
6.4 Response of the pH-Sensitive Hydrogel Microvalve.....	96
6.5 Results and Discussion .....	97
6.6 Concluding Remarks.....	98

## CHAPTER 7

### **Light Driven Hydrogel Microactuator ..... 99**

7.1 Introduction.....	99
7.2 Photo-Responsive Hydrogel Microactuator .....	101
7.3 Fabrication of bR Activated Hydrogel Microactuator .....	102
7.3.1 Fabrication of the HEMA-AA Hydrogel .....	103
7.3.2 Fabrication of the bR functionalized porous substrate.....	104
7.4 Microactuator Response.....	106
7.4.1 Photoelectrochemical characteristics of the microactuator .....	107
7.4.2 Swelling characteristics of the microactuator .....	109
7.4.3 Response reversibility of the hydrogel microactuator .....	114
7.4.4 Microfluidic valve activated by the bR based pH-gradient generator	116
7.5 Concluding Remarks.....	118

## CHAPTER 8

### **Conclusions ..... 120**

8.1 Thesis Summary.....	120
8.2 Thesis Contribution.....	123
8.2.1 Production of bacteriorhodopsin .....	123
8.2.2 The Development of bR self-assembled monolayer .....	124
8.2.3 Fabrication of the optically driven pH gradient generator.....	125
8.2.4 Fabrication of the optically driven microactuator.....	126
8.3 Limitations and Recommendations for Future Work .....	127
8.3.1 Purple membranes distribution on the substrate .....	127
8.3.2 Optimizing the generated pH gradient .....	127
8.3.3 Swelling dynamics of the microactuator hydrogel .....	128
8.4 Final Thought .....	128

### **Bibliography ..... 129**

### **Curriculum Vitae ..... 139**

## LIST OF TABLES

Table 3.1 Materials and media used to grow <i>Halobacterium Salinarium</i> cells.....	31
---	----

## LIST OF FIGURES

Figure 2.1 Schematic diagram of a <i>Halobacterium salinarium</i> cell. A two-dimensional crystalline purple membrane provides proton transport and membrane-bound ATP synthase enables the photosynthesis of ATP from ADP..	16
Figure 2.2 General Structural description of purple membrane patches containing bR. A bR protein in the membrane. Its carboxy terminus is located inside the cell and the amino terminus is located outside the cell....	17
Figure 2.3 Detailed structural description of the bR. The seven transmembrane helices are labelled from A to G. The retinal Schiff-base and the amino acids are most relevant for proton transport..	19
Figure 2.4 Photo-isomerization of the bR retinal from (a) all-trans to (b) 13-cis in bR. The retinal has covalent bond with Lys-216 via a protonated Schiff base. When absorbing a photon, the retinal isomerizes around the C13=C14 bond. (Based on Gai <i>et al.</i> , 1998).	20
Figure 2.5 Basic photochemical cycles of bacteriorhodopsin, when exposed to visible light ( $h\nu$ ), for both the aqueous (a) and dry forms (b) (Groma <i>et al.</i> , 2001). The subscripts refer to the peak wavelength for the identified intermediate..	21
Figure 2.6 Spectral absorbance of the bR produced at the University of Western Ontario. Note that visible light ranges from approximately 400nm to 700nm.	23
Figure 2.7 An electrostatic difference map associated with the primary photochemical event of bR..	25

Figure 3.1 Illustration drawing of the Bacteriorhodopsin in its biological <i>Halobacterium salinarium</i> cell.....	30
Figure 3.2 Photograph of the 1.0 L fermentation process of the <i>Halobacterium salinarium</i> cells .....	32
Figure 3.3 Photograph of the 10.0 L fermentation process of the <i>Halobacterium salinarium</i> cells .....	33
Figure 3.4 Photograph of the density gradient formed the purple membrane band. ....	35
Figure 3.5 Spectral optical density of the bR produced at the University of Western Ontario. Note that visible light ranges from approximately 400nm to 700nm. ....	36
Figure 3.6 Fabrication of oriented bR films by the EPS technique. PM patches transport onto the anode due to its more negatively charged cytoplasmic side. ....	37
Figure 3.7 Preparation of a bR film by the LB technique. The cytoplasmic side of PM is more hydrophilic (facing into the water) than the extracellular side (facing the air). ....	39
Figure 3.8 Schematic drawing of multiple PDAC/PM layers as fabricated by the LBL technique (He <i>et al.</i> , 1998).....	40
Figure 3.9 Illustration of the self-organized and self-assembled photoelectric dry layer on Au substrate. ....	41
Figure 3.10 AFM analysis of the bare gold coated substrate. ....	43
Figure 3.11 The simplified structure of the self-assembled bR-biotin-streptavidin-biotin-thiol-Au film .....	44
Figure 4.1 Basic structure of bacteriorhodopsin purple membrane patches. A bR monomer penetrates through the membrane where its carboxy terminus is located inside of the cell and the amino terminus is located outside of the cell.....	47

Figure 4.2 Fundamental photochemical cycles of bacteriorhodopsin, for (a) the aqueous phase, where the proton pumping starts with the release of a proton during the L→M transition and finish with a proton uptake during the M→N transition (Edman <i>et al.</i> , 1999) and (b) the dry bR, where only K, L and M intermediates are observable and no proton pumping across the protein membrane. ....	50
Figure 4.3 SEM photograph of the self-assembled ultra-thin bR layer, with a magnification factor of 200. Enlarged area shown in upper right corner (taken in the Nanofabrication facility, the University of Western Ontario) .....	52
Figure 4.4 AFM analysis of the self-assembled ultra-thin bR layer. Two cross-sectional profiles are shown (taken in the surface science facility in the University of Western Ontario). .....	53
Figure 4.5 Experimental apparatus used to test the photoelectric properties of the photocell and equivalent electronic circuit for the light responsive bR thin layer. ..	55
Figure 4.6 Small-amplitude random photoelectric response of the bare Au substrate. ....	56
Figure 4.7 Measured voltage difference across the bR layer on a 0.185 cm <sup>2</sup> substrate as a function of light exposure time. Six pulses with increased time durations of light exposure are shown. ....	57
Figure 4.8 Enlarged view of the photocell response to the second light pulse. Illumination was intermittently reduced to 50% of intensity at 1800 s. ....	58
Figure 4.9 Enlarged view of the photocell response showing voltage buildup toward steady-state over the duration of the sixth light pulse in Figure 4.7. ....	59
Figure 4.10. Measured voltage difference across the 0.0925 cm <sup>2</sup> pixel for a sequence of varying input pulse widths (0.0625s, 0.125s, 0.25s, 0.5s, 1s, 2s, 4s, 8s, 15s, and 30s). .....	60
Figure 4.11. Relationship between the width of the light pulse and maximum voltage difference generated by the bR photocell. ....	61
Figure 4.12. Relationship between light intensity and bR photocell response .....	62

Figure 5.1 Layered structure of an optically driven pH gradient generator used to transport hydrogen ions ( $H^+$ ) between two adjacent ionic solutions separated by a porous substrate. ....	68
Figure 5.2 Sequence of steps used to fabricate a PDMS microfluidic chip.....	72
Figure 5.3 SEM photograph of the PDMS based microfluidic chip. ....	74
Figure 5.4 SEM photograph of the self-assembled ultra-thin bR film on porous PAA substrate with a magnification factor of 3000. Enlarged area shown in upper right corner .....	75
Figure 5.5 Experimental photocell response to a light pulse. ....	76
Figure 5.6 AFM analysis of the self-assembled ultra-thin bR layer on PAA substrate. Two cross-sectional profiles (A-A', B-B') are shown. ....	77
Figure 5.7 Schematic drawing of the microfluidic test device used to perform the experiments. The dimensions are given in $\mu m$ . ....	78
Figure 5.8 Change in pH of the ionic solution in reservoir R1 as a function of light exposure. The pH gradient transducer has an active surface that is $0.2cm^2$ . ....	80
Figure 5.9 Change in steady-state pH of the solution in reservoir R1 as the intensity of light striking the transducer increases. ....	81
Figure 5.10 Measured pH in the R1 solution as the electrode probe is moved away from the bR-PAA transducer surface. The instrument used to record the solution's pH had a sampling time of 1 second and resolution of 0.01 pH units. ....	82
Figure 5.11 Change in pH over time of the two reservoirs separated by the bR-PAA transducer when exposed to an 18mW light source (-o- for R1, -□- for R2). ....	83
Figure 5.12 Comparison between the experimental observations -o- (every 100 <sup>th</sup> sample is shown with circular mark) and theoretical model ( <u>  </u> ) used to predict the temporal change in pH for the R1 solution when exposed to a constant light source .....	85
Figure 5.13 The change in pH of the target solution is sufficient to cause a phenolphthalein indicator dye to change colour. The optically driven proton pumps	

of the bR-PAA pH gradient generator cause the solution in R1 to transform from a light greenish blue (pH 5.10) to a darkened, more intense blue (pH 5.31). .....	87
Figure 6.1 Volume transitions of acidic and basic hydrogels under pH gradient activation .....	91
Figure 6.2 Schematic drawing showing the hydrogel network structure.....	92
Fig. 6.3 Steps in micromolding a PDMS microfluidic chip .....	94
Figure 6.4 pH-sensitive (HEMA-AA) microvalve at pH 3 and pH 10, respectively (Nanofabrication Facility UWO). .....	96
Figure 6.5 Swelling of 155 $\mu\text{m}$ (HEMA-AA) pH sensitive microvalve. ....	97
Figure 7.1 Schmatic drawing of the bR activated hydrogel structure. ....	101
Figure 7.2 Schmatic drawing of the ions flow through the activated hydrogel. ....	102
Figure 7.3 SEM photograph of the Au-coated PAA substrate. ....	105
Figure 7.4AFM photograph of bio-functionalized Au-coated substrate showing surface topology. ....	105
Figure 7.5 Measured voltage difference across the bR layer on a 0.096 $\text{cm}^2$ substrate under continuous light exposure. ....	108
Figure 7.6 Recorded photocurrent based on the measured voltage difference across the bR layer on a 0.096 $\text{cm}^2$ substrate under continous light exposure. ....	109
Figure 7.7 Schmatic drawing of the test chip. ....	110
Figure 7.8 Photograph of the test setup .....	111
Figure 7.9 Schematic drawing of the (a) deswelled hydrogel, and (b) swelled hydrogel valve. ....	112
Figure 7.10 Photograph of the (a) deswelled hydrogel and (b) swelled hydrogel valve. The photographs are taken in the same scale. ....	112

Figure 7.11 The change in diameter of the HEMA-AA hydrogel actuator. ....	113
Figure 7.12 The change in length of the HEMA-AA hydrogel actuator. ....	113
Figure 7.13 The change in volume of the HEMA-AA hydrogel actuator. ....	113
Figure 7.14 Photograph of the actuator in the microfluidic channel. ....	114
Figure 7.15 Change in microactuator cross-sectional area. ....	115
Figure 7.16 The reversibility of the microactuator response in the microfluidic channel. .....	116
Figure 7.17 Photographs of the actuator in the microfluidic channel in configuration (a) deswelled phase and (b) swelled phase. ....	117
Figure 7.18 Change in microchannel opening. ....	118



## NOMENCLATURE

A	Area of substrate
$A_{bR}$	Area of one bacteriorhodopsin of the hexagonal molecule
AA	Acrylic acid
ADP	Adenosine Diphosphate
AFM	Atomic Force Microscopy
SEM	Scanning Electron Microscopy
ATP	Adenosine Triphosphate
Arg	Arginine acid
Asp	Aspartic acid
Au	Gold
BR, bR	Bacteriorhodopsin
BS	Basal Salt
( $C_t$ )	Total Capacitance
CID	Charge Injection Device
CM	Culture Media
DNase	Deoxyribonuclease
( $E_{ph}$ )	Photovoltage Source
EFS	Electrophoretic Sedimentation
FIB-SEM	Focused Ion Beam Scanning Electron Microscopy
Glu	Glutamic Acid
HEMA	2-hydroxyethyl methacrylate
HCl	Hydrochloric acid
<i>H.S.</i>	Halobacterium Salinarum

ITO	Indium Tin Oxide
K216, Lys 216	Lysine 216
KCl	Potassium chloride
mH	Mass of the hydrogen ion
MS	Media Salts
$n_{pho}$	Number of photons received by one bR hexagonal molecule
$n_{max}$	Maximum number of photons processed by One bR hexagonal molecule
NaCl	Sodium chloride
NaOH	Sodium hydroxide
$N'_p$	Maximum rate of proton pumping by one bacteriorhodopsin molecule
LB	Langmuir-Blodgett
LBL	Layer-by-Layer adsorption
LOC	Lab-on-a-Chip
PAA	Porous Anodic Alumina
PBS	Phosphate Buffer Saline
PDAC	Poly(diallyldimethylammonium chloride)
PDMS	Polydimethylsiloxane
$pKa$	Phase transition point
PM	Purple Membrane
RM	Rich Media
SAM	Self-Assembled Monolayer
SU-8	Photoresists

UV	Ultra Violet Beam
$V_C$	Volume of Fluid in the Reservoir
WT	Wild Type bR
$\mu$ -TAS	Micro-Total Analysis Systems
$\eta$	Surface coverage fraction factor
$\varphi$	Surface porosity

# CHAPTER 1

## INTRODUCTION

### 1.1 The Problem

Microactuators are critical components of microelectromechanical systems because they convert the input signal into mechanical motion needed to perform useful work. These microactuators or the transducers as they often called are made from functional structures that can receive and process the input signal and then act with the suitable response. Their actuation has been considered to be the building block of mechanical work generators such micro-objects manipulators and flow control valves of microfluidic chips. One of the important technological challenges is how effectively drive microactuators such as microfluidic valves. The microfluidic valves are necessary active components of microfluidic systems that control the micro-fluid supply for the chemical and biochemical processes that are performed on the microfluidic chips. However their operating techniques require accessing the system physically to activate these valves such as the electrical and chemical techniques. In the electrically driven microvalves the electric leakage is highly expected, whereas triggering the chemically operated microfluidic valves can only be done by changing the chemical composition of the surrounding fluid. Electrical based techniques might make an interaction or cross-talk with biochemical processes on the chip as most of biochemical processes are electrical sensitive processes.

On the other hand the replacement of the working fluid in the chemical way to activate the microvalves might affect the processes on the microfluidic chip as the working fluid usually made to assist the chemical and biochemical processes on the microfluidic chip. These difficulties have limited their practical usage. One of the most advanced techniques have been considered for activating microfluidic actuators is the use of light beams as a power provider and control signal carrier. However the reported technologies on the optically driven microsystems are developed based on the photo-

thermal effect. Unfortunately the photothermal effect necessitates keeping the microvalve in very narrow temperature ranges which is not suitable for many practical applications. Looking towards the biological systems for inspiration, the optical system of the human vision for example is based on the photo-electro-chemical interaction between the light beam and the visual rhodopsin. In this manner it can be considered an optical to electro-chemical transducer. Whereas the biological muscles produces mechanical work when activated with an electro-chemical input. These two inspiring biological concepts interested the author to bring them together in one complete mechanism that generates mechanical work when powered with optical signal. This thesis supports the viability of employing one of the biologically synthesised visual rhodopsins known by bacteriorhodopsin protein and artificially fabricated smart material called hydrogel as a building block of novel optically driven microsystems. This system can work only by developing an effective technique for building monolayers of the self-assembled bacteriorhodopsin proton pumps, fabricating a suitable hydrogel and then creating the overlap working zone that can operate these different constituting components in the same time with degrading the performance of each other. Only then is it possible to demonstrate its effectiveness by driving smart hydrogels to control fluid flow on microfluidic chips as proof of concept.

## **1.2 Optofluidics**

The term “optofluidics” implies to an emergent research field that combines optical and microfluidic technology to create highly versatile systems (Fainman *et al.*, 2010; Monat *et al.*, 2007). The advances in the microfluidic technology enable creating changeable and reconfigurable optically driven systems (Fainman *et al.*, 2010). Microfluidics has numerous advantages over solid hardware components including smooth interface, diffusion capability, and good molecular transport characteristics. On the other hand, the optical signal is characterized with the high sensitivity, can be localized to single-cell for nanosurgery (Jeffries *et al.*, 2007), can manipulate objects and fluids suspended in fluids, and moreover it is the fastest known information carrier. Since the appearance of the optofluidic field in 2003, its promise has been demonstrated by the accomplished

advances in broad technological challenges. Heng *et al.* in 2006 generated novel non-expensive optofluidic microscope, which is able to capture on-chip high resolution imaging (Heng *et al.*, 2006). The integration of the microfluidics with the optics has also facilitate the fabrication of reconfigurable three dimensional microlenses (Rosenauer *et al.*, 2008), and the fabrication of in-situ magnetic microactuators in microfluidic channels (Chung *et al.*, 2010). Furthermore, the ability of trapping bio-functionalized micro-objects has been demonstrated (Domachuk *et al.*, 2007).

The biological organisms undergo in large number of interactions with the environment throughout their lifecycle. Their high sensitivity allows them to detect and discriminate between very small changes in their surroundings. The small size and energy efficiency of the biological materials can make them a promising choice for developing unique transducers for sensing and actuation. The integration of bio-materials with microsystems has leaded to significant advances in wide range of challenging applications such as creating flexible photocells (Wang *et al.*, 2005) and self healing materials (Ratner 2007). During the biological generation of bio-materials, the natural evolution optimized their constituting bio-molecules and assembled them in three dimensional structures, allowing them to process and store large amounts of information in very small volumes.

One of the most attractive classes of bio-materials for generating more versatile microsystems is the photosensitive proteins which enable the generation of very fast and remotely powered and controlled microsystems. The Photosensitive proteins can generate electrical signal form the incident light beams. This property has motivated intensive exploration of such biomaterials within the technological community. To date, light is the fastest and most effective technique of carrying power and information. Over the past three decades, scientists have closely studied the structures and functions of various photosensitive proteins to understand the real mechanism of the biological energy conversion. Among the light activated bio-molecules, *bacteriorhodopsin* (bR) protein is the most notable example. It shows light sensitive properties similar to that of *rhodopsin*, a protein found in human eyes. Compared to other photosensitive proteins, bR is characterized with its high thermal and photochemical stability, thereby exhibiting superior long-term stability and thus making it technologically promising. BR is promptly

becoming an advanced building block material for fabricating bioelectronic systems, as it exhibits high applicability potentials in light sensing, artificial vision and parallel associative memories, and optical actuation.

### **1.3 Optical Actuation in Microfluidic Systems**

Microfluidic systems are integrated technologies used to manipulate very small amounts of fluid for a variety of medical and industrial applications. The design and fabrication of complex microfluidic systems requires various building blocks that enable fluid transport, directional flow, pumping, sample preparation, separation, mixing, detection, and in situ chemical reaction. One of the greatest design challenges has been controlling the directional flow of fluid through the constituent microchannels. Flow control is achieved by microactuating devices, such as valves, that perform mechanical work in response to an external command or control signal. The device can be separated into two parts: the actuator shell and the method of actuation. The shell is the basic mechanical structure of the actuator and, often, contains deformable or moving parts. The main function of any shell design is to provide a mechanism for the desired actuation method to produce useful work. The actuation method is the means by which a control signal is converted to a force that is applied to the actuator shell and generates physical movement. The output of the overall system is the desired response given as a displacement, force, or pressure value. An example of a micro-valve is a flexible diaphragm driven by piezoelectric, electrostatic, electromagnetic, or thermo-pneumatic actuator (Kovacs 1998). These micro-valves typically offer small displacements, in range of tens of microns. However, they are large in size, expensive to fabricate, and not easily integrated into existing microfluidic channels (Liu *et al.*, 2002).

Light powered and driven microactuators offer several interesting design features and, therefore, are becoming more popular in developing micro-system technology. All-optical circuits and devices have advantages over conventional electronic components because they are activated by photons instead of currents and voltages. In many of these designs the photons provide both the energy into the system and control signal to initiate the desired response. Furthermore, optical systems are free from current losses, resistive

heat dissipation, and friction forces that greatly diminish the performance and efficiency of conventional electronic or electro-mechanical systems. The negative effects of current leakage and power loss are greatly amplified as design engineers strive for product miniaturization through the exploitation of nanotechnology.

Hydrogels are composed of hydrophilic or hydrophobic cross-linked polymeric networks with a fluid filling the interstitial spaces of the network. Due to their hydrophilic, hydrophobic, and elastic nature these hydrogels are primarily used for drug delivery systems and biomedical instrumentation. In general, hydrogels represent a promising class of materials for microfluidic applications that demand low stressing components and the formation of tight seals that prevent fluid leakage.

Light sensitive hydrogels are often driven by one of three approaches. The first approach is to exploit molecules that can undergo volume changes when exposed to specific wavelengths of light. Ishihara *et al* (Ishihara *et al.*, 1984) investigated the swelling properties of 2-Hydroxyethyl methacrylate with azobenzene molecules as the side groups. The azobenzene molecule is a UV sensitive molecule that can make a 180° rotation around a carbon double bond. The rotation of the azobenzene group around the carbon double bond induces structural rearrangement. The maximum volume change that was observed with this structural rearrangement was 14% in 6 hours at 25°C. An alternative approach exploits light ionized molecules in a neutral hydrogel network. In this context, Ishikawa and Kitamura (Ishikawa *et al.*, 1994) used polyacrylamide microgels that have triphenylmethane leuco cyanide as the light ionizable molecule. UV light ionizes this molecule inducing repulsive forces that drive the hydrogel to swell. It was reported that the photo-dissociation of this light sensitive chromophore occurs in less than 60 seconds. The equilibrium time for an 11µm particle is about 1 hour, while for a 180 µm particle it takes more than 55 hours.

Utilizing the swelling and de-swelling properties of temperature responsive hydrogels is the third approach. These temperature responsive hydrogels are polymer networks that have N-isopropylacrylamide as the backbone monomer. This monomer has a transition temperature of around 32°C. Suzuki and Tanaka (Suzuki *et al.*, 1990) utilized heating power of a light beam raise the temperature of the material. The synthesized



hydrogel contained N-isopropylacrylamide as the main constituent and trisodium salt of copper chlorophyllin as a light sensitive chromophore. Discontinuous volume transition was observed around 31.5°C. The diameter of the sample shrank from about 240µm to 100µm in response to a temperature increase from 25°C to 40°C. Mamada *et al* (Mamada *et al.*, 1990) investigated the response of a N-isopropylacrylamide gel with the photosensitive molecule bis(4-(dimethylamino)phenyl) (4-vinylphenyl) methyleluocyanide as a side group. Juodkazis *et al* (Juodkazis *et al.*, 2000) studied the effect of laser radiation on the temperature responsive hydrogel N-isopropylacrylamide. The experiments confirmed that radiation forces can alter the phase transition process by shifting back the volume transition temperature in the range of 10°C. Sershen *et al* (Sershen *et al.*, 2005) incorporated optical absorption particles to drive the temperature responsive hydrogel poly[N-isopropylacrylamide-co-acrylamide]. The optical absorbing particles that were used are gold-colloid nanocomposites hydrogel that collapse when illuminated under green light and gold nanoshell hydrogel that collapses in response to near IR light. Both hydrogel composites have fast responses and can reach final state in 5s when fabricated in micron scale.

## 1.4 Motivation of the Present Work

Over the last three decades, optical driven systems using biologically synthesised materials have evolved into very efficient transducers. Biological transducers can be extremely sensitive; for example, the retina of human eyes can respond to individual photons (Baylor *et al.*, 1979). These optical transducers can also respond to wide range of light intensities through the range of the light spectrum. Transmitting signals of the control information and power signals through bio-processors facilitate the natural and optimum data compression and processing, and minimizing the external wiring and hardwares of the electrical, chemical and mechanical systems.

Within the last decade scientists and engineers have strived to create absolute optically driven transducer for sensing and actuation to benefit from the unique characteristics of the light radiation. The sequential developments for creating the optically activated transducers includes the development of the photoelectric devices,

then hybrid photoelectric using bioelectronics photosensitive proteins and then recently photomechanical transducers based on the photo-thermal phenomenon. Most of the reported photo mechanical systems exploited the photo-thermal effect. In essence the reported photo mechanical systems exploited the photo-thermal effect. In essence the reported photomechanical transducers are activated by the heat associated with the light illumination where the focus was to generate enough heat from the light radiation to drive temperature sensitive polymers, or to induce thermal expansions. In micro-scale the most successfully optical driven transducers are systems that integrated with the temperature sensitive hydrogels based on the poly(*N*-isopropylacrylamide) monomers. These hydrogel actuators exhibited good functionality in microfluidic valves (Sershen *et al.*, 2005; Richter *et al.*, 2008; Lou *et al.*, 2003).

However, in order to extend the thoughts for designing optically driven micro transducers without experiencing the photo-thermal effects, the biological organisms were considered as examples of complete integrated systems. One of the interesting examples is the conversion of the optical beams received by the eye receptors into mechanical motion in its muscles. The eye receives the incident light beam by the retinal rhodopsins. These rhodopsins release protons to make an electrochemical gradient. The generated electrochemical gradient is considered as the input signal to activate the eye muscles to make mechanical motions (Forrester *et al.*, 1996; Batterbury *et al.*, 2009 Malmivuo *et al.*, 1995). This photomechanical energy conversion technique is taken in the present research as an inspiring point for designing true photomechanical system.

Bacteriorhodopsin is currently considered to be the most promising photo-responsive biomaterial that can preserve its functionality when integrated with artificial systems. However, despite all of reported performance when exposed to light beams, this protein has not been fully understood because most of the reported work focused on the bulk performance of thousands of not properly oriented and assembled layers. Therefore it has not been standardized as an “engineering” material. Most of the researchers who are investigating the theory behind bR functionality are within the fields of biochemistry, and biophysics, which made their findings, models, and conclusions are not presented in a way that is easily applicable in engineering systems. The fundamental findings of researchers from different background are usually expected to have good degree of similarity. However, their conclusions and analysis are based on their background

oriented methods, which can lead to contrasting findings. Furthermore in engineering, the designers study the theory and applicability in artificial systems. The core motivation of studying the bR protein is to investigate its performance at the monolayer level to understand the reality of the bR behaviour because it is found in the living bacterial cell in the form of monolayers. The study of the bR performance at the monolayer level not only enhances its applicability in engineering practices, but also facilitates fabrication of the thinnest photosensitive layer in the domain of nanometers.

The constituting a component that processes the received signal from the bR monolayer in the introduced optically driven microactuator is hydrogel actuating shell, which converts the electro-chemical signal into mechanical work to be used in microscale actuation and control. The objective of this part of the research is to develop a suitable pH gradient hydrogel that can function in a common electrochemical domain with bR monolayer, so that a directed light source can be used to activate and power the micro-actuator. This photo-responsive material should not generate a significant temperature increase that can affect the surrounding fluid. Finally, this micro-actuator should form a seal that prevents undesirable leakage when blocking a channel and conform to all possible channel geometries.

## **1.5 Objectives and Scope of this Work**

The core of this thesis is to investigate the electrochemical signal that is produced by the bR monolayer when exposed to light and applying it to the hydrogel actuation shell of the sensing and actuation transducer. Many researchers investigated the performance of bR in artificial environments in the dry and wet forms. However most of conducted work focused on thick films larger than 20  $\mu\text{m}$  fabricated with non-specific directional organization methods. The use of nonspecific organizing methods creates bR film consists of thousands of randomly stacked monolayers. As the bR protein is directional proton pump, the films of randomly stacked monolayers can never give clear picture of the bR performances. At this point there are several key questions that arise when working with this bio-material:

1. What is the signal pathway of the photoelectric effect in the dry bR monolayer?
2. What is the signal pathway of the photoelectrochemical effect in the wet bR monolayer?
3. How the generated signal be converted into mechanical work?
4. What are the parameters affect the photosensitive monolayer response?
5. How the photosensitive monolayer response can be optimized?
6. How can the photosensitive monolayer response be exploited in a practical sensing and actuating application?

Understanding the bR and theory behind the signal conversions when exposing the bR monolayer to light beams in the dry and wet environments is underlying objective of this research. By doing so, it provides a means of developing clear understanding to describe the signal generated by the dry and wet bR monolayer photoreceptor, which in turn allows standard engineering design and analysis methodologies to be employed. For engineers and technologists to effectively integrate bR monolayer based photoreceptor with microfluidic chip, an appropriate theoretical model must be available. Because this is the first time bR monolayer based photoreceptor is introduced, no readily applicable model has been described in prior literature and therefore, the development of a meaningful model is a primary objective of this dissertation.

In order to have clear understanding of the signal conversions processes; one must understand the proton transport mechanism in the wet bR, and the charge separation process in the dry bR. A suitable mathematical relationship must be defined between input light parameters and proton pumping, and concentration evaluation within the ionic medium. In other words, the proton pumping within single bR molecule must somehow be interpreted into pH gradients that are observed across the photosensitive monolayer. Special care is taken in developing mathematical model that relate input light signal to the final generated pH gradient. The developed model describing the proton pumping response of bR monolayer, is proven via theoretical simulation and experimental analysis.

The fundamental component that affects the generated pH gradient is the bR photosensitive monolayer. The main key factors that contribute in the final response are subdivided into fabrication factors and operation parameters. The fabrication method and its affecting factors to create photosensitive monolayer are studied to produce high surface coverage, and therefore to be able to generate measurable absolute electrochemical response without using amplification circuits. On the other hand the operation parameters such as light beam parameters (intensity, wavelength), area of the photosensitive surface, volume, and strength of the ionic solution are optimized. The fabrication process, and the associated factors, and operation parameters are optimized to create an optofluidic transducer able to convert the incident light into electro-chemical potentials to be used as an input signal to the hydrogel actuator shell.

The final question is related to the applicability of the generated electrochemical potentials in sensing and actuation. In the living cell, the generated pH gradients provide the necessary energy for synthesizing adenosine triphosphate (ATP) from adenosine diphosphate (ADP) which is required for the bacterial cell activities and cell movements (Wang *et al.*, 2005; Hampp, 2000; Voet *et al.*, 2006). The fabrication bR photocell in the form of monolayer based photo-electro-chemical transducer makes it much closer approximation to a biological system. This molecular architecture makes bR a well-suited material for light sensing and for actuation of pH sensitive hydrogels. The final investigation of the created photosensitive nano layer is exploring the limits and capability of activating microfluidic valves.

Even though building photosensitive system anatomically mimics the biological systems is beyond the scope of this project. This thesis introduces photo-electro-chemo-mechanical system that physiologically mimics the rhodopsins based biological systems, and biological muscle and intended to discuss a large breadth of topics covering the fabrication and operation of the photosensing photo-actuation based on dried and wet bR monolayers. Topics of the thesis range from fundamental physics and biochemistry to engineering design, and applications.

## 1.6 Overview of the Thesis

The remainder of this thesis is organized into eight chapters. Chapter 2 provides a detailed overview of bacteriorhodopsin proton pump. Its structure and photosensitive characteristics are described in detail, providing deep view on the material's characteristics, and behaviours. This background knowledge establishes the foundation needed for the design and analysis described in subsequent chapters. The property most relevant to this work is bR's photoelectric and photo-electrochemical responses, which are generated by the phototransduction processes.

In order to fabricate bR based photo-responsive transducer, the bR proton pumps must be directionally organized and irreversibly immobilized onto Au coated substrate. The methods of organizing and immobilizing bR layers are reviewed in Chapter 3. However, the biotin labelling method was used to recognize and label the extracellular side of the bR, and self assembly technique based on biotin-thiols and streptavidin was used to allow linking the bR purple membranes directionally to the Au substrate. The introduced methodology was used for the dried, and the wet bR monolayer. This chapter also provides details of the fabrication method.

Chapter 4 investigates the photovoltaic characteristics of the molecularly organized bR based monolayer. The phototransduction process of the dried bR monolayer is investigated. The photo-cycle of the dried bR is significantly different from wet or aqueous bR because it is based on charge separation, whereas the wet bR photo-cycle is based on the transport of protons. The photovoltaic stability, power intensity and exposure duration are studied. The transient and steady state responses are investigated. Mechanical deformations of the bR structure are explained based on the photovoltaic characteristics. Factors that affect the fabrication process and operation performance are optimized for creating high performance photo-responsive monolayer without using signal amplification circuits.

Chapter 5 studies the photo-electro-chemical signal transduction of the aqueous bR (wet bR) monolayer. The aqueous bR monolayer works as proton pumping station made from arrays of parallel arranged proton pumps. The photo-electro-chemical activity of the bR monolayer is studied based on the pH changes in the surrounding ionic

medium. The affect of the input power and the distance between the pumping station and the measuring point are investigated to make clear understanding of the pH kinetics in the microchannels. A mathematical model is formulated to describe the phenomenon. This chapter further validates the proposed theoretical model and provides a basis for optimizing photodetector performance for a given application.

The fabrication procedures and response characteristics of the pH-gradient activated hydrogel micro actuator are described in Chapter 6. As proof of applicability, the chapter describes how the pH-gradient activated hydrogel can be operated in larger microsystem with very specific electro-chemical environment so that it can be integrated with the bR based photo-electro-chemical transducer. It was fabricated in a comparable geometry, and operated in electro-chemical environment similar to the targeted environment with the based bR photo-electro-chemical transducer. The tests are performed in Polydimethylsiloxane (PDMS) microfluidic chip because of its optical properties, so that it can be integrated in the optically driven microfluidic systems. The swelling response characteristics of the pH-sensitive hydrogel are investigated and the limitations are discussed.

Design, fabrication and evaluation of hydrogel microactuator activated by the bR based monolayer are described in Chapter 7. Several optically driven microactuators are constructed from the temperature sensitive hydrogels and operated by the photo-thermal effect which limit their usefulness in engineering and biomedical applications. By using the bR based monolayer, the microactuator can be operated remotely at wide range of temperatures. The signal transduction process, pathway, and the photo-electro-chemo-mechanical transformations are investigated. The performance characteristics of the prototype are analyzed to demonstrate the viability of utilizing bR monolayer as an engineering material for new and innovative sensing and actuating transducer. As proof of applicability of the developed micro-actuator in microfluidic chips, bR activated hydrogel micro-valve was integrated with PDMS based microfluidic chip to create the optically driven microfluidic valve. The microvalve swelling kinetics and characteristics are investigated. The response characteristics and limitations are discussed.

Chapter 8 summarizes the contributions of this thesis. It also recognizes the limits of the project and provides suitable recommendations for the future studies, and investigations.



## CHAPTER 2

### REVIEW OF BACTERIORHODOPSIN

#### 2.1 Photosensitive Proteins

A variety of biological and electrochemical processes are powered and controlled with solar radiation. The light triggered organisms generate photoreceptors that detect and process light beams into usable form of energy. Among the photosensitive structures, nourishing chlorophylls and visual rhodopsins are the most known photo triggered structures. In plants the protein complex chlorophylls which is found in their green leaves photosynthesizes glucose and starch to be part of their life cycle. On the other hand most of the mammals have photosensitive proteins in their eyes known by visual rhodopsins. The light driven rhodopsins are used for sensing.

Rhodopsins in living biological organisms are functioning in two distinct ways when exposed to light beams. The bacteriorhodopsin (bR), and halorhodopsin act as energy converters from the photonic form into electronics phase, whereas rhodopsins SRI, and SRII are acting as visual phototaxis that regulate the flagellar motors of the cell in order to control its movements in the medium. The rhodopsins proteins have responsive molecule known by the retinal that trigger series of electrostatic changes leading structural conformational changes once exposed to light beams. Upon illuminating the retinal of the bR with light beams, a series of photo-electro-chemical and chromic changes leads to structural and conformational changes occur in the protein. The generated signal from these changes is utilized in each organism in the way that supports continuing its life cycle. In the *Halobacterium salinarium* bacterial cells the rhodopsin protein convert light beams into pH gradient that provides energy required for the cell activities. Whereas in the human eye the generated signals from rhodopsin protein are transformed into nerve impulses to be sent to the brain to contribute in constructing the surrounding images. Despite the final product of the photosensitive proteins when

exposed to the photonic energy, basically, they convert the photonic energy into electrochemical potential used in each particular organism uniquely.

In 1967, purple membrane was discovered as a specialized component of the cell membrane of the salt-loving organism called *Halobacterium salinarium* (Henderson and Unwin, 1975). The purple membranes (PM) are isolated in irregular sheets of 5nm thickness. Each PM fragment contains 75% bacteriorhodopsin (bR) in trimeric cells and 25% lipids in hexagonal symmetry (Hampp, 2000). Each bacteriorhodopsin (bR) molecule contains functional molecule called retinal. The retinal purple color dominates the entire PM. At low oxygen levels, *Halobacterium salinarium* bacterial cells grow the purple membrane (PM) sheets that have the capability to convert radiant sun light to gradient in the concentration of the hydrogen ions across the cell wall which is interpreted as pH gradients. These pH gradients provide the necessary energy for synthesizing adenosine triphosphate (ATP) from adenosine diphosphate (ADP) which is required for the bacterial cell activities (Wang *et al.*, 2005; Hampp, 2000). Biologically, the ATP is known to be the energy transfer agent that diffuses in the cell to energize its cellular molecular processes, and cell movements (Voet *et al.*, 2006). Interestingly enough, the ATP can be considered as the agent that transfers energy currency of life to the bacterial cell. This photosynthesis in bR is fundamentally different from the chlorophyll-mediated photosynthesis that is found in plants. In the chlorophyll based photosynthesis, the energy conversion starts with electron charge separation whereas in bR the process of conversion of light energy into usable form of energy starts by pumping hydrogen ions across the membrane to produce an electrochemical potential.

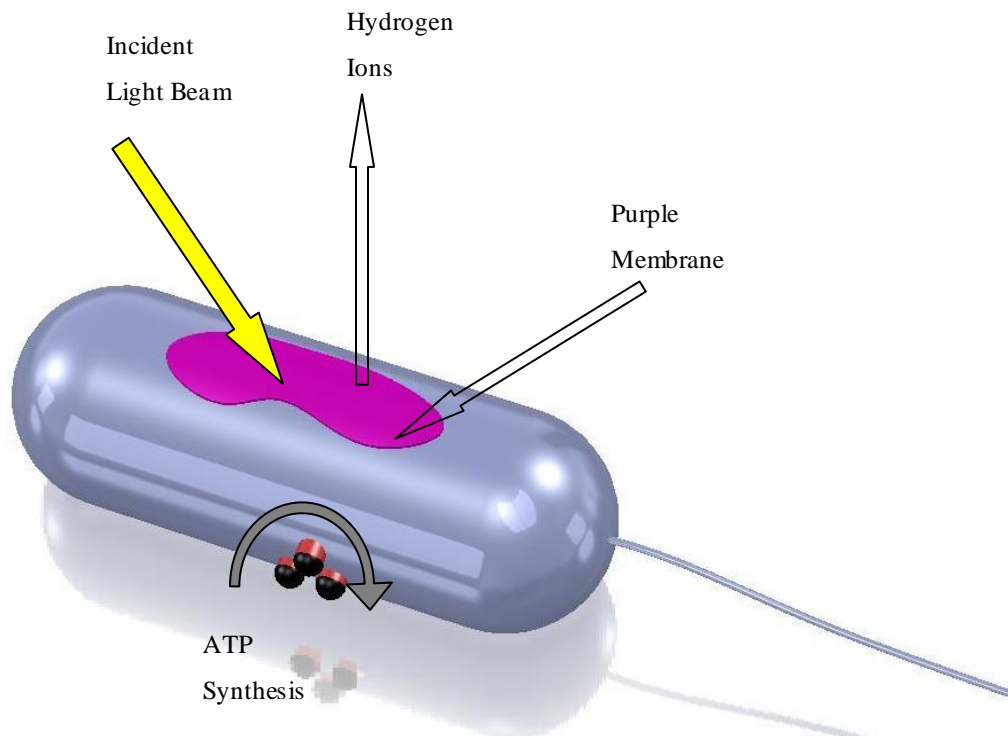


Figure 2.1 Schematic diagram of a *Halobacterium salinarium* cell. A two-dimensional crystalline purple membrane provides proton transport and membrane-bound ATP syntheses enable the photosynthesis of ATP from ADP.

## 2.2 General Structure of Purple Membrane and Bacteriorhodopsin

Bacteriorhodopsin proton pump is the only protein in the purple membranes of *Halobacterium salinarium* living cell. Under oxygen limited conditions the cell membrane grows purple membrane patches in the form of hexagonal two-dimensional crystalline lattice of bR, Figure 2.2. The bR molecules are arranged in directionally oriented arrays with lipid filling the inter-molecular spaces forming monolayer-thick PM patches. The molar ratio of the lipid to the bR molecules is 10:1 (Blaurock and Stoeckenius, 1971).

The PM patches are characterized their irregular lateral dimensions, where the average diameter can be up to 5  $\mu\text{m}$ , whereas they have uniform thickness of 5nm. The PM proved high functional and structural stability over several years of light exposure. In the wet or aqueous medium it keeps its stability at relatively high temperature of 80°C

and at harsh chemical environments for pH values from 0-12 in the presence of high ionic strengths up to 3 M NaCl (Hampp, 2000). The PM preserves its photoelectric activity in dry environment and can keep functioning up to 140 °C (Shen *et al.*, 1993).

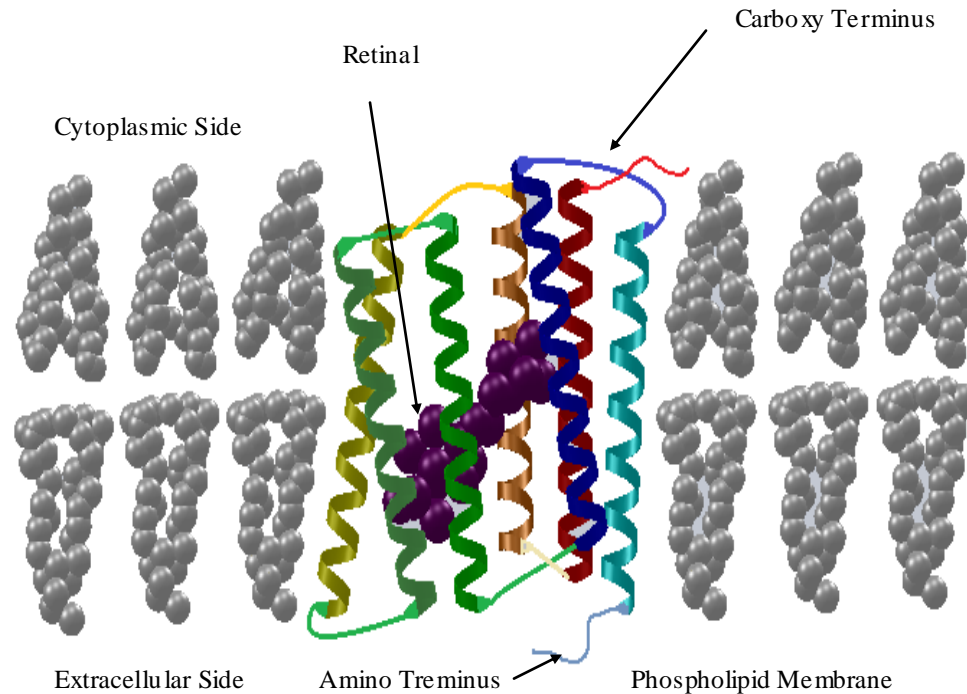


Figure 2.2 General Structural description of purple membrane patches containing bR. A bR protein in the membrane. Its carboxy terminus is located inside the cell and the amino terminus is located outside the cell.

The two dimensional structure of lipid-bR in the PM is the base of the thermal and chemical stability in the dry and wet environments. Each bR molecule converts the light radiation into electrochemical energy by pumping protons from the cytoplasmic side to the extracellular side of the membrane without allowing passive diffusion of protons back into the cell.

The bR is a retinal protein complex that consists of two main components: a protein molecule body and the retinal molecule. The retinal is simply known by Vitamin A aldehyde. The bR structure consists of 248 amino residues in a polypeptide chain arranged in seven  $\alpha$ -helices (Henderson *et al.*, 1990). The  $\alpha$ -helices are labelled in the

literature from A to G, as shown in Figure 2.3. The retinal is linked to  $\epsilon$ -amino group of lysine-216 (K216) of the G helix with covalent bonding via a protonated Schiff base (Lemke and Oesterhelt, 1981). The seven transmembrane helices contain the retinal residue, amino-acid residues and water molecules within a structural cavity (Lanyi, 1998). This cavity, which is also known by the proton transport pathway, shields the chromophoric group of the retinal from the possible external environmental influences. The Schiff base divides the proton pathway into two channels; traditionally referred to as the extra cellular and cytoplasmic half-channels. The extracellular part contains several charged residues; the most notable of them is anionic Asp85. This residue is considered to be the main component of the counter-ion to the Schiff base and is also the proton acceptor once the Schiff base deprotonated during the proton pumping process. The residues Asp212, Arg82, Glu204, and Glu194 have roles in the proton release to the extracellular side during the pumping process. In contrast, the cytoplasmic part contains mostly hydrophobic residues except the protonated Asp96 which is considered as the proton donor to the Schiff base. The proton pumping process is found to be influenced by many single mutations of these residues. However, the pumping process is completely abolished only when Lys-216 or Asp85 are replaced.

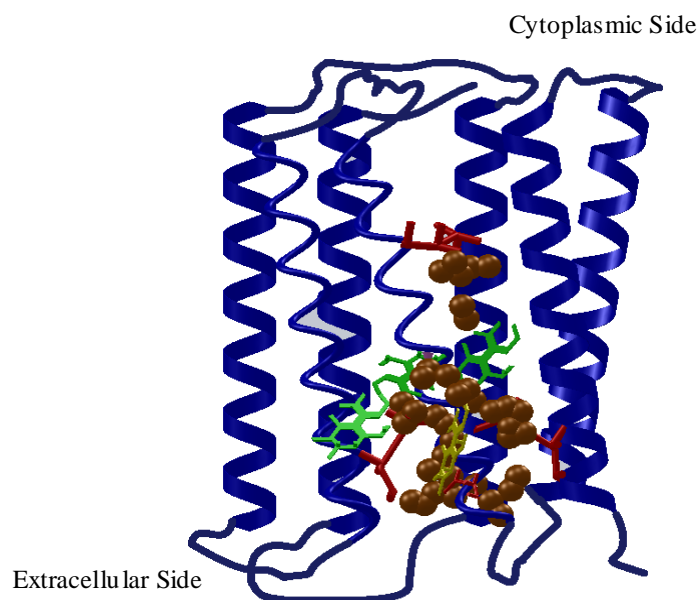


Figure 2.3 Detailed structural description of the bR. The seven transmembrane helices are labelled from A to G. The retinal Schiff-base and the amino acids are most relevant for proton transport.

### 2.3 Photoelectrochemical Cycles of Bacteriorhodopsin

The retinal of bacteriorhodopsin proton pump is a natural chromophore that exists only in one of two configurations: *all-trans* and *13-cis* (Maeda *et al.*, 1977). In the dark, the bR molecules contain mixture of these two retinal configurations; it is called “dark-adapted”. Once bR molecules exposed to the light radiation the molecules that are in the *13-cis* configuration ground their state to be at the *all-trans* retinal configuration. This is considered as the starting point of the photocycle, which is also known by “light-adapted” state. Basically the proton pumping process does not occur in the dark-adapted bR. When the bR molecules receive the activating light beams, the retinal undergo in an isomerisation process around the C13=C14 double-bond to transform the retinal configuration from *all-trans* to *13-cis* configuration, as shown in Figure 2.4 (Gai *et al.*, 1998). The retinal isomerisation is followed by proton transport from the cytoplasmic to the extracellular side of the membrane, which is interpreted as converting the incident light energy into chemical energy (Lanyi, 1993). The proton pumping process is accompanied by a thermal structural relaxing photocycle with several intermediate states.

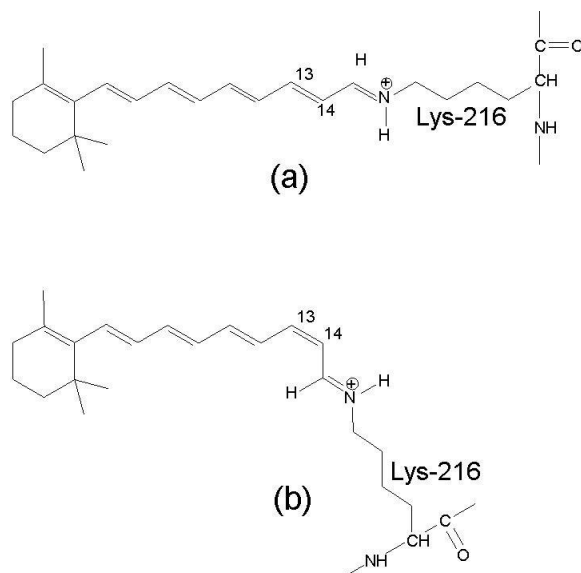
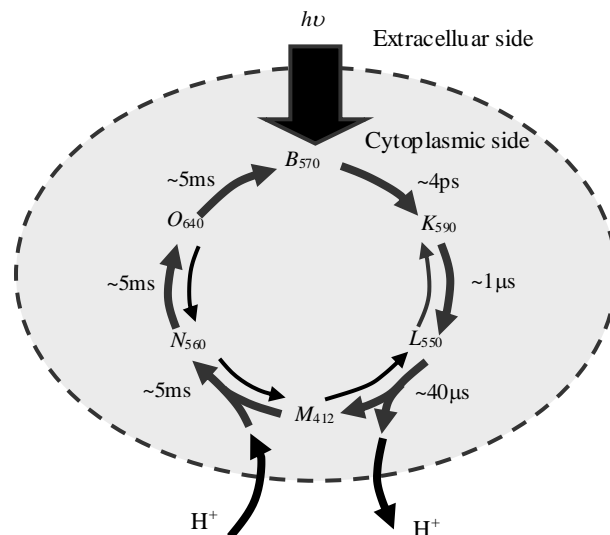


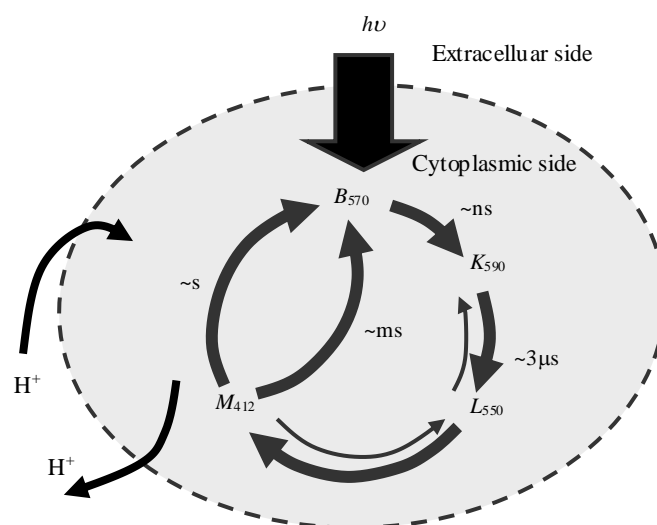
Figure 2.4 Photo-isomerization of the bR retinal from (a) all-trans to (b) 13-cis in bR. The retinal has covalent bond with Lys-216 via a protonated Schiff base. When absorbing a photon, the retinal isomerizes around the C13=C14 bond. (Based on Gai *et al.*, 1998)

Prior studies have shown that the kinetics of the bR photocycle depend on the level of humidity in the sample (Váró *et al.*, 1983; Korenstein *et al.*, 1977). The photocycle and proton transfer kinetics of dried bR film differ from aqueous, or wet, bR because of dehydration (Korenstein *et al.*, 1977; Cao *et al.*, 1991; Groma *et al.*, 2001; Wang 2006; Wang *et al.*, 2007). In the bulk aqueous form, Figure 2.5a, the bR molecules act as a light-driven proton pump.

The absorption of a photon by the bR molecule initiates the isomerization of retinal from all-trans to 13-cis conformation, followed by proton transport across the cell membrane. The PM proton transfer starts with the release of a hydrogen ion (H<sup>+</sup>) during the L550→M412 transition and ends with an ion uptake during the M412→N560 transition. The light induced intermediate states of the photocycle correspond to activation, proton dissociation, proton translocation, proton association, and relaxation.



(a) Multistate intermediates of the aqueous bR photocycle.



(b) Limited intermediate of the dried bR photocycle.

Figure 2.5. Basic photochemical cycles of bacteriorhodopsin, when exposed to visible light ( $h\nu$ ), for both the aqueous (a) and dry forms (b) (Groma *et al.*, 2001). The subscripts refer to the peak wavelength for the identified intermediate.

When the bR molecules are exposed to light illumination, they all return to the ground state B. This step is considered as the start point of the photocycle. The photocycle consists of photo-driven thermal intermediates with distinct photo-absorption



maxima. Fundamentally, the photocycle's intermediates are wavelength driven transitions, where each intermediate can proceed by thermal relaxation to the next state or switch back to the ground state B, based on the received photo excitation. All of the intermediates are before the proton release and after the proton uptake. The transition of the bR that occur between releasing proton and up-taking another proton is considered as an irreversible transition, where the nitrogen atom in the Schiff base becomes no more accessible to the extracellular side of the proton way half-channel, then open the cytoplasmic side of the half-channel and close the extracellular half. The sequence of the proton release-uptake is a pH-based process, where at  $\text{pH} \geq 7.0$  the proton release precedes the proton uptake, whereas at  $\text{pH} < 7.0$  the proton uptake precedes the proton release (Ludmann *et al.*, 1992). These simultaneous structural re-arrangements are considered to be the origin of the vectorial proton transport through the bR protein. In the wild-type bR proton pump a complete photo-cycle needs approximately 10 ms (Dancshazy *et al.*, 1986).

However, when the humidity level in the bR film falls below 90%, the later N560 and O640 intermediates are no longer observed and fewer protons are transferred across the PM (Ganea *et al.*, 1997). As shown in Figure 2.5b, only the K590, L550 and M412 intermediates of the dry bR are involved in the photochemical cycle. The dry bR protein returns to its ground state (B570) through several paths, each with a different lifetime (Varo *et al.*, 1991). Furthermore, the only available ions for dry bR film are those enclosed within the structure of the bR purple membrane proton pumps (retinal ions).

Both aqueous and dry bR purple membranes have the same spectral absorbance, Figure 2.6, and exhibit a peak photo-excitation response at 568 nm. The optical absorbance at a given wavelength is related to the ratio of light intensity transmitted through a sample to the original incident light intensity.

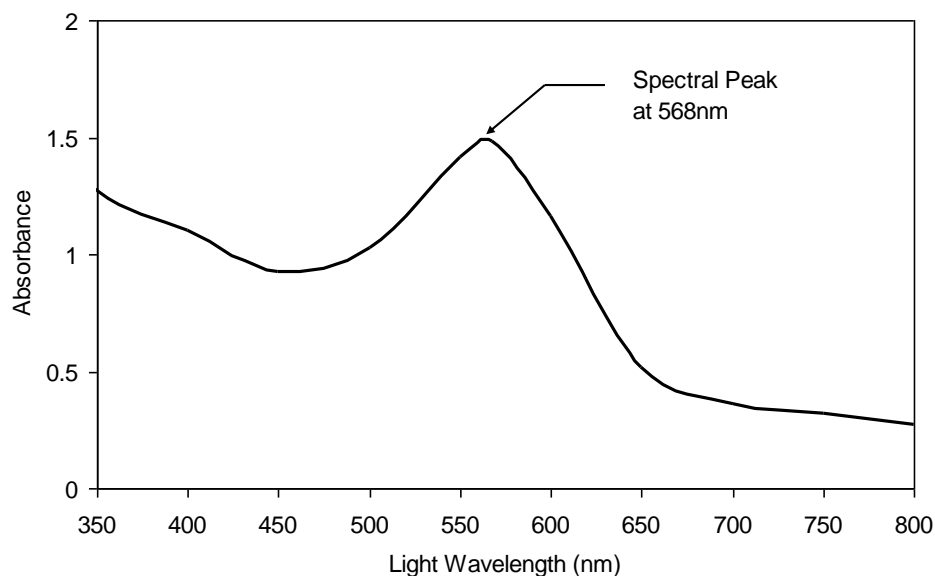


Figure 2.6 Spectral absorbance of the bR produced at the University of Western Ontario. Note that visible light ranges from approximately 400nm to 700nm.

## 2.4 Photoelectric Properties of Bacteriorhodopsin

The photoelectric characteristics and response of bR based systems is the resultant of the light-bR interaction and its photocycle kinetics. In other words the charge dynamics within the bR protein can be directly related to the intermediate kinetics of the photocycle. When bR receives light beams, it starts the charge translocation process, and the sub sequential structure deformations needed to generate charge gradients (Lanyi, 1993). This charge activity can be detected with monitoring the potential difference. The existence of such voltage difference and the temporary changes in the polarity and amplitude can be directly related to the proton transfer across the PMs.

The photoelectric response of bR array can be described as the collective responses of all bR pumps. However the response of each bR pump includes two photoelectric components (Hong, 1999). The first component is the proton translocation across the PM which represent the vectorial proton pumping action from the intracellular side to the extracellular side in the presence of aqueous medium. The second component of the photoelectric response is originated from the charge displacement and

recombination within the bR molecule. This component is essential in the dry bR based photoelectric films where it is less sensitive to the moisture content. The charge displacement and recombination does not lead to net voltage difference as it occurs inside the bR pump channel.

The organized PMs generates electric signal once exposed to light radiation. The generated light signal contains three major components with different lifetimes. The fastest component shows its viability within 100 ps in the opposite direction of the proton pumping pathway. The other two photoelectric components take place in microsecond and millisecond range and are in the same direction of the proton transport (Liu, 1990). The internal charge dynamics, proton dynamics, and non-proton ion dynamics may all contribute in the photoelectric components. Theoretically, the photocycle lifetimes should coincide with the photoelectric components. However, the lifetimes of the PM photocycle components are not in full agreement with the detected responses (Wang, 2006). This might occurred due to the use of classical methods to organize and adsorb the PMs on the electrodes surface. The other possible reason, which is believed to have less contribution in the photoelectric activities, is the influence of the surrounding conditions such as salt concentration.

The very fast rise-time (picoseconds range) of the bR photoelectric response is achievable with using ultra-fast laser pulsing. This rapid response is generated from expected processes (Birge, 1999). The first possible reason is the instantaneous change in the electron density associated with electronic excitation in the protonated Schiff-base polyene during the retinal isomerisation of the retinal in bR. The change in the electron density is interpreted by moving an electron with 2.49 Å on the polyene chain toward the nitrogen atom, which leads to making the C14C15H=NH-Lys more negative, Figure 2.7. The generated electrostatic change between the C14C15H=NH-Lys and the two near negative Aspartic acid residues supports the photopolymerization around the 13-*cis* double bond, and thus starting the earlier photochemical processes. Once bR is photoexcited the isomerisation process take place within 200 fs. This photochemical which occurs within 200 fs is the fastest so far known photoreaction. This ultra-fast response shows promising. This isomerization process occurs within 200 fs following photoexcitation. To date, this is the fastest known biological photoreaction, and thus

shows great potential candidate for high-speed photoelectric applications. The second expected reason is that: the protonated Schiff moves away from the negative counterion in the stage of forming the *K* state intermediate. This second process dominates the photoelectric response. Similar photoelectric responses are found in the visual rhodopsin of vertebrates which is known by the early receptor potential (ERP).

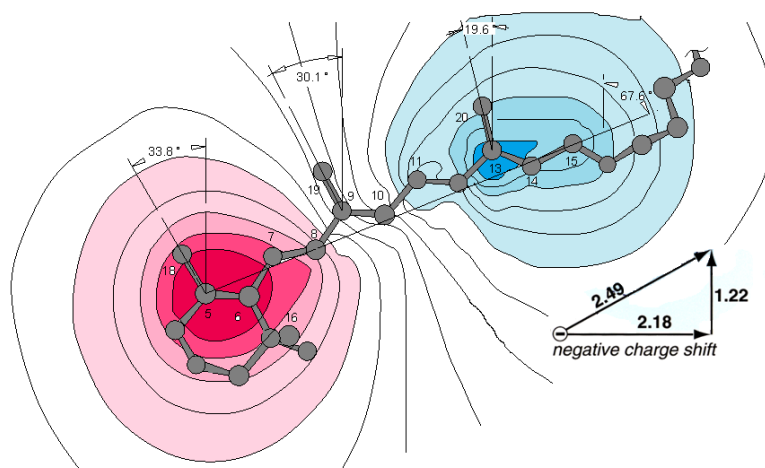


Figure 2.7 An electrostatic map of the primary photochemical event of bR.

## 2.5 Applications of Bacteriorhodopsin

The unique characteristics of bR proton pump starting from its thermal and chemical stabilities, high quantum efficiency, photochromical, photoelectrical, and photoelectrochemical characteristics, and functional viability when immobilized in artificial systems, make bR a promising candidate for various applications. Since its discovery, bR has been used in different devices such as the photochromic, and photoelectric applications. Recently the interests focus in the development of an alternative method for organizing bR accurately and permanently, and its impact on the photoelectric and photoelectrochemical characteristics.

### 2.5.1 Photochromic applications

The unique photochromic characteristics of bR have enabled creating all-optical logic gates, optical memories, parallel associative processors, and holographic interferometry (Sharmar and Roy, 2004; Renner and Hampp, 1993; Cullin *et al.*, 1995; Birge *et al.*, 1999). These techniques are based on the photochromic characteristics of bR, where each bR proton pump individually absorb the incident photons and launch a reversible photocycle. Bacteriorhodopsin can go in reversible transitions between the photocycle intermediates by exploiting the photo-responsivity of bR at different wavelengths. Furthermore bR can be genetically engineered to generate different spectral shifts and longer lifetimes at certain intermediates for improved photo-responsivity (Bräuchle *et al.*, 1991). Organizing bR within the photoresponsive film remains at this point a technological challenge for generating higher performance bR based systems.

### 2.5.2 Photoelectric applications

The photo-responsivity of bR enabled producing bio-photocells for sensing and imaging technologies. However, bR proton pumps have to be directionally organized as pumping sense is a fundamental condition for detectable responses. The photoelectric characteristics of bR immobilized on conductive substrates have been investigated with the different substrates. Indium tin oxide (ITO) coated glass and plastics, gold, Platinum are the most used electronic substrates (Saga *et al.*, 1999). However, for the micro and nano applications different substrates are proposed as potential candidates for immobilizing bR such as the gate terminal of a GaAs-based MOSFET and nano-black lipid membranes (Xu *et al.*, 2004; Horn and Steinem, 2005).

Most of the worldwide reported bR based system focused on generating electric potential when exposed to light beams with different configurations and applications. Miyasaka *et al.* (1992) developed a bR based 8×8 pixel cell of image photodetection. Haronian and Lewis (1992) studied the methods that can be used without losing the bR functionality. The researchers deposited a 50 μm × 50 μm pixels array pixels is created by depositing bR onto a continuous ITO electrode, then ablating both film and substrate using an argon-fluoride excimer laser. Martin *et al.* (1997) introduced protein-silicon hybrid photoreceptor array. The researchers built a high-resolution bR-silicon photocell,

using the detection grid of a charge injection device (CID) as the substrate for a bR-polymer film. This structure integrates processing circuit to monitor the bR photoresponse. Libertino *et al.*, (2003) deposited non-oriented bR film on Si and SiO<sub>2</sub> substrates.

The bR-based photoelectric and photochromic systems have shown functional mimic of the biological vision as the bR good degree of functional similarity with the biological eye *rhodopsin*. The bR showed inherent of processing simple vision information. Several research groups focused on two essential functions including feature extraction and pattern recognition. The function of feature extraction involves detection and position of spatial and temporary variations in the image intensity which is very important in the edge enhancement and motion detection applications. In the biological vision systems, the basic edge detection systems are formed from the ganglion cell receptive field. This formation is referred to a zero-crossing filter. An artificial receptive field based on bR photodetector has been developed by Takei *et al.* (1991) and Yang *et al.* (1998). BR is also used in building parallel processing units based on the neurobiological principles (Haronian and Lewis, 1991). The researchers introduced bR based rapid reprogrammable neural network architecture with the capability of including large synapse matrix.

The photoelectric responsivity and characteristics that is shown by bR based artificial systems have been exploited in making unique motion detection systems capable of detect the motion and edge information in real time Miyaska and Koyama (1993). Moreover, a position-sensitive motion sensor that is able to detect the object's motion at certain positions and times based on bR has shown promising performance. From the pattern and color recognition bR exhibited viable functionality. Min *et al.* (2001) constructed bR based sensor at different configurations able to make image extraction and pattern recognition. On the other hand, colour recognition sensors based on bR has shown functional responsivity (Frydrych *et al.* 2000, Choi *et al.* 2001) when trained the neural networks for colour space recognition.

## CHAPTER 3

# PRODUCTION AND IMMOBILIZATION OF BACTERIORHODOPSIN

### 3.1 Introduction

Bacteriorhodopsin (bR) is a biologically produced protein in a living organism called *Halobacterium salinarum* (formerly *Halobacterium halobium*) from the Archaea domain of life. The *Halobacterium salinarum* is a unicellular organism that grows and produces optimally in high salt concentration. This light-sensitive protein which is biologically formed in the marsh archaeobacteria *H. salinarum* has been extensively studied as an organic photosensitive material for a variety of engineering applications including photocells and optical memory (Hampp 2000; Wang *et al.* 2005). The biological growth protocols in the laboratory and the molecular level organizing of the bR molecules have been established and presented in this chapter.

### 3.2 Production of Bacteriorhodopsin (bR) Protein

Bacteriorhodopsin (bR) is a biologically produced protein in a living organism called *Halobacterium salinarum* (formerly *Halobacterium halobium*) from the Archaea domain of life. The *Halobacterium salinarum* is a unicellular organism that grows and produces optimally in high salt concentration near saturation, warm temperature near 37°C, and low oxygen levels. At the point of salt saturation, the oxygen level is approximately five times lower than in clean water. At this oxygen low level, *Halobacterium salinarum* cells grow 5nm thick purple membrane (PM) sheets that have the capability to convert radiant sun light to instantaneous gradient in the concentration of the hydrogen ions across the cell wall which is interpreted as pH gradients. These pH gradients provide the necessary energy for synthesizing adenosine triphosphate (ATP) from adenosine diphosphate

(ADP) which is required for the living cell activities (Wang *et al.*, 2005; Hampp, 2000). Biologically, the ATP is known to be the energy transfer mechanism agent that diffuses in the cell to energize its cellular molecular processes, and cell movements (Voet *et al.*, 2006). Interestingly enough, the ATP can be considered as the driver mechanism that transfers energy currency of life to the bacterial cell. This instantaneous process is repeatable as long as there is a continuous generation of pH gradients across the cell walls.

Unlike non-automated events, the process of generating pH gradients is understood to be consists of a fully automated sequence of photo-electro-chemical events at molecular level that is triggered by photon reception and completed with the pumping of hydrogen atoms to the extracellular medium. These processes are physically hosted by the purple membrane (PM) patches. In essence, each PM patch works as a hardware unit that contains an array of biological nano-processors known by bacteriorhodopsin (bR) protein which has an approximate volume of  $56.7\text{nm}^3$  (Henderson *et al.*, 1990; Henderson, 2007) and lipid filling to seal the bR intermolecular spaces. Structural analysis of the PM patches showed that, the bR proteins are arranged in parallel hexagonal crystalline lattice forming two-dimensional arrays. Each array is molecularly built by a multiple of the ratio of ten lipid molecules per one bR molecule (Sumper *et al.*, 1976). This qualitative and quantitative assembly acquired the purple membrane patches at that low-scale their unique mechanical flexibility and robustness and their chemical and thermal stability (Wang *et al.*, 2005; Hampp, 2000), Figure 3.1.

In nature these planar purple membrane patches which might cover up to 80% of the bacterial cell, utilize a broad range of wavelengths contained within the visible band of solar radiation to provide energy to the living bacterial cells.



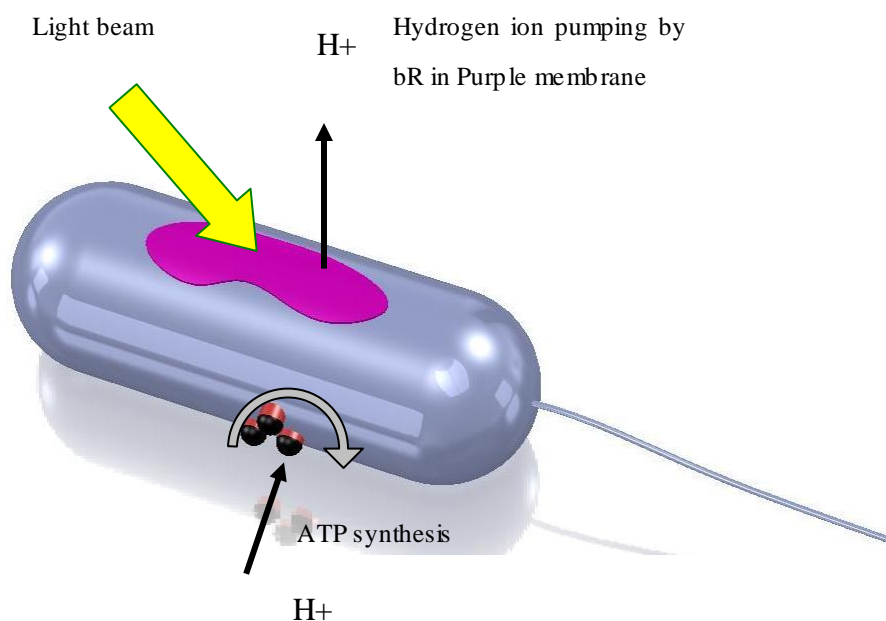


Figure 3.1. Illustration drawing of the bacteriorhodopsin in its biological *Halobacterium salinarum* cell. (This is similar to Figure 2.1)

### 3.2.1 Materials for fermentaion of *Halobacterium salinarum* growth media

The *Halobacterium salinarum* wild type (WT) strain was a generous gift from Dr. Robert Birge (Department of Chemistry, University of Connecticut, Storrs, Connecticut, USA). Uracil (item number U1128) provided by Sigma-Aldrich; Peptone Bacteriological (item number LP0037) provided by Oxoid Ltd; Tryptone (Stoke number Fulka T7293) provided by Sigma-Aldrich; Sodium chloride NaCl (Item number S640) provided by Fisher Scientific, MgSO<sub>4</sub> (anhydrous) (Item number M63) provided by Fisher Scientific, KCl (Stoke number 7447-40-7) provided by Fisher Scientific, tri-Sodium citrate·2H<sub>2</sub>O (Stoke number 0754-12) provided by Mallinckrodt, 5N NaOH (item number SS254) provided by Fisher Scientific; yeast extract; Agar (Stoke number A360) provided by Fisher Scientific; DNase (Deoxyribonuclease, 541 units/mg (item number AMPD1 – Amplification grade) provided by Sigma-Aldrich; Percoll (item number 17-0891-01) provided by Amersham Bioscience. Dylasis tubes of 20µm wall thickness, flat width 25m, and volume of 1.98 ml (item number 21-152-18) provided by Fisher Scientific.

### 3.2.2 Fermentaion and growth media

The *Halobacterium salinarum* wild type (WT) have been grown in four phases with specific medium suitable for the growth process for each phase. The mediums used are: media salts, culture media, and rich media. Table 3.1 shows the standard composition for the scales used in this research work. The medias can be scaled up or down with the same ratios.

Table 3.1 Materials and media used to grow *Halobacterium salinarum* cells.

Media name	Composition
Media Salts (MS) (10.0 L)	<ul style="list-style-type: none"> <li>• 2.5 kg NaCl, 97.7 g MgSO<sub>4</sub> (anhydrous), 30 g tri-Sodium citrate·2H<sub>2</sub>O, 20 g KCl, 10L of MilliQ water.</li> </ul>
Culture Media (CM) (1.0 L)	<ul style="list-style-type: none"> <li>• 1.0 L media salts, 3 g yeast extract, 5 g tryptone.</li> <li>• pH adjusted to 7.2 using 5N NaOH.</li> <li>• Autoclave for 30 min.</li> </ul>
Rich media (RM)	<ul style="list-style-type: none"> <li>• 1.0 L media salts, 10 g peptone</li> <li>• pH adjusted to 7.2 using 5N NaOH</li> <li>• Autoclave for 30 min.</li> </ul>
Uracil stock solution	<ul style="list-style-type: none"> <li>• 0.5 m uracil added to 200 mL de-ionized water</li> </ul>
Basal salt (BS)	<ul style="list-style-type: none"> <li>• Rich media without peptone</li> </ul>
Culture Media Plates (1.25 L) Should be done each two to three months to transfer the cell line so that keep it life for longer	<ul style="list-style-type: none"> <li>• 1L Culture Media, 18.8 g Agar, 250ml ddH<sub>2</sub>O</li> <li>• pH set to 7.2 using 5N NaOH</li> <li>• Autoclave</li> <li>• Dry plates 12-17 hrs at 37 °C before using</li> <li>• Store at 4 °C</li> </ul>

**Phase I (one colony in 5mL):** one pick of the *Halobacterium salinarum* colony cells picked using toothpick and placed in 5 mL of culture media in a test tube. 100  $\mu$ L of 2.5 mg/mL uracil stock solution is immediately added. The mixture is exposed to continuous white light illumination and the temperature is adjusted to 39 °C for 7 days. The swirly and cloudy appearance can be noticed in 4 days when the growth is going well.

**Phase II (100 mL fermentation):** 1 mL of phase I cells added to 100 mL of rich media. 2 mL of 2.5 mg/mL uracil stock solution is immediately added. The mixture is exposed to continuous white light illumination and the temperature is adjusted to 39 °C. This phase is conducted in 1.0 L bioreactor with stirring speed of 50 rpm for 7 days.

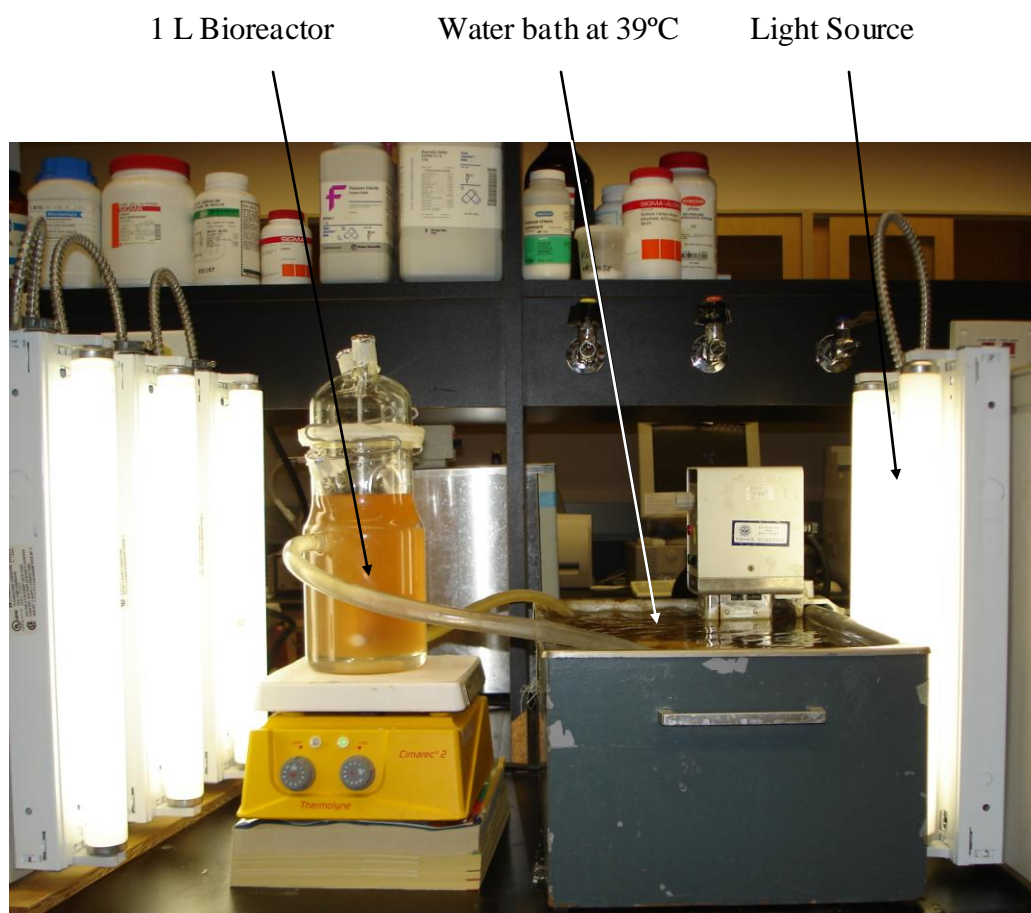


Figure 3.2 Photograph of the 1.0 L fermentation process of the *Halobacterium salinarum* cells.

**Phase III (1.0 L fermentation):** 1.0 L of phase I cells added to 9.0 L of rich media. 200 mL of 2.5 mg/mL uracil stock solution is immediately added. The mixture is exposed to continuous white light illumination and the temperature is adjusted to 39 °C. This phase is conducted in 1.0 L bioreactor with stirring speed of 50 rpm for 7-10 days, Figure 3.2.

**Phase IV (10.0 L fermentation):** 10.0 L of phase I cells added to 900 mL of rich media. 18 mL of 2.5 mg/mL uracil stock solution is immediately added. The mixture is exposed to continuous white light illumination and the temperature is adjusted to 39°C. This phase is conducted in 10 L bioreactor with stirring speed of 50 rpm for 7-10 days, Figure 3.3.

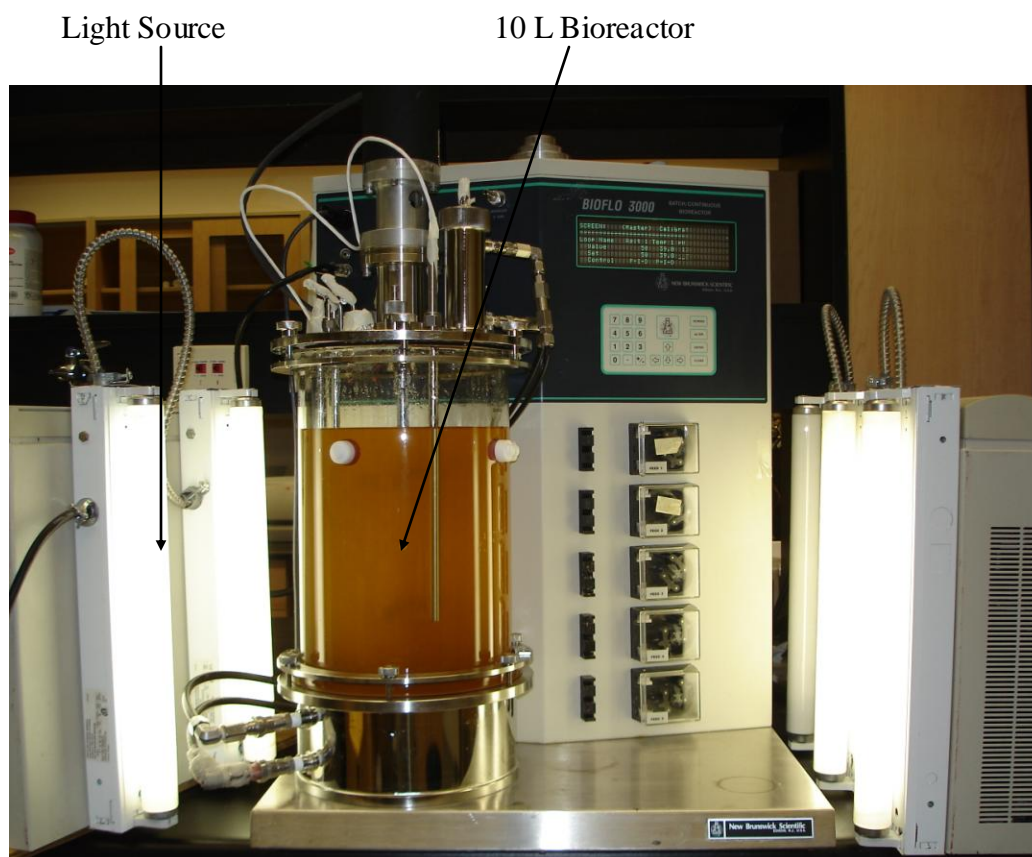


Figure 3.3 Photograph of the 10.0 L fermentation process of the *Halobacterium salinarium* cells.

### 3.2.3 Extraction and purification of bacteriorhodopsin (bR)

The produced *Halobacterium salinarum* cells were harvested using 1.0 L centrifuge tube volume at 5000 rpm for 30 minutes cycles at 4°C. The collected cells from the harvesting process were re-suspended in 300 mL of basal salt solution. The suspension was treated by adding 5 µL of DNase. The DNase reduces the viscosity of the lysate which reduces the possible deterioration of DNA by hydrolysis. Then, the resulted suspension was stirred on stirring plate with magnetic bar for 3 to 4 hours at room temperature.

The resultant solution was transferred into dialysis tube with minimum air bubbles, and then immediately well sealed using the tube clips. The sealed tubing was placed in flask containing 0.1 M NaCl solution for 15 hours at 4°C. The flask was completely covered with aluminum foil to prevent the light-cells interaction. The difference in the salt concentration from 4M to 0.1M generates osmotic pressure difference between the intra-cellular and the extracellular sides of the *H. S.* cell walls. This amount of osmotic pressure was found to be enough to break the cell walls without damaging the bacteriorhodopsin (bR) proton pumps. Once the microorganism was lysate the purple colour can be noticed clearly.

The resulted lysate was centrifuged at 50,000g (22,000 rpm Sorval centrifuge with rotor T-1270) for 30 minutes at 4 °C. The supernatant was discarded while the sediment was re-suspended in 300 mL of 0.1M NaCl. The re-suspension process was carefully performed by scrubbing the bottom of the centrifuge tubes gently and mixed using a vortexer. The suspension was centrifuged another time at the same conditions and then suspended in 0.1M NaCl. The resulted sediment was suspended in de-ionized water.

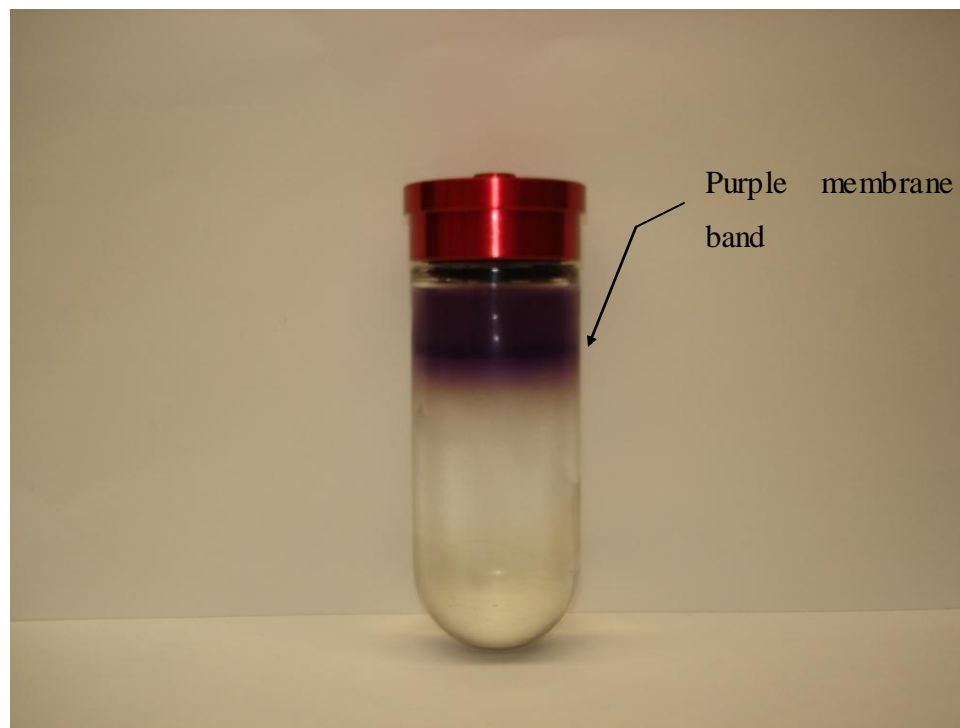


Figure 3.4 Photograph of the density gradient formed the purple membrane band.

The final suspension was centrifuged and suspended in 25% percoll solution and then centrifuged for 2 hours at 50,000 g (22,000 rpm Bekman) and 4 °C. The percoll is linear gradient self-forming when centrifuged at greater than 10,000 g. The purple band was extracted and then suspended in 25% percoll for one more time to get ride of the cell wall fragments and the unwanted molecules when centrifuged for 2 hours at 4°C, Figure 3.4. The purple band was suspended in de-ionized water, and then centrifuged at 50,000 g (22,000 rpm Sorval centrifuge with rotor T-1270) for 30 minutes at 4°C. The last step of centrifuging and re-suspending in the de-ionized water was repeated number of times until the solution conductivity was around 10 $\mu$ S/cm, which means clean protein suspension. Once it is purified, the optical response of the bR suspension was tested in the spectrophotometer  $\mu$ Quant from BIO-TEK Instruments, Figure 3.5. The optical density peaks shows a ratio of 1.8422:1. This ratio indicates that the used bR suspension is within the acceptable range of purification. Oesterhelt and Stoeckenius considered the bR suspension of peaks ratio 2:1 is acceptable, so that, the used bR suspension is within

the acceptable range. In general, it is recommended to have the bR purified within the peaks ratio that ranges (2.5-1.5):1.0. Low purification leads to the generation of weak light to electrochemical energy conversion, and over-purification (peaks ratio less than 1.5:1.0) may lead to degrading bR electrochemical properties.

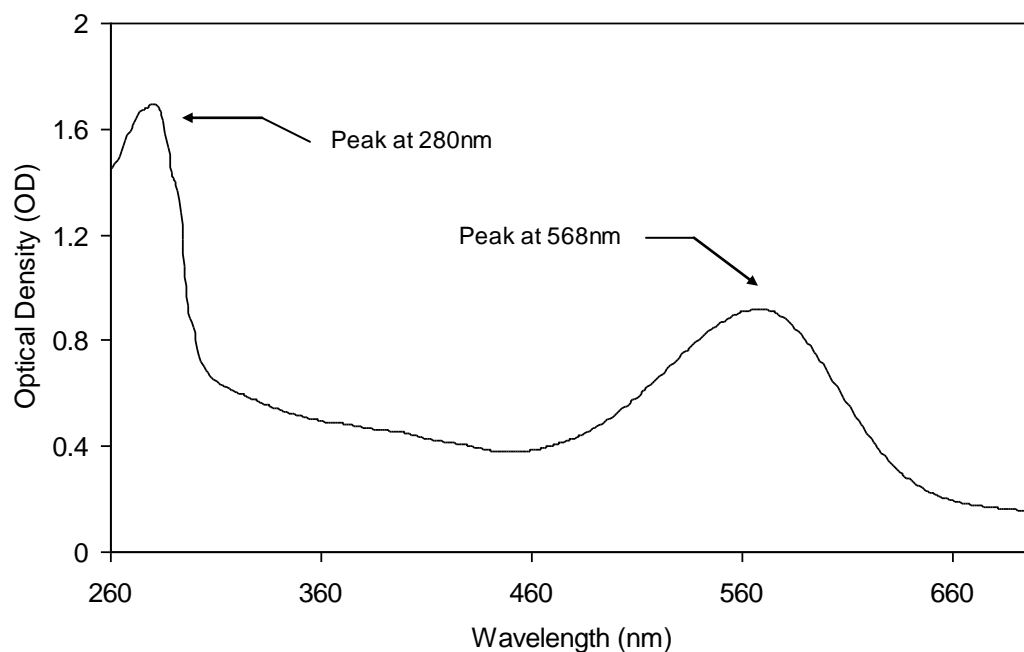


Figure 3.5 Spectral optical density of the bR produced at the University of Western Ontario. Note that visible light ranges from approximately 400nm to 700nm.

### 3.3 Review of Immobilization Methods

Incorporating bacteriorhodopsin (bR) biomaterials into practical devices is a critical technological challenge because bR is a directionally functioning proton pump. Whenever there is non-even directional organization, signal cross-talk occurs and signal deterioration is expected. On the other hand thickness of the photo-sensitive layer plays significant role in determining the final dimensions and performance of the photo-responsive devices. The capability of achieving ultra-thin photo-responsive layer enables fabricating ultra-thin photo-responsive devices.

Several methods are commonly in use to adsorb bR on electrodes; these methods include these include Langmuir-Blodgett deposition (LB), electrostatic layer-by-layer adsorption (LBL), Electrophoretic sedimentation (EPS), antibody-mediated monolayer based on the self assembly method and immobilization within polymer gels. All of these methods have shown measurable signals. However the successful detection of the photoelectric performance is in-part attributed to the functioning capability no matter the position of bR molecule is and the stable crystalline structure. Among these methods EPS, LB, and LBL are considered to be the most common methods in fabricating photoelectric and photochromic devices as they showed measurable signal. These techniques are briefly described in the following subsections.

### 3.3.1 Electric field sedimentation (EFS) technique

The Electric Field Sedimentation utilizes the difference in negative charge density between the opposite sides of the PM to generate a dipole moment that is specifically directed from the cytoplasmic side to the extracellular side. This method is used with dry films and gel capsulated bR (Dér *et al.*, 1985), Figure 3.6. However, this method of film fabrication is problematic because both sides of the protein are negatively charged with only a small measurable difference (-1.8 charge/bR: -2.5 charge/bR at pH 6.6 (He *et al.*, 1999) making it nearly impossible to properly specify orientation of the PM patches. Consequently, the EFS immobilization technique attracts both sides of the PM patches with no specificity regarding whether it is on the cytoplasmic or extracellular side.

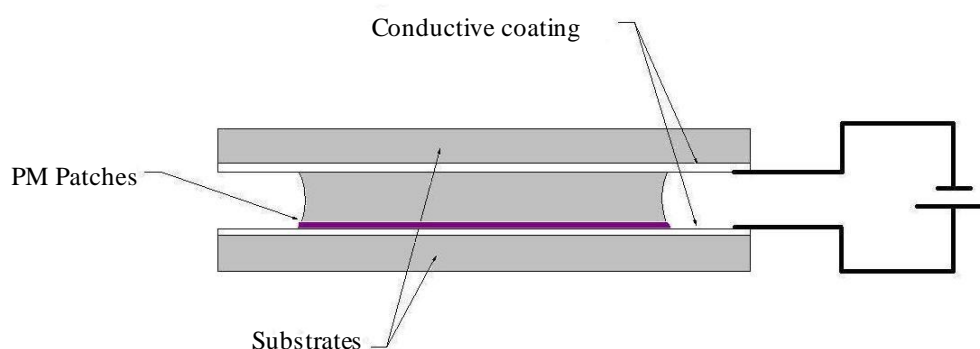


Figure 3.6 Fabrication of oriented bR films by the EPS technique. PM patches transport onto the anode due to its more negatively charged cytoplasmic side.



Further, the thin dry films fabricated using the EFS technique are often characterized by a surface roughness of approximately 200nm (Xu *et al.*, 2003), and a film thicknesses between 10-150 $\mu$ m (Wang *et al.*, 2005; Xu *et al.*, 2003; Zhang *et al.*, 2003). The relatively thick film indicates that thousands bR layers are stacked together on the cathode surface. The reported large surface roughness suggests that not all PM in the final layer of the film will make direct contact with the opposite electrode during operation and, thereby, the signal will be weaker than expected.

### **3.3.2 Langmuir-Blodgett deposition (LB) technique**

The LB method is a common technique used to produce ordered thin films of biomolecules that have amphiphilic characteristics (Pepe and Nicolini, 1996). In this technique, the amphiphilic molecules are spread across the aqueous surface in a trough, and then pushed by a dynamic barrier and transferred onto a solid substrate by a horizontal or vertical dipping, Figure 3.7. The repeatable use of this method can produce multi-layered films. Naturally when PMs are spread on the aqueous surface their cytoplasmic side orient towards the water and the extracellular side towards the air, because the cytoplasmic side of the PMs is more hydrophilic than the extracellular side. There are attempts to improve this method by using different enhancing ways such as the use of antigen/antibody molecular interactions (Koychi *et al.*, 1994), and applying electric field which help in enhancing the film orientation. Even though the LB method can be used in producing very thin film, its PMs are subject to denature in most of the organic solvents. Although thinner bR films can be fabricated using the LB technique, published studies (He *et al.*, 1999; Yamaguchi *et al.*, 1993) have shown that the PM patches that comprise the thin film exhibit random directional orientation.

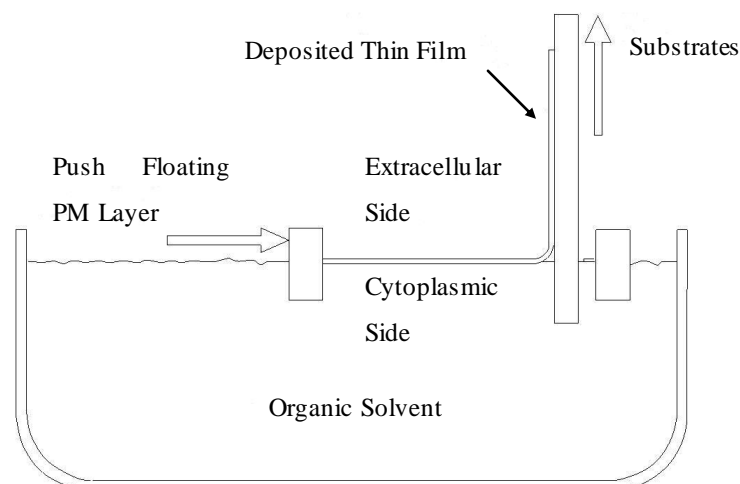


Figure 3.7 Preparation of a bR film by the LB technique. The cytoplasmic side of PM is more hydrophilic (facing into the water) than the extracellular side (facing the air).

### 3.3.3 Electrostatic layer-by-layer adsorption (LBL) technique

The electrostatic layer-by-layer technique is a reliable method for assembling oppositely charged layers on substrates. This technique fundamentally depends on the strong electrostatic interactions between oppositely charged polyelectrolytes (He *et al.*, 1998). The purple membrane is characterized with its asymmetrically charged surfaces, which makes it good candidate for LBL built architectures. One of the electrolytic materials that made with the PM a reliable bi-layers is poly(diallyldimethylammonium chloride) (PDAC). Figure 3.8 provides schematic description of the LBL architecture based on the interaction between the PDAC/PM. At pH values greater than 5, the PM exhibits more negative charge density on the cytoplasmic side than the extracellular side. This difference in the charge density between both sides of the PM is taken as the reference line for building the LBL based PM multi-layered architectures. Even though, this technique is used with several biomolecules and polymers, it is not considered as a reliable method with PM because it depends on the difference in the charge density between both sides of the PM. The difference in the charge density between both sides of the membrane is small enough to do not the PM directionality.

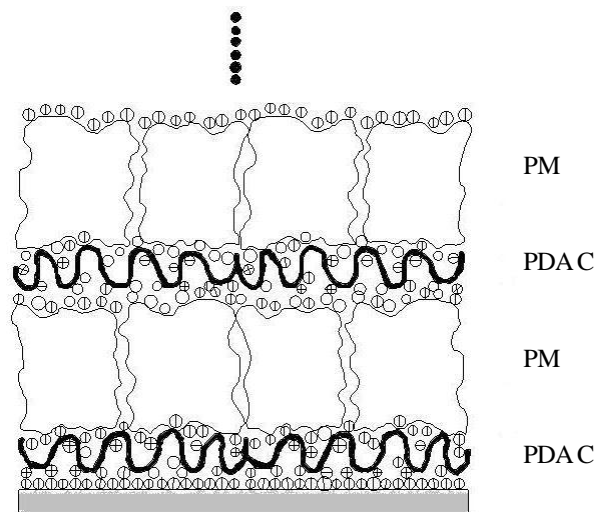


Figure 3.8 Schematic drawing of multiple PDAC/PM layers as fabricated by the LBL technique (He *et al.*, 1998).

### 3.3.4 Self-assembly of PMs using biotin labelling

To properly exploit the material in an engineered system, it is necessary, therefore, to control how the bR proton pumps are adsorbed onto the substrate. Orientation specificity can be achieved by using either the antigen–antibody immobilization method (Koyama *et al.*, 1994), the genetically engineered bR protein (Schranz *et al.*, 2007), or the biotin labelling technique (Henderson *et al.*, 1978; Chen *et al.*, 2003; Ren *et al.*, 2006). Although the antigen– antibody technique produces satisfactory orientation of the bR, the process is very lengthy because it is necessary to synthesize antigens, monoclonal antibodies, and bi-antibodies. On the other hand, using genetically modified bR protein might not be very convenient to designers without knowing the detailed characteristics of the generated product. Producing the genetically engineered PMs also necessitates genetic modifications to the protein in order for the PM to be connected to the gold substrate via thiols. In contrast, the biotinylation technique introduced in this paper uses only one reactive residue that is located at the extracellular side of bR, and it can be accessed at a specific pH, making biotin labelling a highly repeatable and reproducible process at the molecular level.

The biotin labelling and streptavidin recognition technique employs selective molecular labelling, recognition, and adsorption to enable the self-assembly of proteins and other biological material at very specific sites on the sensing surface. This highly selective immobilization technique has been used to build a variety of integrated biosensors for detecting *E. coli* bacteria (Gau *et al.*, 2001), and bacteriophages (Gervais *et al.*, 2007), as well as to develop molecular switches (Stayton *et al.*, 1999). The self-organized and self-assembled bR monolayer created using the biotin labelling and streptavidin recognition technique is schematically shown in Figure 3.9.

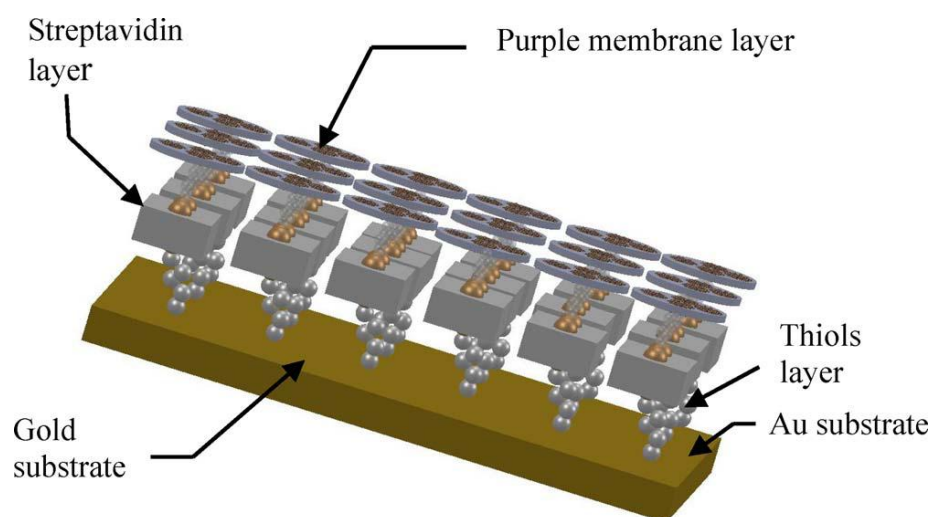


Figure 3.9 Illustration of the self-organized and self-assembled photoelectric dry layer on Au substrate.

The fabrication of this thin photoelectric layer requires molecular recognition of the extracellular side of the bR proton pumps using biotin (Henderson *et al.*, 1978) and then building a self-assembled thiol monolayer on the gold substrate. The spontaneous adsorption of the labelled bR proteins on the thiol monolayer is achieved by a streptavidin molecular recognition and binding technique.

### 3.4 Fabrication of Self-Assembled bR Monolayer

The fabrication processes of self-Assembled bR proton pumps monolayer involves using with addition of the purified bR Purple membranes Biotin-XX, SSE (was acquired from Invitrogen, [www.invitrogen.com](http://www.invitrogen.com)), biotinylated and hydroxyl-terminated thiols (were purchased from nanoScience Instruments, [www.nanoscience.com](http://www.nanoscience.com)). Streptavidin (was obtained from Sigma-Aldrich), 5×5×0.1mm Anodic Aluminum oxide ceramic membranes (were provided by Synkera Technologies, Inc., <http://www.synkera.com> ). The fabrication process can be divided to three major steps: biotin labelling of bacteriorhodopsin, substrate preparation and activation, and adsorption of the ordered bR monolayer. These fabrication steps are provided in details in the following subsections.

#### 3.4.1 Biotin labelling of bacteriorhodopsin

Biotin labelling of the bR PMs is simply recognizing the extracellular side and making a permanent bond between Lysine-129 and Biotin-XX. The Biotin-XX is often called biotin ester. The biotin labelling and bonding procedure used in this research was based on the method described by Henderson (Henderson and Stubb, 1978; Chen *et al.*, 2003) and involves adding 100µl of 20mg/ml biotin ester in dimethyl formamide to 2ml of 1.9mg/ml PMs suspended in 0.1M sodium bicarbonate at pH 8.5. An orbit shaker was used to mix the solution for 2 hours at 20°C. The mixture was then centrifuged and re-suspended in 0.1M sodium bicarbonate at pH 8.5. This step was repeated three times and then left for approximately 12 hours to remove weakly coupled biotin to the hydroxyl groups of the PMs. The resultant biotin-protein suspension was then dialyzed against two changes of phosphate buffer saline (PBS) at pH 7.4. Once completed, the biotinylated bR proteins were suspended in PBS at a pH of 7.4 for the final assembly.

#### 3.4.2 Substrate preparation and activation

Gold (Au) surfaces are characterized with their high affinity for thiol adsorption thereby enabling permanent bonds to be formed between the HS terminal of the thiols and the Au surface. The 0.231cm<sup>2</sup> substrate was first covered with 3nm adhesive titanium layer and then coated with a 75nm Au layer. The surface scan of the bare gold substrate, Figure

3.10, using an atomic force microscope (AFM) showed a relatively smooth profile with an average surface roughness of 0.672 nm and a maximum peak to valley deviation of less than 5 nm.

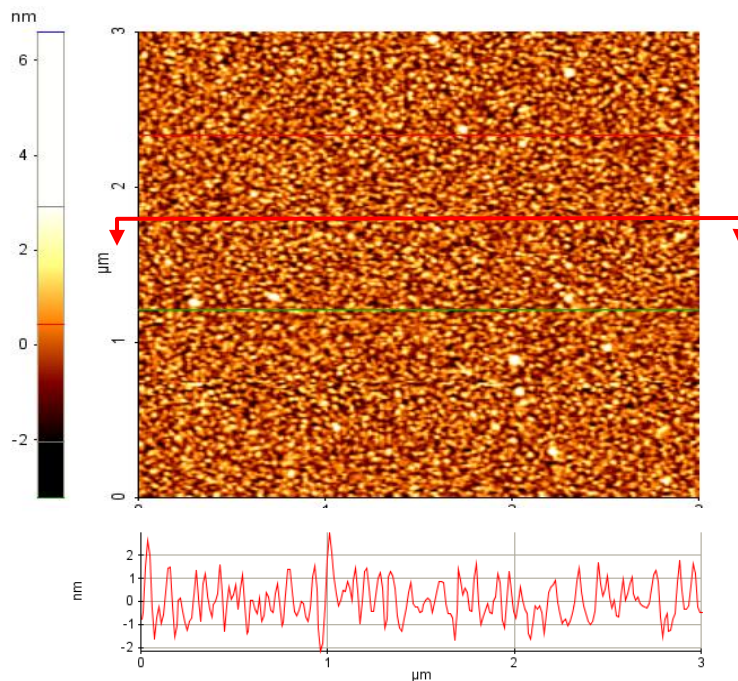


Figure 3.10 AFM analysis of the bare gold coated substrate.

The Au coated substrate was then incubated in  $4.5 \times 10^{-4} \text{M}$  mixture of biotin terminated thiol and the hydroxyl terminated thiol dissolved in ethanol for 4 days at room temperature. The mass ratio between the biotin-thiol, and hydroxyl-thiol was 1:4. The final step involved washing the prepared substrate with ethanol, milliQ water, and phosphate buffer saline (PBS) at pH 7.4.

### 3.4.3 Adsorption of the ordered bR monolayer

The thiol-coated substrate was incubated in 1 ml of 0.25 mg/ml streptavidin in PBS at pH 7.4 for 30 minutes at room temperature. The surface was then washed thoroughly with PBS at pH 7.4. Finally the streptavidin covered substrate was incubated in the biotinylated bR for 60 minutes at room temperature. The basic structure of the bR-biotin-

streptavidin-biotin-thiol-Au after the labelled immobilization process is illustrated in Figure 3.11.

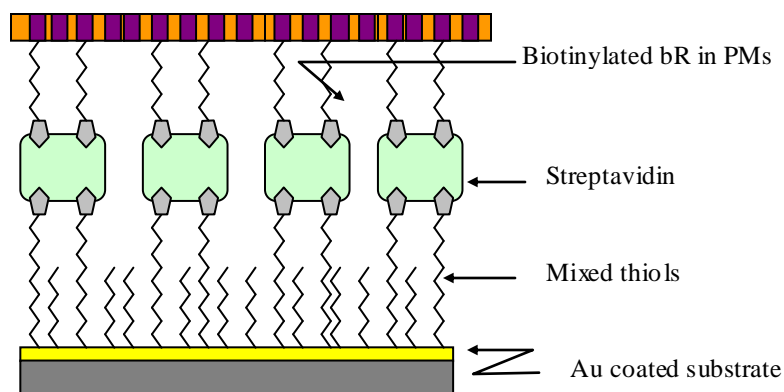


Figure 3.11 The simplified structure of the self-assembled bR-biotin-streptavidin-biotin-thiol-Au film.

### 3.5 Concluding Remarks

The bacteriorhodopsin proton pumps are produced in the laboratory by reducing the oxygen level in the growth media and providing continuous supply of the light beam. The *Halobacterium salinarum* cells compensate the shortage in the oxygen levels by creating natural proton pumps in the cell walls. These proton pumps generate pH gradients for providing the necessary energy for synthesizing adenosine triphosphate (ATP) from adenosine diphosphate (ADP) which is required for the bacterial cell activities. Upon reaching the cells maturity, walls of the *Halobacterium salinarum* cells are broken and bR proton pumps are selectively extracted and purified.

The fabrication of molecularly organized bR monolayer based on the molecular recognition and self-assembly impacts the system performance as it mimics the ideal bR organization in cell walls of the *Halobacterium salinarum* living organism. In this structure the extracellular side of the PM would face one direction. Several methods for organizing bR have been discussed in this chapter, including EFS, LB, LBL, and self-assembled bR monolayer. The use of self-assembly way in organizing the bR can generate a height degree of organizing without losing the photo-activity. The bR

monolayer produced by using biotin labelling to permanently label the extracellular side of bR and assembling in it on bio-functionalized Au-substrate using streptavidin protein enables the formation of consistent and vectorially oriented bR monolayer. The self-assembled bR monolayer is used for fabricating the dry bR based photoelectric chip and the photoelectrochemical chip.



## CHAPTER 4

# PHOTOELECTRIC CHARACTERISTICS OF A SELF-ASSEMBLED BR MONOLAYER

### 4.1 Introduction

The photoelectric films are the first step towards the absolute optically driven hydrogels as they convert solar radiation or the photon energy inherent in a focused light beam into electric form of the energy. The sole component of the created film is the light activated organic material harvested from the *Halobacterium salinarium* microorganism called bacteriorhodopsin (bR) proton pump in purple membranes, Figure 4.1, as described in Chapter 3. When exposed to visible light, each bR molecule acts as a simple proton pump which transports hydrogen ions from the cytoplasmic to the extracellular side through a transmembrane ion channel that connects both sides of the membrane. The crystalline structure is the basis of the bR material's chemical and thermal stability. The PM has been shown to be stable for several years while being exposed to prolonged periods of sunlight. The PM even preserves its photochemical and photoelectric activity under dry conditions, and can withstand relatively high temperatures of up to 140°C. Moreover, the bR purple membranes continue to function as a proton pump under very harsh chemical conditions such as extreme acidic and alkaline environments that are often considered corrosive for semiconductor technology (Hampp, 2000).

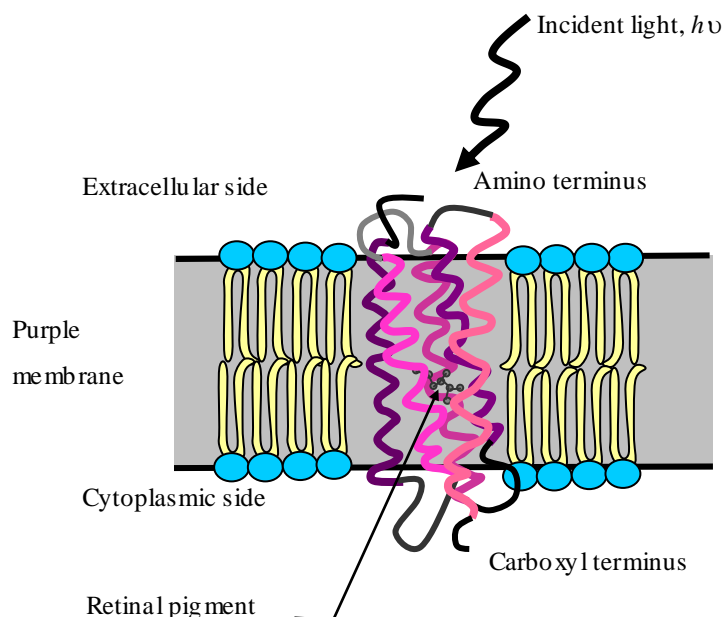


Figure 4.1 Basic structure of bacteriorhodopsin purple membrane patches. A bR monomer penetrates through the membrane where its carboxyl terminus is located inside of the cell and the amino terminus is located outside of the cell. (Al-Arife *et al.*, 2011)

Over the past two decades researchers have exploited the proton transfer mechanisms of bacteriorhodopsin PMs to develop a variety of engineered photoelectronic and microelectromechanical systems (Wang *et al.*, 2008; Lensu *et al.*, 2004; Roy *et al.*, 2010; Al-Arife *et al.*, 2010). The light responsive behaviour has been used to create novel bioelectronic imaging arrays (Wang *et al.*, 2008) and color sensors (Lensu *et al.*, 2004). As well, bR coated microcavities have been recently introduced as a mechanism for developing all-optical switches (Roy *et al.*, 2010). The bacteriorhodopsin based photoelectric structures can also be used to induce volumetric phase transitions in pH sensitive polymer gels. The flow of ions from the photon activated bR changes the pH value of the ionic solution that surrounds the hydrogel actuator or microvalve (Al-Arife *et al.*, 2010). The chargeable polymeric network undergoes a measurable geometric change when the pH of the ionic solution is shifted to the phase transition point  $pK_a$  (Li *et al.*, 2002).

From the perspective of MEMS and microfluidic system design, all of these light responsive devices require the bR to be properly immobilized on the surface of an electrode in order for the PM to act as a directional proton pump. The measured photoelectric signal from each cell electrodes is the combined response of numerous PM proton pumps. Unfortunately, a thin film fabrication technique that produces PM patches with a mixture of both cytoplasmic and extracellular sides being adsorbed on the same electrode will result in a significantly weakened photoelectric response. In other words, the resultant signal arising from two bR pumps with opposite orientation is zero (Schranz *et al.*, 2007). Consistent orientation of the PM patches on the electrode surface is, therefore, necessary for efficient photon to ion flow and charge separation.

## **4.2 Phototransduction Process in Dried bR Films**

The fabrication methodology can deeply influence the molecular architecture of the bR based photocell, and thereby affects the photocell performance. The differences in the cells performances can also be noticed with the small differences in the fabrication methods. Therefore, the influence of the photosensitive cells preparation conditions on the phototransduction process need to be described.

### **4.2.1 Role of water molecules in proton pumping process**

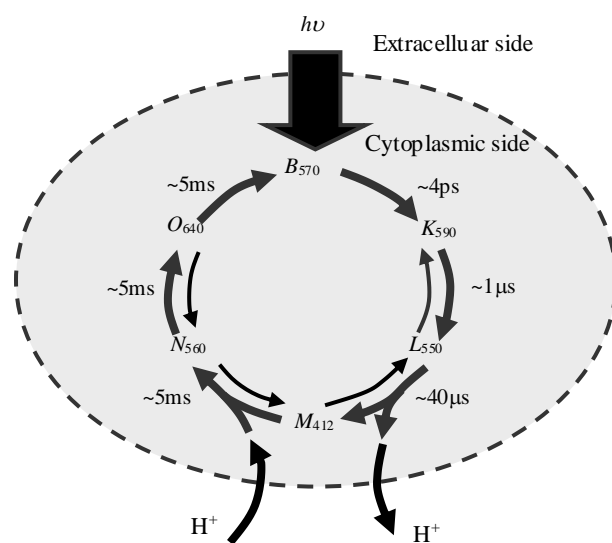
The published studies concluded that the fundamental function of bR depends on the in part on the presence of several water molecules in the proton transfer channel (Murata *et al.*, 2000). The water molecules located between the Schiff base and the key amino acid residues have a critical role in forming a hydrogen-bonding network that constitutes the proton translocation pathway, and in keeping the protonated Schiff base structure stable.

The water molecule that is located between the Schiff base and Asp 96 is considered to be indispensable for the protonation of the Schiff base. However the unprotonated state of the Schiff base is an energetically favourable structure. So that, the transfer of the proton from the Schiff base occurs spontaneously, no matter of whether a water molecule is available.

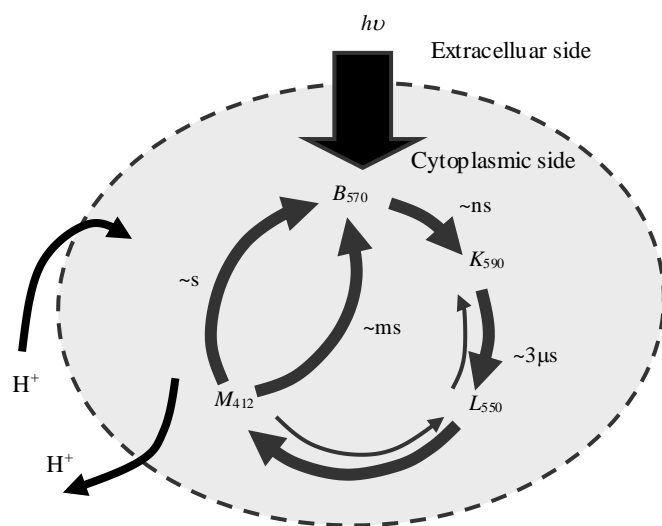
### 4.2.2 Dehydration effects on photochemical cycle and proton pumping

Several studies have shown that the kinetics of the bR photocycle is influenced by the level of humidity (Korenstein and Hess, 1977; Váró, 1981). The photocycle and proton pumping activity are fundamentally different from the wet bR photocycle and pumping activity due to the change in the degree of humidity (Cao *et al.*, 1991; Groma *et al.*, 2001). In the aqueous bR based film, each bR molecule acts as a light driven proton pump. When exposed to light each bR enables its retinal protein to undergo in photoisomerization from all-*trans* and 13-*cis*, followed by proton pumping from the cytoplasmic to the extracellular side of the cell membrane. Figure 4.2 (a) provides the fundamental photocycle of bR, where the proton pumping is initiated with the release of a proton in the  $L \rightarrow M$  intermediate transition and finished with the proton uptake in the following  $M \rightarrow N$  transition during the photocycle (Edman *et al.*, 1999).

On the other hand, the dry bR film acts fundamentally different from the aqueous bR based cells. It was noticed that, when the medium humidity in the bR film becomes less than 90%, the *N* intermediate is no longer observable, the basic intermediates are accelerated, and less protons pumped across the protein (Ganea *et al.*, 1997). The last intermediate of the dried bR photocycle is the *M* state, and then the Schiff-base is reprotonated. Coupling of the conformational changes of all of the intermediates are hindered in the dry bR; this disables switching the accessibility of the Schiff-base the extracellular to the cytoplasmic side and proton pumping does not take place (Ganea *et al.*, 1997). When exposing the dry bR to a nanosecond laser pulse, the photocycle becomes slower and the protein returns to its ground state in different intermediates with noticed lifetimes, indicating different paths of the proton back to the Schiff-base (Váró and Lanyi, 1991). Figure 4.2 (b) provides a basic illustration of this process.



(a)



(b)

Figure 4.2 Fundamental photochemical cycles of bacteriorhodopsin, for (a) the aqueous phase, where the proton pumping starts with the release of a proton during the  $L \rightarrow M$  transition and finish with a proton uptake during the  $M \rightarrow N$  transition (Edman *et al.*, 1999) and (b) the dry bR, where only K, L and M intermediates are observable and no proton pumping across the protein membrane. (Al-Arife *et al.*, 2011)

### 4.3 Surface Coverage of the Substrate with Biotinylated bR

Ideally the proposed bR immobilization process would result in an ultra-thin layer of PM that covers the entire Au substrate. However, experimental observations confirm that monolayer fabrication methods do not produce a continuous uniform monolayer of closely arranged membranes (Schranz *et al.*, 2007; Horn and Steinem 2005). The sporadic distribution of PM fragments on the substrate may be the result of small electrostatic repulsive forces between the constituent fragments. These forces likely arise because individual fragments have a net negative charge above the purple membrane's isoelectric point (Hampp 2000; He *et al.*, 1999).

In this study the surface coverage on the substrate was examined by using a focused ion beam scanning electron microscopy (FIB-SEM) at the University of Western Ontario's *Nanofabrication Facility*. Figure 4.3 shows a photograph of the fabricated photoelectric film and it is clear from the image that the PM fragments (dark patches) cover significant, but not all, areas of the Au substrate. The mass density of the PM fragments deposited on the gold substrate was calculated by assuming the layer of purple membranes acted as a parallel plate capacitor (Horn and Steinem 2005) and found to be  $0.9467\text{ng/cm}^2$ . It is important to recognize that the substrate surface topology (ie. roughness), concentration of thiols, concentration of the streptavidin, and concentration of the biotinylated purple membranes all play a critical role in determining the final distribution of PMs on the gold substrate.

An important feature of the proposed fabrication technique is that very thin photosensitive "layers" can be deposited on the substrate. Direct experimental measurement of the photosensitive layer's thickness is difficult because the observed values are dependent on the precision and sensitivity of the instrument. Conventional techniques such as optical ellipsometry, reflectance spectroscopy, capacitance metrology, and atomic force microscopy (AFM) in contact mode can be used to measure the layer thickness but these measurements will be distorted due to poor lateral resolution (Casuso *et al.*, 2007) and the non-rigid structure of the purple membrane patches. Furthermore these instruments measure a small area (usually few square micrometers) and then compute value with the assumption that the whole surface has uniform properties.

However, the electrostatic nature of purple membranes allows the formation of gaps between fragments resulting in uneven coverage of the substrate.

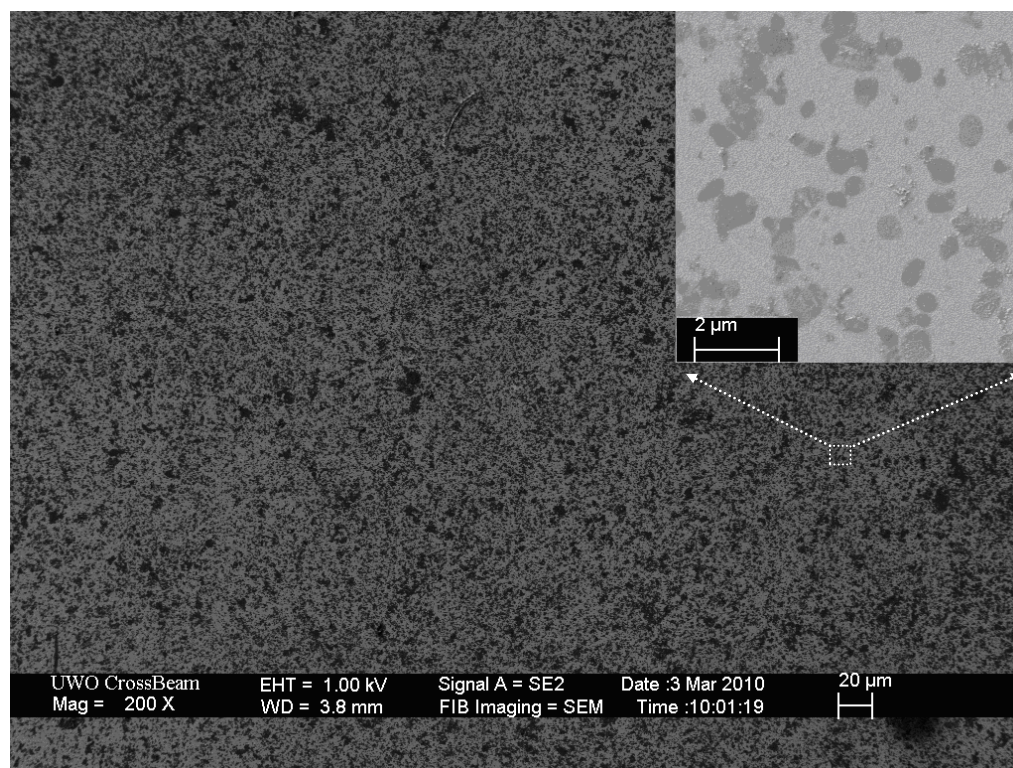


Figure 4.3 SEM photograph of the self-assembled ultra-thin bR film, with a magnification factor of 200. Enlarged area shown in upper right corner (taken in the Nanofabrication Facility, the University of Western Ontario)

The experimental photocell is comprised of a single self-assembled bR layer on the substrate. The entire photo responsive layer was fabricated under identical conditions and, therefore, it is reasonable to generalize measurements of a small window as being representative of the entire surface. The thickness of the bR-biotin-streptavidin-biotin-thiol-Au architecture was measured and characterized using an atomic force microscopy (AFM) in the “jumping mode” where individual scans, Figure 4.4, were made at randomly selected locations. The images and profile readings confirm that the immobilized dry thin bR monolayer exhibits an overall thickness between 12 to 12.33nm. Although the bR has not been deposited uniformly across the substrate surface, it does provide a significant amount of coverage at this thickness.

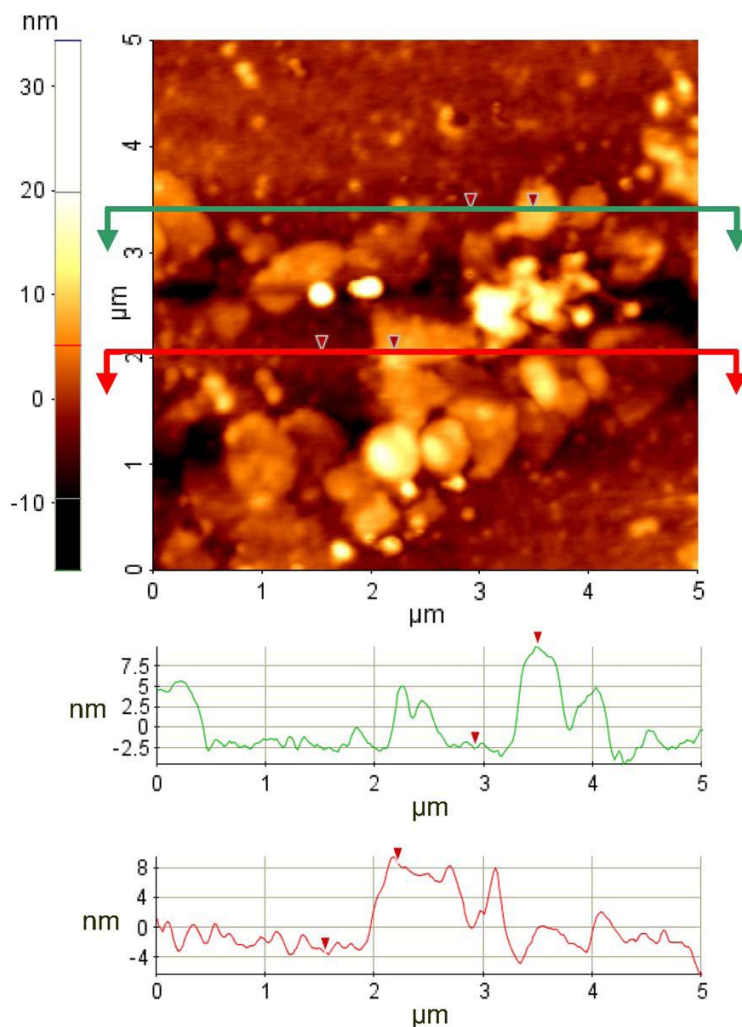


Figure 4.4 AFM analysis of the self-assembled ultra-thin bR layer. Two cross-sectional profiles are shown (taken in the Surface Science at the University of Western Ontario).

Since the dimensions of the constituent components of the self-assembled monolayer are known, it is also possible to theoretically compute the thickness of the photosensitive layer. The individual purple membranes have a thickness of 5 nm (Hampp 2000); the streptavidin is 5.8 nm thick (Gast *et al.*, 1999); and the biotinylated thiols form a 2.7 nm thick monolayer (Kossek 2009). Therefore, the overall thickness of the photosensitive layer in its aqueous phase is calculated to be around 13.5 nm. This theoretical analysis validates the AFM measurements. The small difference between the measured thicknesses of the dry bR and the calculated thickness of the aqueous bR is



believed to arise from the reduction in water content during the drying process of the actual bR film.

#### **4.4 Investigation of Photoelectric Response of the bR Monolayer**

The photoelectric response characteristics of the bR monolayer were measured under various exposure times to laser light pulses (fixed wavelength, variable intensity). For these measurements a photocell was created by placing the thin bR film between its Au substrate and an optically transparent indium tin oxide (ITO) contact glass plate. The Au and ITO surfaces act as microelectrodes to permit a closed electronic circuit to be formed.

##### **4.4.1 Experimental setup**

The photocell constructed from bacteriorhodopsin PMs can be modeled by a simple equivalent electronic circuit (Wang, *et al.*, 2005; Horn and Steinem 2005; Xu, 2003; Walczak *et al.*, 2008) as shown in Figure 4.5. The Photovoltage source ( $E_{ph}$ ) is formed by the light responsive bR monolayer. The total capacitance ( $C_t$ ) represents the combined affect of the chemical capacitance arising from the charge displacement process and the biological capacitance of the purple membranes. The total resistance is a result of the purple membrane resistance and the contact resistance between the bR monolayer and the electrodes. For this study, the space between the microelectrodes is determined by the physical flatness of the electrodes and the thickness of the bR monolayer architecture (approximately 12.33nm). An in-depth discussion about mathematically modeling the bR behavior and developing a more detailed electronic circuit model can be found in the work by Wang (Wang, 2006), Xue (Xue, 2003) and Wang *et al.* (Wang *et al.*, 2006).

Once the photoelectric cell was assembled, an 18mW, 568nm laser was used to provide a continuous source to the photocell, Figure 4.5. The 568nm light source was used in the experiments because the peak photo-excitation of bacteriorhodopsin occurs at this wavelength (Hampp 2000). The voltage differences were measured using an Agilent 34420A nano-volt/micro-ohm meter. The space between the microelectrodes is determined by the physical flatness of the electrodes and the thickness of the bR

monolayer architecture (approximately 12.33nm). No additional signal processing or amplification was performed in an effort minimize distortions to the experimental readings.

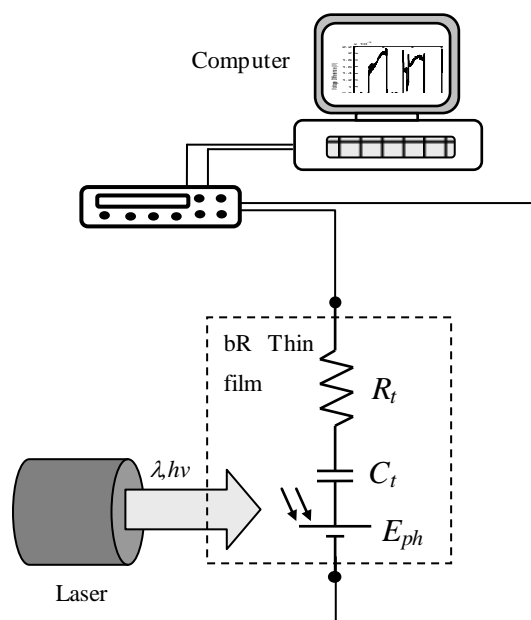


Figure 4.5 Experimental apparatus used to test the photoelectric properties of the photocell and equivalent electronic circuit for the light responsive bR thin layer. (Al-Arife *et al.*, 2011)

#### 4.4.2 Photovoltaic response of bR monolayer to continuous light illumination

Prior to testing the fabricated thin bR film, several simple controlled experiments were performed to investigate the photoelectric characteristics of the bare gold substrate, thiols adsorbed on gold, and the streptavidin built on the thiols layer. The experimental conditions for this preliminary test are identical to those to be used for activating the bR photocell. When exposed to an 18mW, 568nm laser source over a prolonged period of time the bare Au substrate exhibits random background noise in the range of -2.5 to 4.0 $\mu$ V as shown in Figure 4.6. Similar small-amplitude random photoelectric noise was recorded for both the thiols absorbed on Au and the streptavidin built on the thiols layer.

The results of these preliminary tests suggest that any measurable photovoltage is generated by the bR-biotin-streptavidin-biotin-thiol-Au architecture and, in large part, originates from the actions of the PM proton pumps.

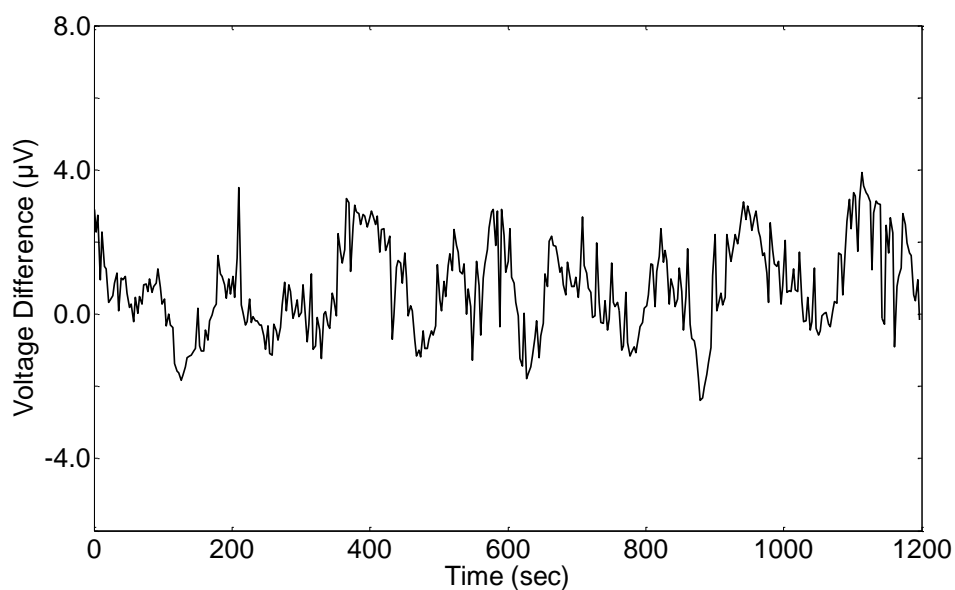


Figure 4.6 Small-amplitude random photoelectric response of the bare Au substrate.

The bR photocell is initially exposed to a series of six consecutive light pulses with varying time durations as shown in Figure 4.7. The light source is an 18mW, 568nm Melles Griot Argon Ion laser with a mechanical shutter. Under dark conditions with no external illumination, the bR thin film exhibits a measurable voltage difference across the electrodes in the range of 0.6 to 0.8mV. The small voltage recorded in the dark state confirms the existence of a difference in charge density between the cytoplasmic and extracellular sides of the bR purple membranes (He *et al.*, 1999; Alexiev *et al.*, 1994).

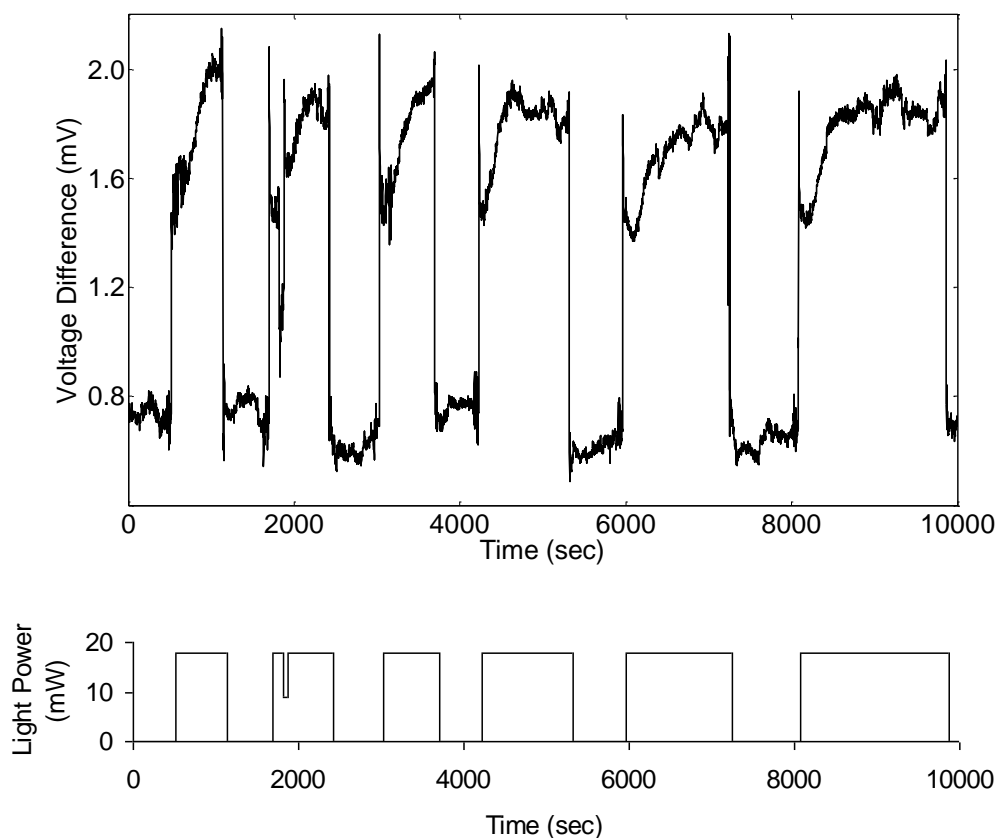


Figure 4.7 Measured voltage difference across the bR layer on a  $0.185\text{cm}^2$  substrate as a function of light exposure time. Six pulses with increased time durations of light exposure are shown.

When light first strikes the photoelectric device there is a rapid 1.4 mV instantaneous increase and subsequent 0.5 mV decrease in the potential across the photocell. The fast signal rise-time is due to the immediate charge separation and release that occurs in less than  $52\ \mu\text{s}$  (Vsevolodov, 1998). After the initial overshoot the signal slowly rises toward a steady state value between 1.8 to 2.1 mV. A rapid drop in the voltage is observed when the light source is turned off. An enlarged view of the photo-response of the bR film for the second light pulse with an intermediate intensity reduction is given in Figure 4.8.

The rapid rise-time and overshoot observed at the onset of the light pulse and subsequent undershoot after the light ceases supports the notion that reversible

mechanical deformations in the bR-protein within the elastic zone of the PM structure occur with the generation of the photo-voltage (Kuhlbrandt, 2000; Subramaniam and Henderson, 2000; Ferrand *et al.*, 1993). Specifically, these reversible deformations of the PM patches influence the surface contact characteristics between the cytoplasmic side of the bR patch and the ITO coated glass surface.

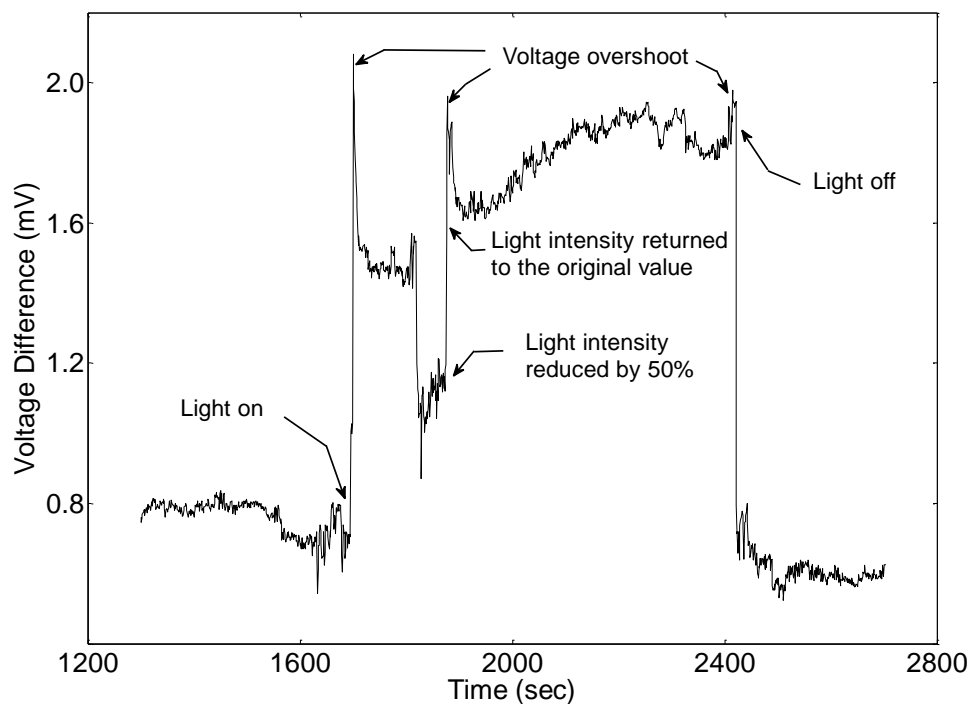


Figure 4.8 Enlarged view of the photocell response to the second light pulse. Illumination was intermittently reduced to 50% of intensity at 1800s.

The enlarged view of the sixth pulse, Figure 4.9, also illustrates the characteristic rapid overshoot, subsequent drop-off and relatively slow signal build-up to steady-state. The entire photo-voltage overshoot occurs within 1 to 3 seconds after the bR layer is first exposed to a step input from an 18 mW, 568 nm laser. Similarly, the drop-off in voltage once the light is removed also occurs within 1 to 3 seconds (Figure 4.7). The relatively slow rise to steady-state for constant illumination is observed for all input pulse widths.

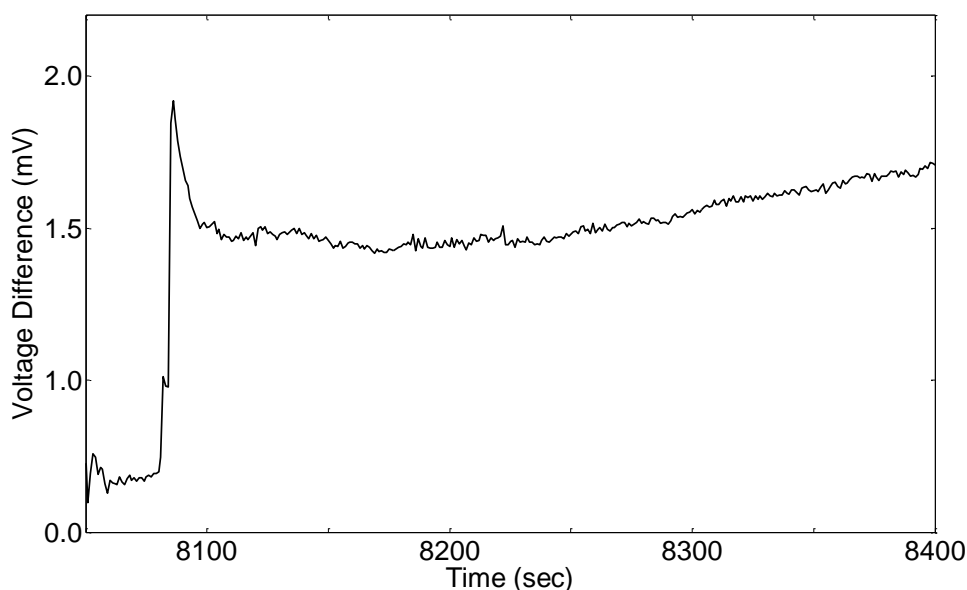


Figure 4.9 Enlarged view of the photocell response showing voltage buildup toward steady-state over the duration of the sixth light pulse in Figure 4.7.

#### 4.4.3 Photovoltaic response of bR monolayer to short light pulses

The photoelectric response of the bR photocell to shorter bursts of light is examined by exposing the device to a sequence of progressively longer light pulses ranging from 0.0625s to 30s as shown in Figure 4.10. Since the experiment does not use peripheral signal amplification circuitry, the results confirm that the maximum voltage difference generated by the photocell is directly dependant upon the light exposure time. Upon closer examination the experimental results show two distinct types of response behaviour, Figure 4.11, based on the width of the light pulse. The first type (Zone I) represents the relative nonlinear response of the photocell to short light pulses with exposure times of less than 4s. These correspond to light pulses a, b, c, d, e, and f in Figure 4.10, respectively. This nonlinear characteristic occurs because the experimental photocell did not reach final steady-state during the brief exposure to light. Light pulses shorter than 0.1s produced no discernable signal beyond the background noise in the system. In contrast, the second type (Zone II) exhibits a linear characteristic because the photocell had sufficient time to reach steady-state for exposure times greater than 4s. These correspond to light pulses g, h, i and j in Figure 4.10, respectively.

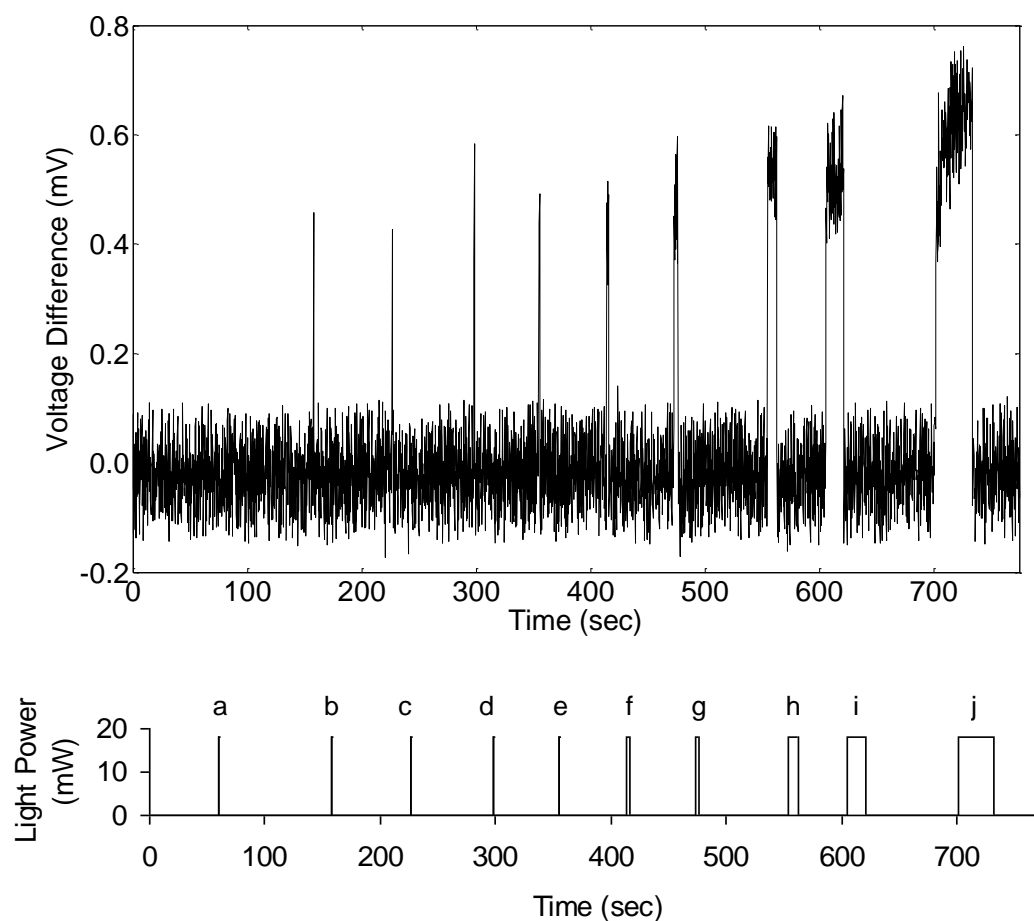
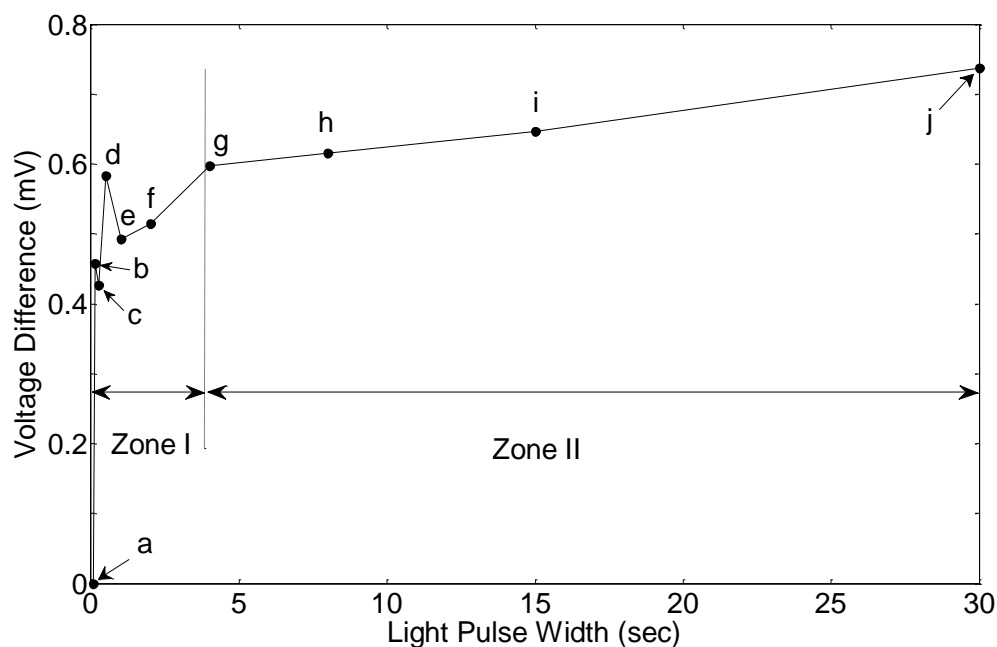


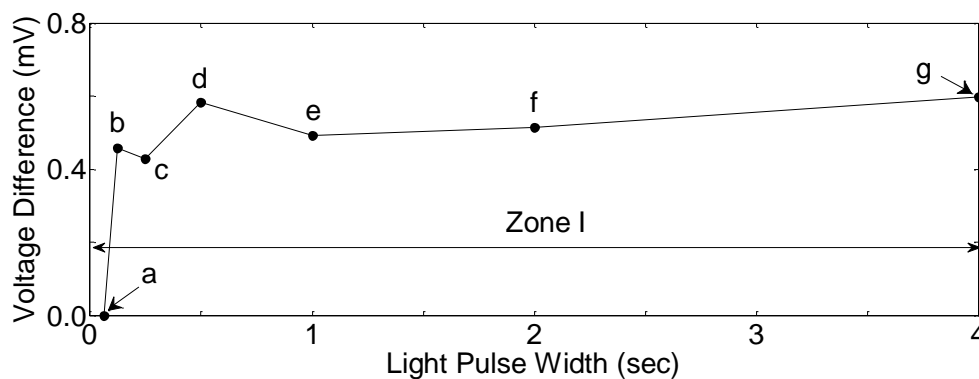
Figure 4.10 Measured voltage difference across the  $0.0925\text{cm}^2$  pixel for a sequence of varying input pulse widths (0.0625s, 0.125s, 0.25s, 0.5s, 1s, 2s, 4s, 8s, 15s, and 30s).

In general, microsystems are expected to detect a noise signal in addition to the system response. The noise signals that are associated with the photoelectric cells are expected to be originated from the photothermal effect as it is the dominating source of noise in the light exposed surfaces (Talgader, 2004; Mohd-Yasin *et al.*, 2010). Both the linear and the nonlinear response zones exhibit similar background noise that ranged from -0.1 to 0.1 mV. The characteristics of the detected background noise did not change significantly under varying light intensity or exposure durations. The amplitude of the noise exhibited by the final fabricated photocell was approximately 0.1 mV, which is larger than the  $4.0\mu\text{V}$  signal associated with the control experiments of the bare gold Au, thiols, and streptavidin structures. This difference in noise is not the result of changes in

illumination but rather the electrical properties of the self-assembled bR monolayer. The bR purple membranes are electrically characterized with the asymmetric charge density between the cytoplasmic and the extracellular sides of the bR purple membranes. In general, the overall steady-state signal-to-noise ratio of photocell is around 21 (2.1mV/0.1mV). The observed fluctuations are considered to be background noise.



(a) Maximum voltage difference for pulses in Figure 4.10.



(b) Enlarged view of zone I (0.0 – 4s)

Figure 4.11 Relationship between the width of the light pulse and maximum voltage difference generated by the bR photocell.



The influence of light intensity on the photocell's response is also investigated by varying the light power of the source from 0-100% as shown in Figure 4.12. Previously published research performed at the University of Western Ontario (Wang *et al.*, 2004) showed that there is a near linear relationship between input light intensity and the photo-voltage response of a bR film. However, these results were observed for a thicker (approx. 30 $\mu$ m) dry bR film fabricated using the EFS immobilization method. The nonlinearity observed in the current study may reflect the differences in charge density of the highly oriented PMs embedded in the ultra-thin monolayer and the less uniformly oriented, and stacked, PMs in the thicker EFS formed layer.

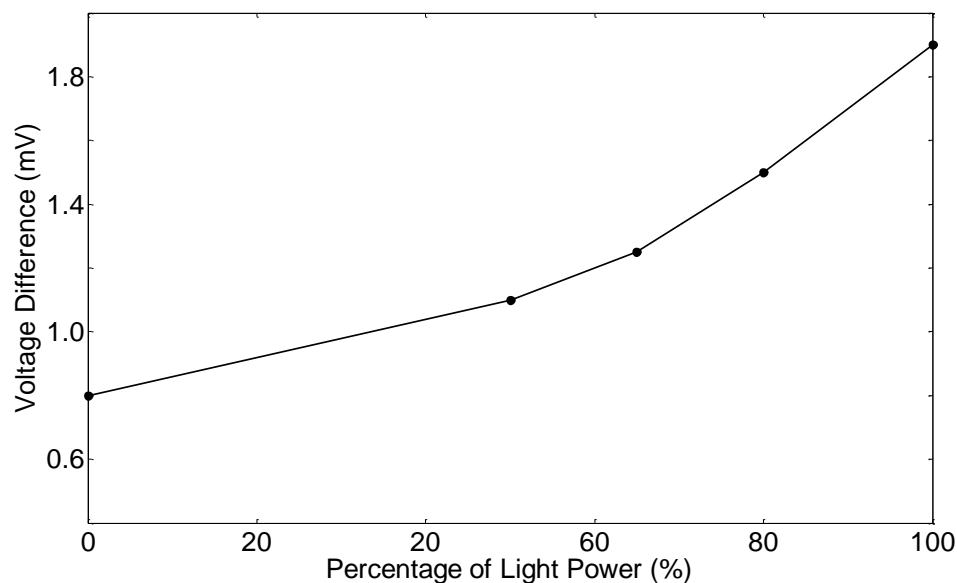


Figure 4.12 Relationship between light intensity and bR photocell response.

#### 4.4.4 Discussion

A self-assembled photoelectric monolayer that functions as a proton pump when exposed to external light has been investigated. The biotin molecular recognition technique was used to label the extracellular side of the bR purple membranes and enable the oriented proton pumps to be efficiently coupled to the streptavidin molecules on the bio-functionalized gold substrate. The thickness of this monolayer was less than  $\sim 12.33/10000$  (1/811) of the thinnest film fabricated using more classical methods such as the electric field sedimentation (EFS) technique. In other words, this method of

orienting and assembling PM patches significantly reduced the amount of bacteriorhodopin needed to cover the same surface area.

Once built on the Au substrate, a functional photocell was created by placing an optically transparent indium tin oxide (ITO) contact glass plate on the ultra thin dry film. The photocell was tested under controlled conditions and found to generate reliable and repeatable photo-voltage signals in the mV range. The temporal response characteristics of the experimental device were similar to that reported in the literature for other bR-based sensors (Wang, 2006; Hong, 2007; Marx, 2007). Several researchers have exploited the rapid rise and initial overshoot behaviour of dry bR film to create light detectors that provide a differential response to a high frequency light pulse train (Wang *et al.*, 2005; Wang, 2006; Hong, 2007; Marx, 2007).

The experimental observations also supported the notion that the PM fragments for a very thin dry bR film will preserve the proton pump ion transport mechanism which had been previously reported in the literature for biotin-streptavidin-bR adsorbed on lipid (Chen *et al.*, 2003) and the aqueous biotin-streptavidin-bR architecture (Ren *et al.*, 2006). Furthermore, the ultra thin monolayer structure does not negatively affect the photoelectric functionality of the dry bR molecules during its photo-cycle.

The relationship between input light intensity and photocell response was also demonstrated (Figure 4.12). The experimental results show a higher degree of nonlinearity than previously published studies (Wang *et al.*, 2004). This observation may reflect the differences in surface charge density for the ultra thin bR film described in this paper and the thicker films created using other immobilization methods. Thicker films contain a larger number of PM patches which are nonspecifically stacked on each other and, often, the resulted contact surface of the film with each electrode contains a mixture of extracellular and cytoplasmic sides of the PM patches. Overlapping PM patches with non-uniform orientation of their constituent bR molecules may cause ions to become trapped inside the film between the stacked monolayers.

## 4.5 Concluding Remarks

The photoelectric analysis and characterization of the dry bR has been experimentally provided in this chapter. The chapter introduced the fabrication methodology for producing ultra-thin bR photoelectric layer, and detailed characterization of the fabricated photosensitive layer. The self-assembled monolayer of oriented bacteriorhodopsin (bR) purple membranes was created on a biofunctionalized gold surface using a biotin molecular recognition technique. The biotin enabled the extracellular side of the bR purple membranes to be precisely labelled. The density of purple membranes on the thin layer ( $\sim 12.33\text{nm}$ ) was experimentally determined to be  $0.9467\text{ng/cm}^2$ . Once fabricated an optically transparent ITO was placed on top of the finished molecular assembly of the bR photocell for experimental testing and performance verification. The experimental investigation of the photocell demonstrated that a  $12.33\text{nm}$  thick bR layer could generate nearly  $0.54\text{mV}/(\text{mW}\cdot\text{cm}^2)$  when exposed to an  $18\text{mW}$ ,  $568\text{nm}$  laser source.

## CHAPTER 5

# PH-GRADIENTS GENERATED BY SELF-ASSEMBLED BR PROTON PUMPS

### 5.1 Introduction

Monitoring and regulating the pH of solutions is an important step in controlling the pH sensitive hydrogel as the phase transition of the hydrogels takes place at specific point of the energy scale and indicated by  $pK_a$ , and pH of the surrounding electrolyte. However due to its importance, the precise control and regulation of pH plays an essential activating variety of biological and chemical processes on Lab-on-a-Chip (LOC) devices and micro-Total Analysis Systems ( $\mu$ -TAS). Externally modifying the pH of a target solution can drive a variety of electro-chemical processes necessary to identify unique proteins, move molecules, and exchange ions between solutions. The microscale control of pH has enabled new methods to be developed for on-chip protein identification, the transfer of large molecules (Suzurikawa *et al.*, 2010), and ion exchange chromatography (Pabst *et al.*, 2008). Other LOC applications that depend on generated pH gradients are the fractionation, separation, and assembly of biologically based molecules such as the human salivary proteins and the collagen bundles (Cheng *et al.*, 2008). From an engineering perspective of this chapter, manipulating the pH of a solution in a microchannel, or reservoir, provides a mechanism for activating and controlling an ionic hydrogel microactuator, or the colour of a phenolphthalein indicator dye for visually monitoring acidity changes in sample solutions (Al-Arife *et al.*, 2010).

In recent years, a number of researchers have developed "on-chip" pH gradient generators for a variety of applications. May and Hillier (May and Hillier 2005) proposed an electrically driven pH gradient generator in 2005. The microscale generator consisted of two electrodes made from a glass substrate covered by an indium-tin oxide layer coated with a platinum catalyst layer. An electric field is then applied to generate a potential gradient in an ionizable solution. The resultant electrical potential induces water

oxidation at different rates along the electrode's surface. The strength of the electric field determines the final pH of the solution.

Suzurikawa *et al* (Suzurikawa *et al.*, 2010) introduced an on-chip electrically powered pH gradient generator activated by two photoconductive electrodes. Each electrode was constructed from three laminated layers on a glass substrate. The laminated layers include a fluorine-doped SnO<sub>2</sub> (F:SnO<sub>2</sub>) layer, an a-Si:H photoconductive layer, and a zinc antimonate (ZnO/Sb<sub>2</sub>O<sub>5</sub>)-dispersed epoxy passivation layer with low conductivity. The photoconductive planar electrode generates a conducting point, which acts as either a photo-anode or cathode, when exposed to an electric field and illuminated by a 1000mW/cm<sup>2</sup> light source. At these conducting points, the electrical field generates hydroxide ions that produce the observed pH gradients. Although this technique leads to rapid generation of pH gradients, the system requires a strong light source and an external electric field to create the local anode or cathode at the conducting points of contact. Both the high intensity light and the external electric field can negatively affect biological samples for some medical applications.

The controlled generation of pH gradients in a solution has also been used as the method for assembling functional membranes in microfluidic devices. Mass transport control for filtration, microdialysis, extraction and gas-liquid exchange in micro-systems can be achieved by integrated membranes (Luo *et al.*, 2010). *In situ* fabrication methods such as photo-polymerization and thermo-gelation have been developed for creating porous structures in microchannels however these techniques can leave residues that are toxic to biological processes. In this context, Luo *et al* (Luo *et al.*, 2010) proposed using *in situ* generated pH gradients to fabricate semi-impermeable chitosan membranes. Rather than using high electric fields that can be problematic for the fabrication of chitosan membranes, the authors chose to exploit a freestanding hydrophilic membrane structure that enabled pH gradients to be generated at the converging interface between a slightly acidic chitosan solution and a slightly basic buffer solution. A simple pumping strategy was then used to create a stable and localized pH gradient. The resultant biofabricated chitosan membranes were experimentally determined to be uniform and permeable to aqueous solutions. The study illustrates that controlling the local pH gradient plays an important role microfluidic device fabrication and operation.

A low-power optically driven pH gradient generator provides an alternative non-invasive mechanism for modifying the target solution's acidity without inducing strong electric fields near the solution or exposing the solution to high intensity illumination and heat. Eroglu *et al* (Eroglu *et al.*, 1994) described a simple biologically-inspired pH gradient generator based on a light-harvesting protein naturally found in the plasma membrane of *Halobacterium salinarium*. In its natural state the bacteriorhodopsin (bR) molecules are carrier proteins that use the sun's energy to transport hydrogen ions from the cytoplasmic to the extracellular side through a transmembrane ion channel that connects both sides of the Archaeobacteria's cell membrane. This early work (Eroglu *et al.*, 1994) showed that light could be used to drive a pH gradient generator. The authors also identified several limitations that occur because of the random orientation of the proton pumps. The directional orientation becomes a critical factor in utilizing biological materials for efficiently pumping H<sup>+</sup> ions in microfluidic channels.

The fabrication procedure for creating a biologically inspired light driven transducer that generates measureable pH gradients in minute quantities of ionic solutions is introduced in this paper. The microscale planar transducer converts an optical signal into a flow of hydrogen ions from a reservoir to a target solution. The transducer or pH-gradient generator, Figure 5.1, exploits the molecular proton pumps found in the purple membranes (PM) of wild type bacteriorhodopsin (bR). The transducer structure is an ultrathin layer of oriented PM patches self-assembled on an Au-coated porous anodic alumina (PAA) substrate. A biotin labelling and streptavidin molecular recognition technique is used to attach uniformly oriented PM patches to the porous substrate and ensure the efficient transport of ions across the transducer surface. The photo-induced proton pumps embedded in the bio-functionalized porous substrate produce a flow of ions that generate a measureable  $\Delta\text{pH}$  proportional to the active surface area and light intensity.

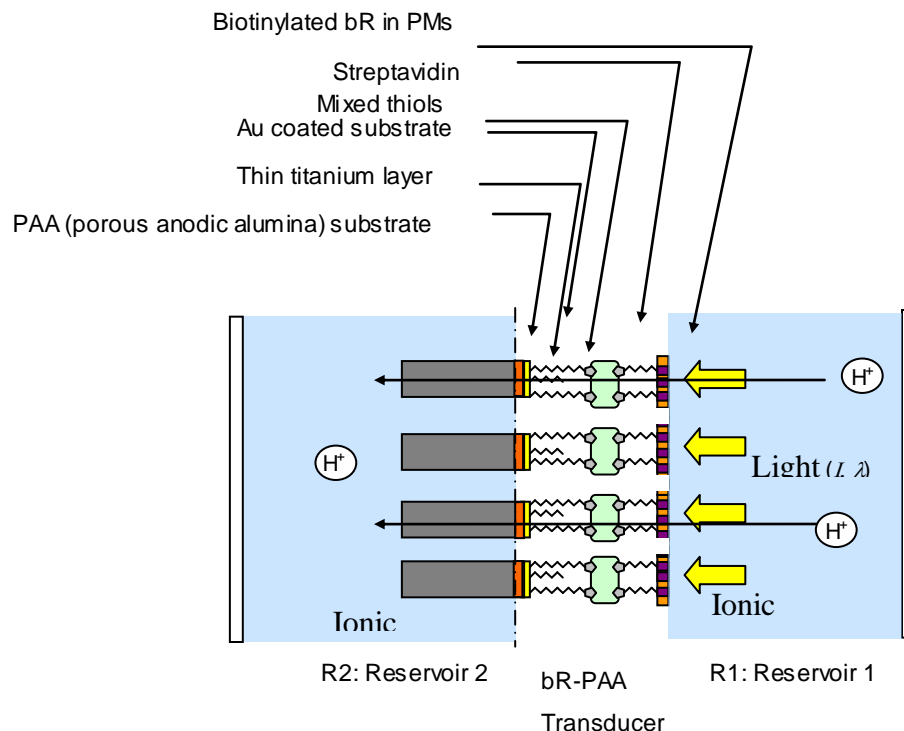


Figure 5.1 Layered structure of an optically driven pH gradient generator used to transport hydrogen ions ( $H^+$ ) between two adjacent ionic solutions separated by a porous substrate.

The functional mechanism for the light activated bR PM proton pumps is described in the following section. The discussion focuses on how the PM patches in the original archaebacteria transport ions across the cell membrane structure. The fabrication method used to orientate and immobilize the extracted bR PM patches on the gold coated porous substrate is summarized in Section 5.3. The materials used are identified and procedural steps are described in detail. Experimental tests used to verify the functional performance of the proposed optically driven pH gradient generator are presented in Section 5.4. A mathematical model of the relationship between the illumination characteristics and target solution's  $\Delta pH$  is developed and verified. Furthermore, a simple experiment is presented to demonstrate how the photon responsive transducer generates a sufficient  $\Delta pH$  to cause a phenolphthalein indicator dye to change colour. Finally, conclusions and directions for future work are summarized in Section 5.5.

## 5.2 The Approach

### 5.2.1 Embedded bR proton pumps

Over the past several decades a number of researchers have attempted to exploit bR proton pumps to change the pH of a target solution. In the late 1970's Ort *et al.*, (1978, 1979) showed that bR molecules can alter the volume of a surrounding fluid when exposed to light. Even though these tests involved non-oriented and randomly distributed PM patches, the experimental results provided clear evidence that the bR proton pumps would maintain their primary function when removed from the living organism. The measured change in volume further supported the notion that the bR pumping activity was the main mechanism for transporting hydrogen ions across the cell membrane and the experimentally observed gradient was not the result of charge translocation or charge transfer through the surrounding conductive medium.

To closer explore this pumping phenomena, Eroglu *et al.*, (1994) immobilized bR material in a 4mm thick polyacrylamide gel membrane using the Electric Field Sedimentation (EFS) technique. The functionality of the modified gel membrane was tested by pumping protons between two liquid filled compartments. Rather than demonstrating the directional pumping of protons from one compartment to the other, the recorded measurements showed a similar simultaneous change in pH of the adjacent compartments. Although this behaviour appeared to contradict the leading hypothesis of the time, the authors explained the results by suggesting an unknown surface phenomenon was acting on the bR-gel membrane. Further studies suggested that the unpredicted response observed by Eroglu *et al* (1994) may have been due to the EFS technique used to immobilize the bR in the gel. The EFS method is non-specific as to how it adsorbs bR pumps on the positive electrode thereby both sides of the bR can become negatively charged with only slight differences being observed (He *et al.*, 1999).

The notion of a light activated membrane for pumping protons between two ionic solutions has been revived in recent years. Lee *et al.*, (2006) used chemical treatment protocols to modify the electrostatic characteristics of bR protein surfaces in an effort to enhance the monolayer surface connect ability to polymeric planar membranes and



vesicles. The key step in their chemical treatment process is the extraction of each bR molecule from its biological membrane and exposing its surfaces to a sequence of pH changes between acidic and basic solutions. Experimental tests on planar bR-gel sheets made by inserting the chemically treated bR in the polymeric membrane showed an absolute  $\Delta\text{pH}$  of 0.1986. The actual response amplitude of bR molecules embedded in the polymeric membrane, however, was much lower than the estimated values. The authors attributed the decrease in efficiency to the chemical protocols used and the possible molecular shielding effect because the transmembrane channels that connect the cytoplasmic side to the extracellular side would become partially blocked (Lee *et al.*, 2006).

### **5.2.2 Self-assembled proton pumps on a porous substrate**

An alternative approach to generating microscale pH gradients using light activated bR proton pumps is introduced in this research. Rather than immobilizing the bR molecules in a polymer gel membrane, the bR PM patches are adsorbed onto a porous anodic aluminum oxide substrate. In this fabrication method an ultrathin layer (~13nm) of oriented PM patches is self-assembled on an Au-coated porous anodic aluminum oxide substrate. The self-assembled monolayer of oriented purple membrane patches from bR is created on a bio-functionalized gold (Au) surface using a biotin labelling and streptavidin molecular recognition technique (Al-Arife *et al.*, 2011). The biotin enables the extracellular side of the bR purple membranes to be accurately labelled and properly oriented to permit the efficient transport of ions in only one direction across the transducer layer.

During the biochemical immobilization process, the biotinylated alkylthiols modify the Au surface using HS- terminals of the thiols and affixes the labelled bR to the functionalized surface using streptavidin-biotin interactions. One of the most reliable methods to build self assembled monolayers is activating the substrate with biotinylated thiols. The thiols are chemical chains that have HS terminal which is characterized with its high affinity to gold, and another terminal that can be permanently activated with biotin. The self-assembly of the labelled bR-proteins on the thiol monolayer is accomplished by a streptavidin molecular recognition and binding capabilities. The biotin

activation of the thiol layer makes the adsorption of the biotinylated bR proton pumps possible by using a streptavidin matrix.

### **5.3 Fabrication of Experimental Analysis**

#### **5.3.1 Preparation of the bio-functionalized porous substrate**

Prior to fabricating the bR monolayer it is necessary to coat the 0.2cm<sup>2</sup> porous anodic aluminum (PAA) substrate with a 3nm layer of titanium and a 22nm layer of gold (Au). The titanium provides a permanent adhesive link between the PAA substrate and Au layer. Gold surfaces are characterized with their high affinity for thiols adsorption thereby enabling permanent bonds to be formed between the HS terminal of the thiols and the Au surface.

Before adsorbing the biotin terminated thiols and the hydroxyl thiols on the substrate, the Au coated substrate was first cleaned for less than 5 seconds with concentrated 'Piranha' solution (70 vol.%H<sub>2</sub>SO<sub>4</sub>, 30 vol.%H<sub>2</sub>O<sub>2</sub>) and rinsed with milliQ water, and then rinsed with pure ethanol. Following the cleaning step, the Au coated substrate is incubated in 0.7mM mixture of biotin terminated thiols and hydroxyl terminated thiols in pure ethanol for 7 days at room temperature in glass tubes in dark room. The used ethanol is first degassed by bubbling nitrogen for 20minutes. The thiols mixture is prepared by adding 100µl of 10mg/ml biotin thiols dissolved in pure ethanol to 400µl of 10mg/ml hydroxyl thiols dissolved in pure ethanol. The formed mixture is diluted by adding 4ml of pure ethanol. The resulted mixture is then sonicated in iced bath for 3-5 minutes until the mixture became homogenous. The final step involves washing the activated substrate with ethanol, milliQ water, and phosphate buffer saline (PBS) at pH 7.4.

#### **5.3.2 Fabrication of the Polydimethylsiloxane (PDMS) microfluidic chip**

The polydimethylsiloxane (PDMS) microfluidic chip that contains the photosensitive chip is first created using a SU-8 micromold. The key steps involved fabricating the test chip (Figure 5.2) involve: creating a photomask, spin coating SU-8 photoresist,

polymerizing the SU-8 mold, and stamping the mold with PDMS to cast the final part in PDMS. Micromolds created from thick photoresists, such as SU-8, enable micro-features with high resolutions to be produced without the need for wet etching. Chemical etching on glass substrates is an expensive process that requires the use of environmentally harmful chemicals such as hydrofluoric acid and nitric acid (Abgrall and Gue 2007; Mourzina *et al.*, 2005)

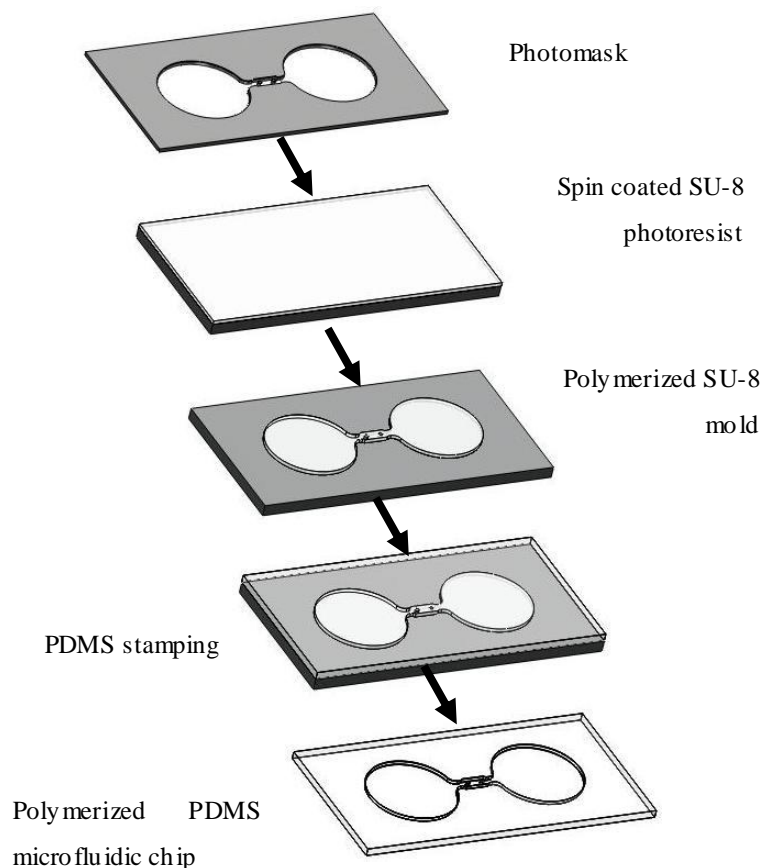


Figure 5.2 Sequence of steps used to fabricate a PDMS microfluidic chip.

For this application, the SU-8 mold for the microfluidic device is created by initially soaking a glass substrate in 20% HCl for two hours and then rinsing it with de-ionized water. Once the glass substrate is dried on a 200°C hot plate for at least 15min it is coated with a thin film of the negative photoresist SU-8 2050. A film thickness of 100µm is achieved by spinning the coated substrate at 500rpm for 5s and then at

1700rpm for 30s. The formed photoresist film is then baked at 65°C on a hotplate for 5min, followed by further heating at 95°C for 30min. The process of baking and cooling the photoresist must be gradual to avoid creating large temperature gradients across the film which cause local stresses that influence surface roughness and introduce cracks. Thermal stresses can also cause the premature separation of the mold from the substrate. Based on experiments it is recommended that the temperature be ramped up in 2-3°C/min increments.

Once completed, the photoresist is exposed to light for 36s. This time exposure is provided in three doses of 12s each, and 1 min rests between doses to avoid overheating. The photoresist coated substrate is baked again for 5min at 65°C and 15min at 95°C. The photoresist is then developed in a SU-8 developer, rinsed with isopropanol for 10s, and dried with compressed nitrogen. Finally, the formed micro mold was hard baked on the hot plate at 200°C for 20min. This last step in the process anneals the mold and prevents surface cracks from forming.

The polymer replicated part is produced from the SU-8 micromold using a PDMS molding process. To complete this step a Sylgard 184 (Dow Corning) kit is mixed and de-gassed using a vacuum desiccators. The PDMS mixture is then poured on the SU-8 mold in a Petri dish, and exposed to a vacuum in order to remove air bubbles trapped at the interface of SU-8 and PDMS. The polymerization process is accelerated by applying homogeneous heating in an incubator at 80°C for 120 minutes. The formed PDMS microchannel, Figure 5.3 is cooled to room temperature, and soaked in acetone for 30min to reduce the adhesion between SU-8 mold and PDMS structure. The PDMS is then gently peeled off in acetone. This last step is very important, especially for designs that have very small features. Before using the PDMS it is very important to convert its surface from the hydrophobic to the hydrophilic nature. Most of the published literature on the nature of the PDMS surfaces indicates that, the surface is made up of repeated -O-Si(CH<sub>3</sub>)<sub>2</sub> groups. When exposed to the oxygen plasma, these groups developed silanol groups (OH) at the expense of methyl groups (CH<sub>3</sub>). The increase in the (OH) concentration in the surface leads to forming stronger intermolecular bonds because the (OH) groups are naturally polar, so that they make the surface highly hydrophilic (Bhattacharya *et al.*, 2005). Practically, the PDMS microchannel is treated with oxygen

plasma in STS Reactive Ion Etch System for 30 seconds to make the channel surface hydrophilic. Once this step has been completed the device is placed in de-ionized water.

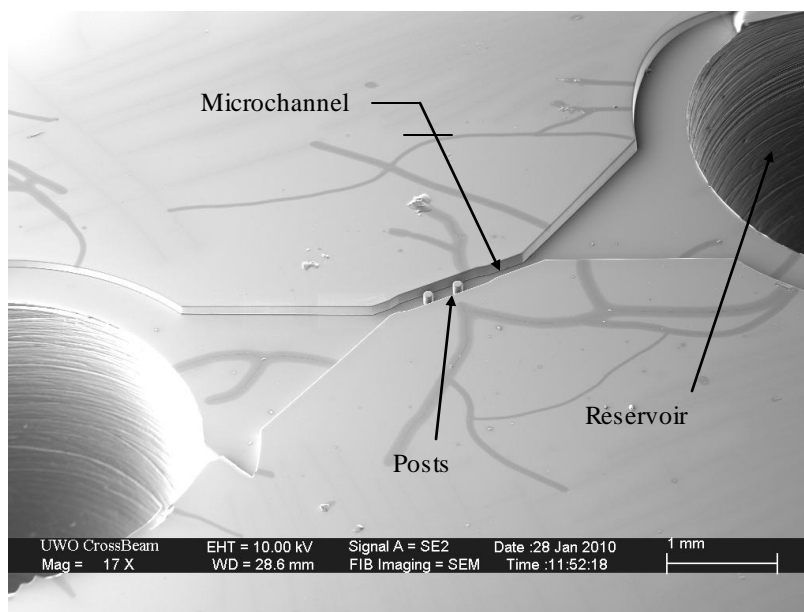


Figure 5.3 SEM photograph of the PDMS based microfluidic chip.

### 5.3.3 Surface coverage of the Au-PAA substrate with biotinylated bR

Although the biotin labelling and self-assembly technique creates a thin layer of bR purple membranes, a closer examination of the porous substrate surface shows that this is not a single contiguous layer rather a sporadic distribution of PM fragments (Al-Arife and Knopf 2010; Horn and Steinem 2005). The electrostatic nature of bR protein produces gaps between the individual PM patches. The surface coverage is examined by using a focused ion beam scanning electron microscopy (FIB-SEM). Figure 5.4 is a SEM photograph of the fabricated photoelectric bR layer and it is clear from the image that the PM fragments (darker areas) cover significant, but not all, areas of the Au substrate.

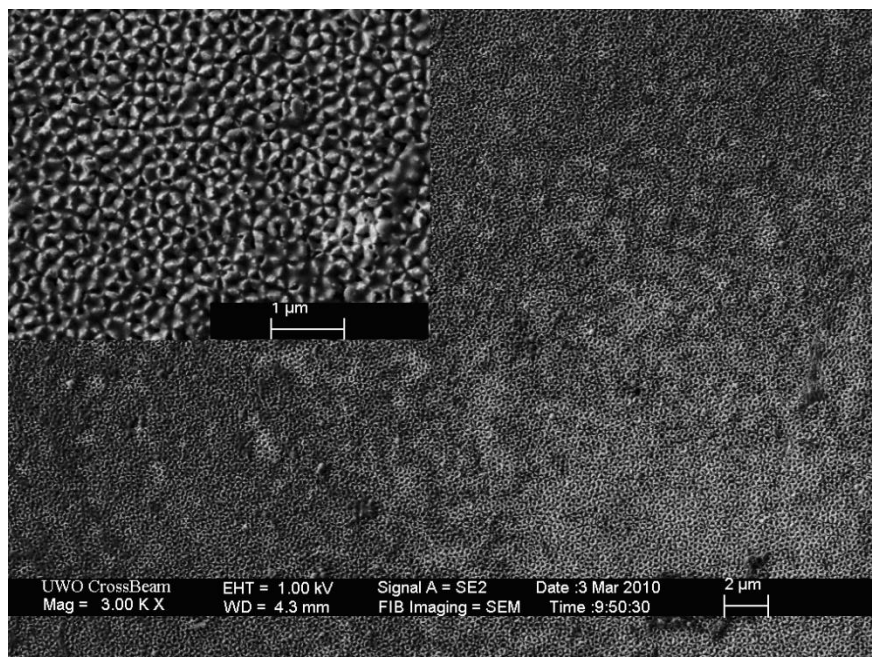


Figure 5.4 SEM photograph of the self-assembled ultra-thin bR film on porous PAA substrate with a magnification factor of 3000. Enlarged area shown in upper right corner.

The mass density of the PM fragments deposited on the Au substrate was calculated by assuming the layer of purple membranes acted as a parallel plate capacitor (Horn and Steinem 2005). Once assembled on the Au coated PAA substrate the photoelectric response characteristics of the self-assembled bR monolayer were measured under fixed light exposure pulse. For these measurements a photocell was created by placing the thin bR film between its Au-PAA substrate and an optically transparent Indium Tin Oxide (ITO) contact glass plate. The Au and ITO surfaces act as microelectrodes to permit a closed electronic circuit to be formed. An 18mW, 568nm light source was used in the experiments because the peak photo-excitation of bacteriorhodopsin occurs at this wavelength (Hampp2000). The voltage differences were measured (Figure 5.5) using an Agilent 34420A Nano-volt/micro-Ohm meter. No additional signal processing or amplification was performed in an effort minimize distortions to the experimental readings. The initial experiments on the photocell demonstrated that a 12.33nm thick bR layer could generate nearly  $1.33\text{mV}/(\text{mW}\cdot\text{cm}^2)$  when exposed to a  $90\text{mW}/\text{cm}^2$ , 568nm laser source for 80 seconds. Based on the

measured the photovoltaic response, and the assumption of considering the self-assembled bR monolayer to act as a parallel plate capacitor, the bR mass coverage density is calculated to be approximately  $2.33\text{ng/cm}^2$ . It is important to recognize that the substrate surface topology (ie. roughness), concentration of thiols, concentration of the streptavidin, and concentration of the biotinylated purple membranes all play a critical role in determining the final distribution of bacteriorhodopsin purple membranes on the gold coated substrate.

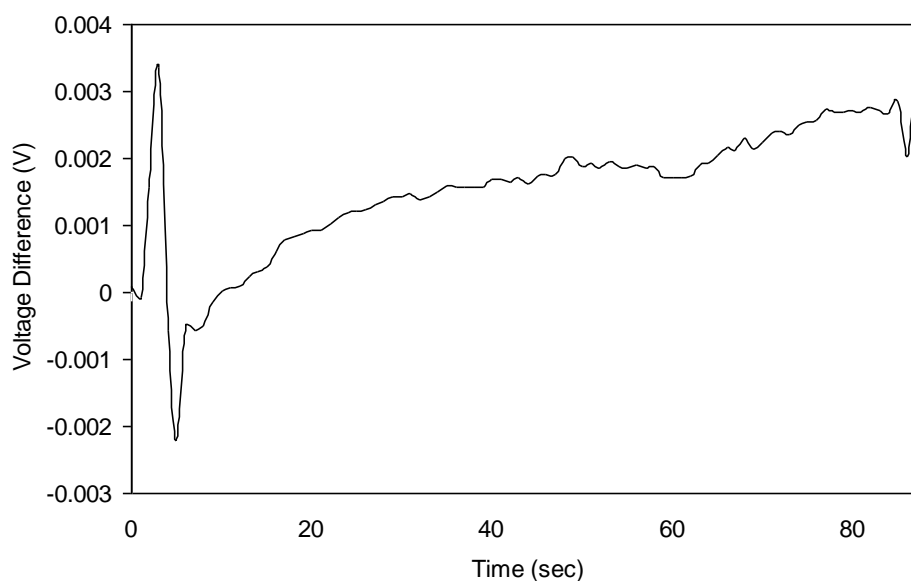


Figure 5.5 Experimental photocell response to a light pulse.

Since the entire photoresponsive transducer was fabricated under identical conditions, it is reasonable to conclude that the measurements obtained over a small window are representative of the entire surface. The surface morphology of the bR-biotin-streptavidin-biotin-thiol-Au-PAA architecture was measured and characterized using an Atomic Force Microscopy (AFM) where individual scans, Figure 5.6, were made at randomly selected locations. The images and profile readings confirm adsorption of the bR monolayer, where the surface profile jumps locally for 40nm. These jumps in the surface profile are higher than the Ti-Au layer which has overall thickness of 25nm. Although the bR has not been deposited uniformly across the substrate surface because of the porosity, it does provide a significant amount of coverage at this thickness.

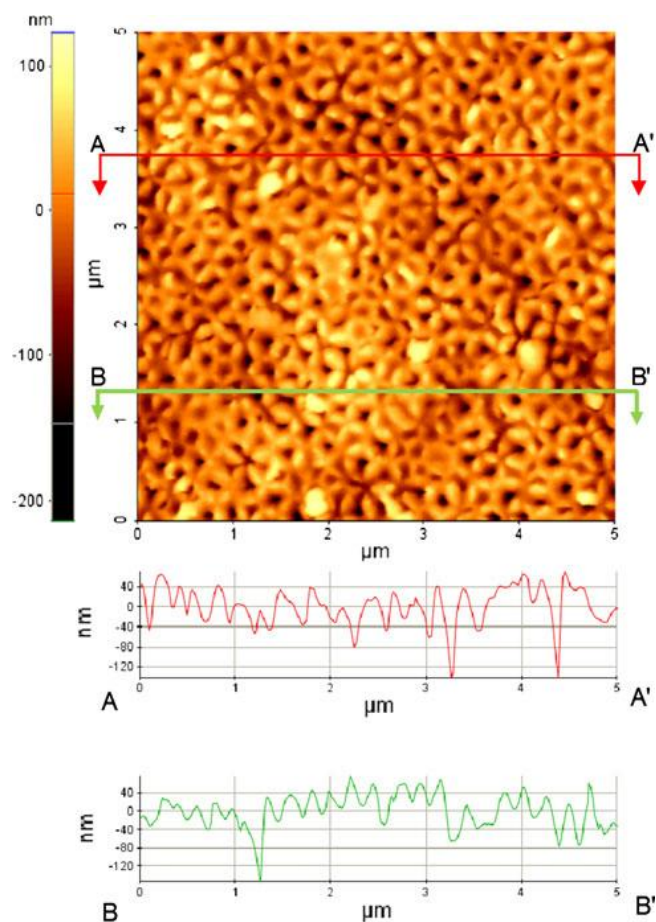


Figure 5.6 AFM analysis of the self-assembled ultra-thin bR layer on PAA substrate. Two cross-sectional profiles (A-A', B-B') are shown.

### 5.3.4 Photo-electro-chemical response based on pH-gradients

The planar bR-biotin-streptavidin-biotin-thiol-Au-PAA (bR-PAA) transducer is inserted into the PDMS device forming pH-controllable semi-porous barrier between two microfluidic reservoirs that contain ionic solutions. The assembly process involves mechanically stretching the flexible PDMS microfluidic device, inserting the bR-PAA transducer at the desired location, and then carefully releasing the polymer chip to tightly seal the edges of the transducer, Figure 5.7. The mechanical seal eliminates any possible contamination that may arise from a chemical adhesive.



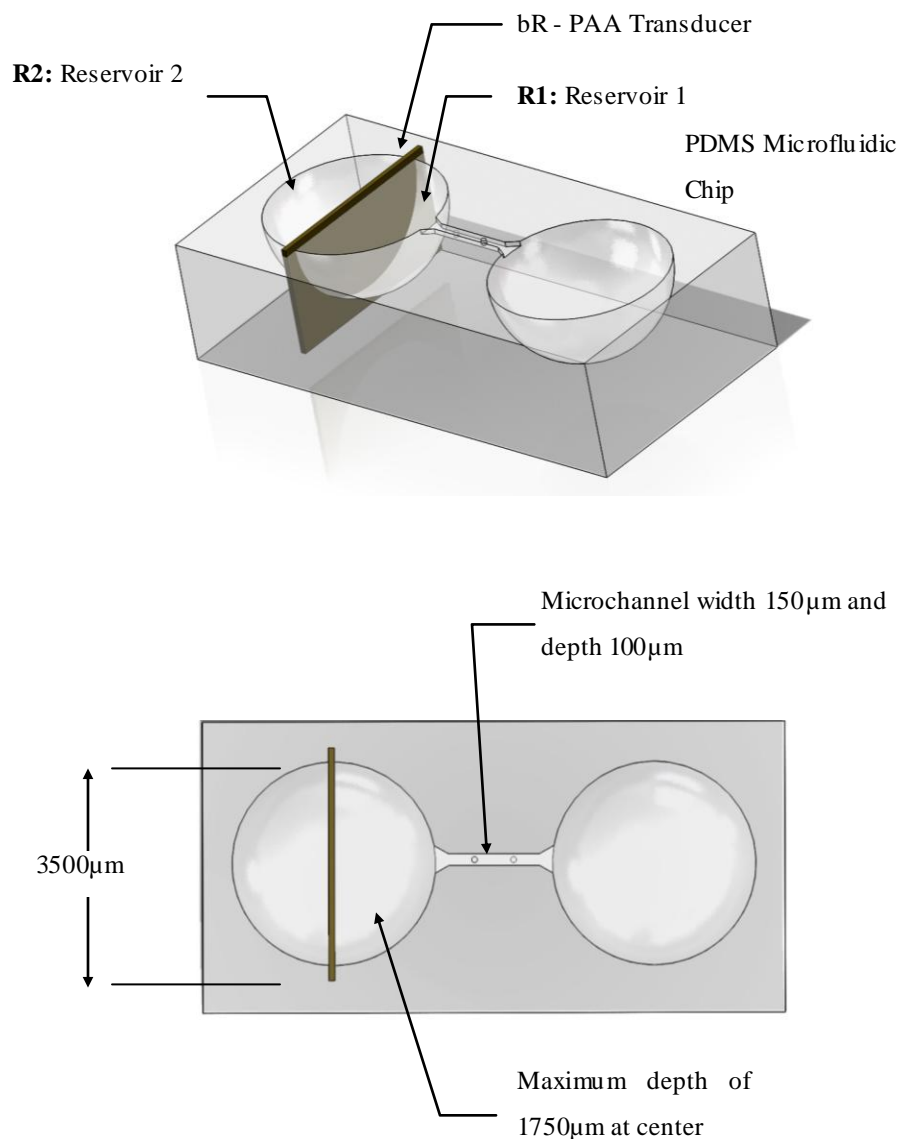


Figure 5.7 Schematic drawing of the microfluidic test device used to perform the experiments. The dimensions are given in  $\mu\text{m}$ .

The photoelectrochemical response characteristics of the fabricated pH-gradient generator are investigated by measuring the change in pH of the solutions under various exposure times to a continuous wave 18mW, 568nm (Melles Griot) Argon Ion laser. The pH changes were measured using a high precision 6230N pH Meter from Jenco

Instruments with a 2.2mm diameter micro-electrode. The electrode is initially inserted at a distance of 250 $\mu$ m from the transducer surface in the reservoir chamber (R1) located adjacent to the immobilized bR. The tip is positioned approximately 60° with the horizontal. The light source is also provided to the same transducer side by a very thin flexible optical fibre placed between the transducer and electrode. The light source was adjusted to provide uniform illumination across the entire photosensitive surface of the bR-PAA transducer. The instrumentation used in experimental study enabled a sampling time of 1 second with a high degree of pH sensitivity of 0.01 pH units. No additional signal processing or amplification is performed to the raw signals in an effort to record undistorted readings.

Prior to testing the pH-gradient generator, several controlled calibration tests are performed to examine the photo-electro-chemical activity of the bare Au substrate, thiols adsorbed on gold, and the streptavidin built on the thiols layer. The experimental conditions for these preliminary tests are identical to those used to verify the performance of fully functioning bR-PAA transducer. When exposed to an 18mW, 568nm laser source the bare Au substrate, and the thiols coated substrate exhibit no measurable photoelectric activity and, therefore, unable to produce a pH-gradient. These preliminary tests confirm that any measureable pH-gradient generated by the bR-biotin-streptavidin-biotin-thiol-Au-PAA architecture originates, in large part, from the actions of the PM proton pumps.

The light response characteristics of the proposed pH gradient generator are investigated by exposing the bR-PAA transducer to different light intensities. The pH of the ionic solutions is selected above 4.5 to avoid any possible interference that might occur at the isoelectric point of the protein. Under dark conditions the ionic solutions separated by the planar transducer exhibits no measurable electro-chemical activity. When the beam from the light source strikes the photo-sensitive bR PM layer, the proton pumps transport H<sup>+</sup> ions residing at the interface of the transducer and ionic fluid into the anodic aluminum oxide porous membrane and then to the solution in the opposite reservoir. As a consequence, the concentration of the H<sup>+</sup> ions in the first reservoir (R1) is decreased producing an increase in the solution's alkalinity as shown in Figure 5.8. At the same time this process increases the H<sup>+</sup> ions and acidity of the solution in the second reservoir.

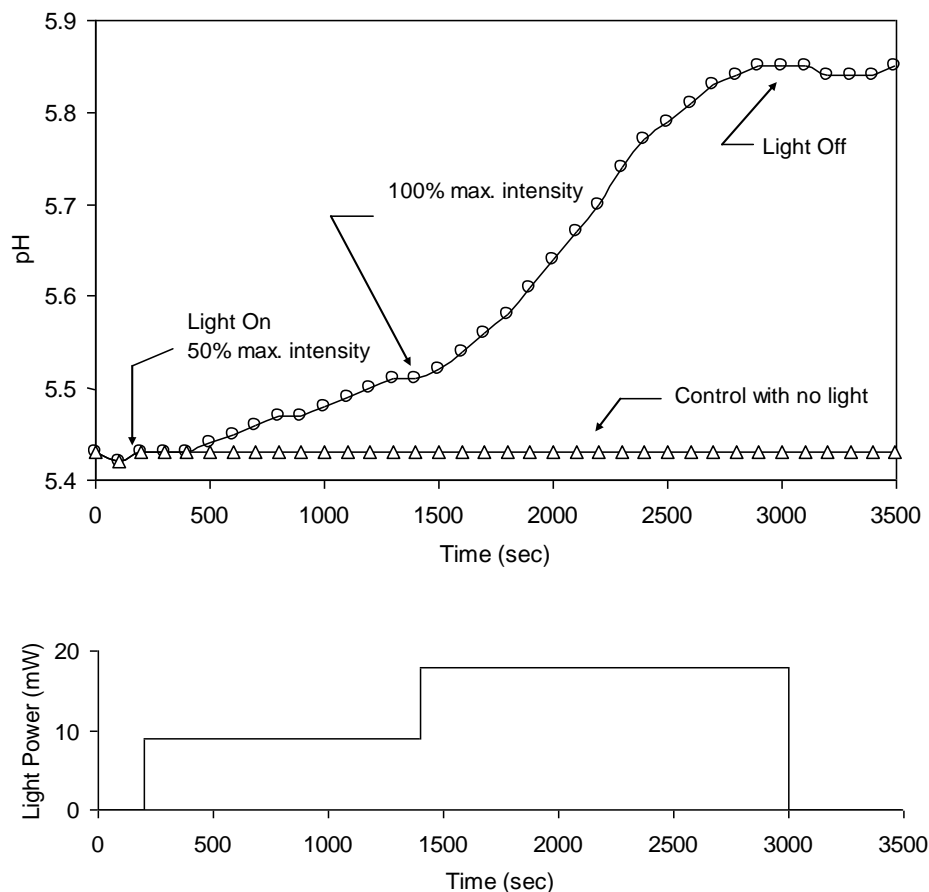


Figure 5.8 Change in pH of the ionic solution in reservoir R1 as a function of light exposure. The pH gradient transducer has an active surface that is  $0.2\text{cm}^2$ .

The measured pH gradient of the solution in R1 is also a function of the light intensity, Figure 5.9. The experimental data suggests that a minimum level of light intensity is necessary to drive the bR proton pumps and generate a significant change in pH. Over a period of 300 seconds, an 18mW light beam generated a pH-gradient that was five times the magnitude observed with only a 9mW source with the same beam diameter. The nonlinear behaviour shown in Figure 5.8 is not unexpected because the observed pH-gradients are the result of combined effects arising from the bR's photoelectric response characteristics and the electrostatic interaction of ions migrating across the bR-PAA transducer.

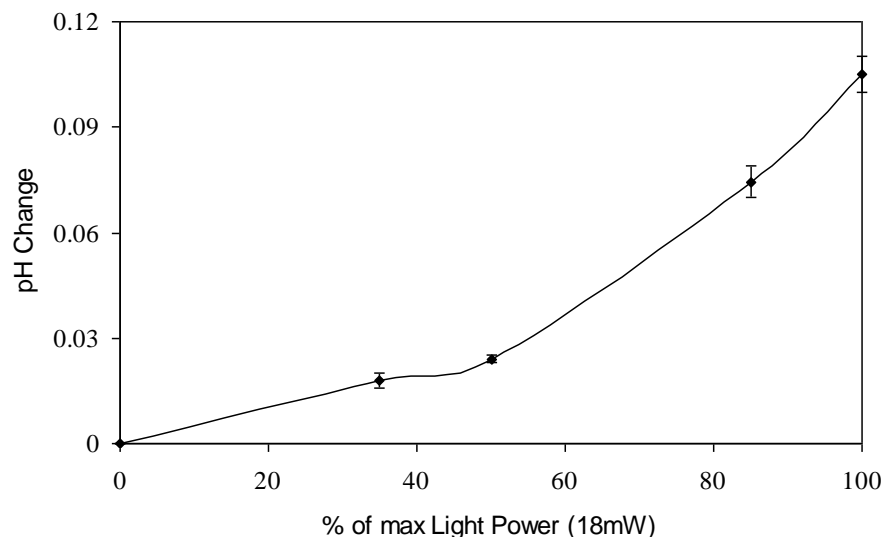


Figure 5.9 Change in steady-state pH of the solution in reservoir R1 as the intensity of light striking the transducer increases.

Furthermore, the light activated bR proton pumping action causes a near instantaneous depletion in the concentration of the  $H^+$  ions along the interface of the bR-PAA transducer with the ionic fluid. This depletion is, however, slowly compensated by the migration of  $H^+$  ions from regions of higher concentration within the same reservoir. Several experiments are performed to investigate this phenomenon. The first test is to record the  $\Delta pH$  in R1 at a distance of  $500\mu m$  from the transducer, and the second at  $1000\mu m$  from the transducer. Figure 5.10 shows the pH build-up at the center of the interface between the bR monolayer on the transducer and the ionic solution when exposed to laser light for only 1500 seconds. At a distance of  $500\mu m$  from the transducer, the pH reaches its maximum value in less than 40 seconds, and then drops off to a slightly lower steady-state value that continues largely unhindered even after the light source is removed. The recorded measurements show that the pH build-up at this location takes more than 450 seconds. In contrast, the pH reaches its maximum value after 300 seconds when the electrode is placed  $1000\mu m$  from the transducer. The increase in response time as the probe is moved away from the transducer is expected because the proton pumping process will initially change only the  $H^+$  ion concentration near the transducer's surface. However, the electrostatic repulsive forces between the

mobile ions will eventually move them randomly through the solution until the concentration is homogenized (Robbins 1972).

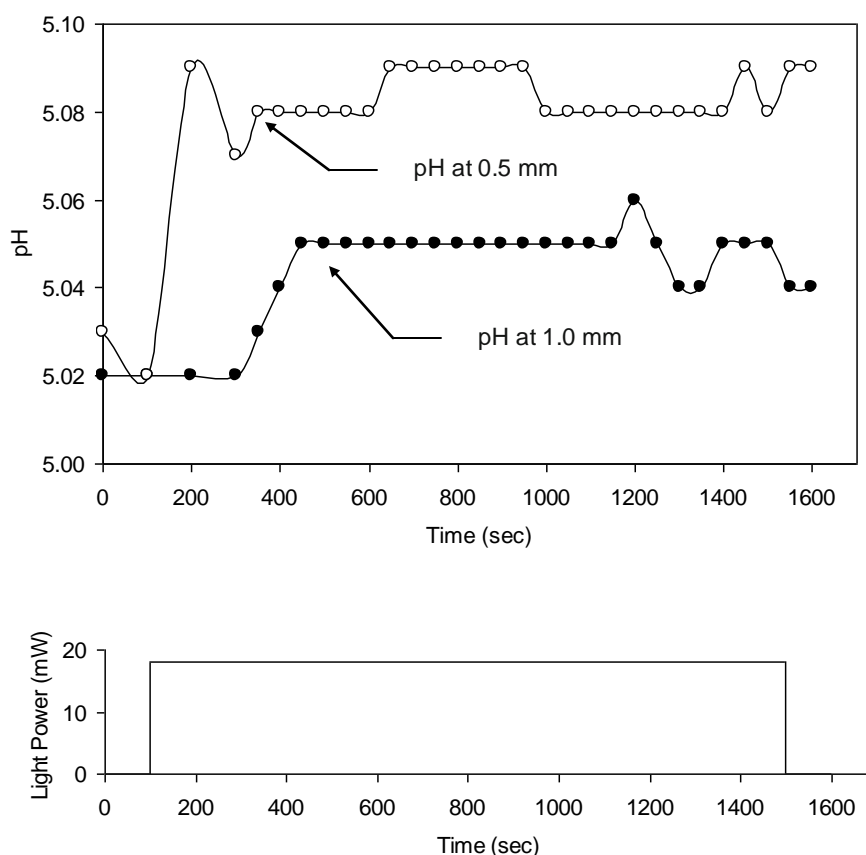


Figure 5.10 Measured pH in the R1 solution as the electrode probe is moved away from the bR-PAA transducer surface. The instrument used to record the solution's pH had a sampling time of 1 second and resolution of 0.01 pH units.

The primary factor that controls the rate in which ions flow across the bR-PAA transducer surface is the density of the bR proton pumps where each pump can transport up to 100 protons/sec ( Hampp 2000). However, there is a physical constraint as to how many bR purple membrane patches can be self-assembled on the Au-coated porous anodic alumina substrate. This fabrication constraint restricts the density of functional proton pumps and thereby limits the response time of the pH gradient generator. It is also important to note that the verification experiments involved the pumping of ions from

reservoirs of equal pH, thereby minimizing the impact of unhindered molecular diffusion of the hydrogen ions through the nano-pores of the bR-PAA transducer. Furthermore, the experiments used in this study demonstrated that the light driven process is unidirectional taking  $H^+$  ions from the reservoir on the bio-functionalized side (R1) of the bR-PAA transducer and transporting them across to the second reservoir (R2). Figure 5.11 shows the corresponding proportional changes in pH of reservoirs R1 and R2 while the bio-functionalized side of the transducer is exposed to light.

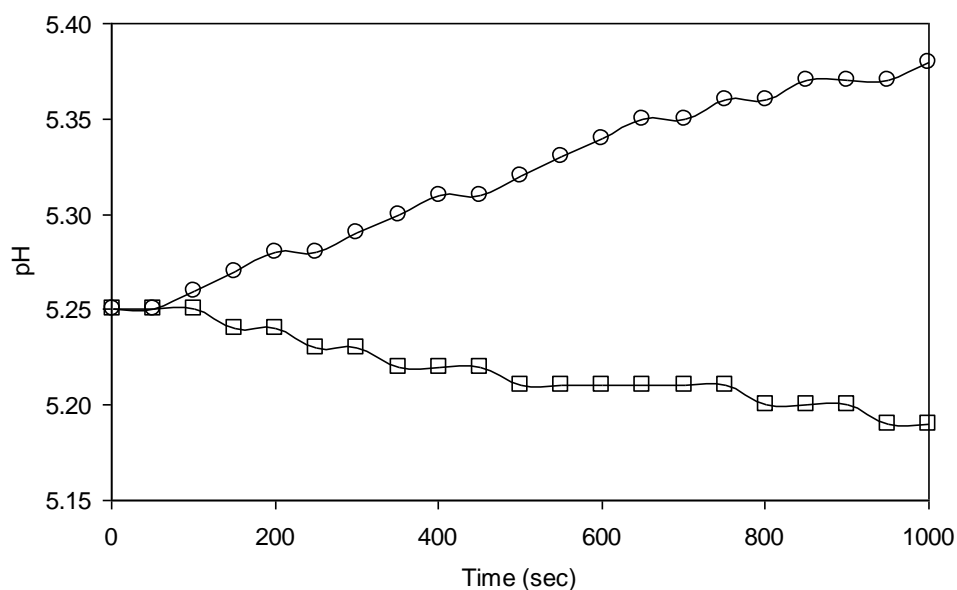


Figure 5.11 Change in pH over time of the two reservoirs separated by the bR-PAA transducer when exposed to an 18mW light source (-o- for R1, -□- for R2).

Although the optically controlled bR-PAA transducer is relatively slow when compared to electrically driven pH gradient generators, the proposed method transports ions between solutions without introducing additional electrical currents. As well the system is remotely driven by a focused beam that can originate from outside the enclosure or reservoir chamber.

## 5.4 Molecular Mechanism for the Light Driven pH Gradient Generation

The proton pumping action of the light-driven bR-PAA transducer changes the molar concentration of the hydrogen ions in the adjacent solutions. The concentration of the hydrogen ions ( $H^+$ ) is theoretically related to the pH scale by a logarithmic function (Voet et al 2006). This relation describes electrochemical potential and changes observed in the non-buffering solutions.

A more detailed model can be developed by considering the molecular level events of the various optically driven bR-PAA transducer components. The net molar concentration of the hydrogen ions can be computed based on the transducer's surface area, the volume of the ionic solution in the reservoir, time duration of the light exposure, and the number of incident photons delivered by the light source. In other words, the ion concentration is

$$pH_t = -\log[H_0^+ + \Delta H_t^+] \quad (5.1)$$

$$pH_t = -\log \left[ H^+ + \left( \eta \varphi \left( \frac{A}{A_{bR}} N'_P \right) \left( \frac{m_H}{V_C} t \right) \left( \frac{n_{pho}}{n_{max}} \right) \right) \right] \quad (5.2)$$

where  $A$  is the area of the substrate that is exposed to light in  $\mu m^2$ ,  $A_{bR}$  is the area of one bacteriorhodopsin hexagonal molecule ( $1.13 \times 10^{-5} \mu m^2$ ),  $N'_P$  is the maximum rate of protons that can be pumped by one bacteriorhodopsin molecule at the optimum wave length (100 proton/sec),  $m_H$  is the mass of the hydrogen ion ( $1.00797/6.0221415 \times 10^{-23}$  grams),  $V_C$  is the volume of the fluid in the reservoir or channel (e.g.  $0.1 \mu L$ ),  $n_{pho}$  the number of photons received by one bR hexagonal molecule,  $n_{max}$  is the maximum number of photons can be processed by one bR hexagonal molecule (100 proton/sec),  $\eta$  is the surface coverage fraction factor (from 0 to 1, it depends on the uniformity of the fabricated bR monolayer), and  $\varphi$  is the substrate surface porosity (15% for the test case).

The expression  $\left(\frac{A}{A_{bR}} N_p'\right)$  in Eqn. (5.2) calculates the surface area of the original substrate exposed to the light source while  $\left(\frac{m_H}{V_C} t\right)$  determines the change in the unit hydrogen ions molar concentration. Finally the expression  $\left(\frac{n_{pho}}{n_{max}}\right)$  calculates the fraction of the maximum number of photons that can be processed by each bR proton pump.

The pumping capacity is dependent upon the ability of each constituent bR molecule to transfer approximately 100 protons per second when exposed to sufficient light energy to initiate the photo-chemical process. Any additional energy beyond the threshold does not increase the pumping rate (Hampp 2000). The comparison with actual experimental data demonstrates the viability of the model to predict proton flow between adjacent reservoirs separated by the bR-PAA transducer, Figure 5.12. However after 1800 second the pH changes became less, which means it is reaching the saturation criteria. This is expected when depleting the concentration of the free hydrogen ions.

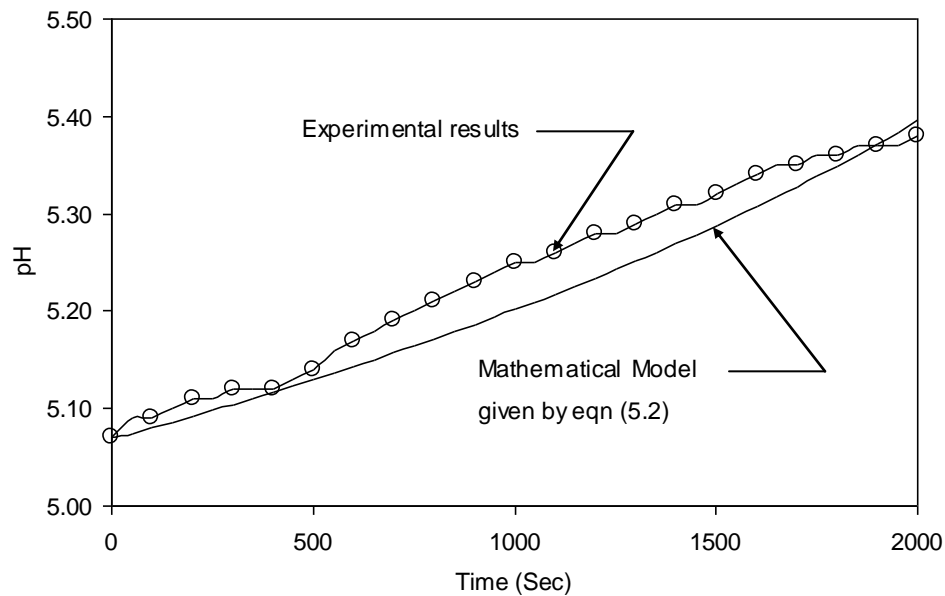


Figure 5.12 Comparison between the experimental observations -o- (every 100<sup>th</sup> sample is shown with circular mark) and theoretical model ( — ) used to predict the temporal change in pH for the R1 solution when exposed to a constant light source.



## 5.5 Monitoring Solution Acidity Using Phenolphthalein Dye

A simple demonstration of the bR-PAA transducer's ability to generate significant changes in target solution pH is shown in Figure 5.13. The ionic solution in R1 contains the 8-hydroxyprene-1,3,6-trisulfonic acid (pyranine) dye at a concentration of 1.3mg/ml (Al-Arife and Knopf 2010). When an 18mW, 568nm light source strikes the bio-functionalized surface of the transducer, the photon activated bR proton pumps transport H<sup>+</sup> ions from R1 to R2 and change the color of the target electrolyte solution in R1 from a pale yellow (pH 5.10) to blue (5.31). The phenolphthalein dye selected for this demonstration test exhibits a visible change in color at a pH of 5.20. The observed changes in color indicate a reduction in H<sup>+</sup> ions and, thereby, a lowering of the solution's overall acidity.

By incorporating pH sensitive dyes in micro-sensors it is possible to provide a visual cue as to changes in pH without the need for sophisticated instrumentation or external hardware to either electronically or optically enhance the signal. It is important to note, however, that the concentration of the indicator dye controls the "saturation" component of the observed color and, therefore, adjusting dye concentrations will produce variations of the same hue.

An interesting variation on this simple monitoring device is an optically driven chemo-photonic sensor (Al-Arife *et al.*, 2010) that responds to the presence of specific phosphate esters by generating chemiluminescence that drives the bR proton pumps which alter the pH of the surrounding solution. Over the past decade the rapid detection of phosphate esters using (dppe)Pt{S<sub>2</sub>C<sub>2</sub>(2-pyridyl)(CH<sub>2</sub>CH<sub>2</sub>OH)} luminophores has been an active area of research because organophosphates are often used to manufacture insecticides, herbicides, and chemical warfare agents (van Houten *et al* 1998). Accurately detecting the presence of phosphate esters is essential for monitoring pollution, chemical spills in industrial facilities, and the release of deadly chemical agents in public spaces.

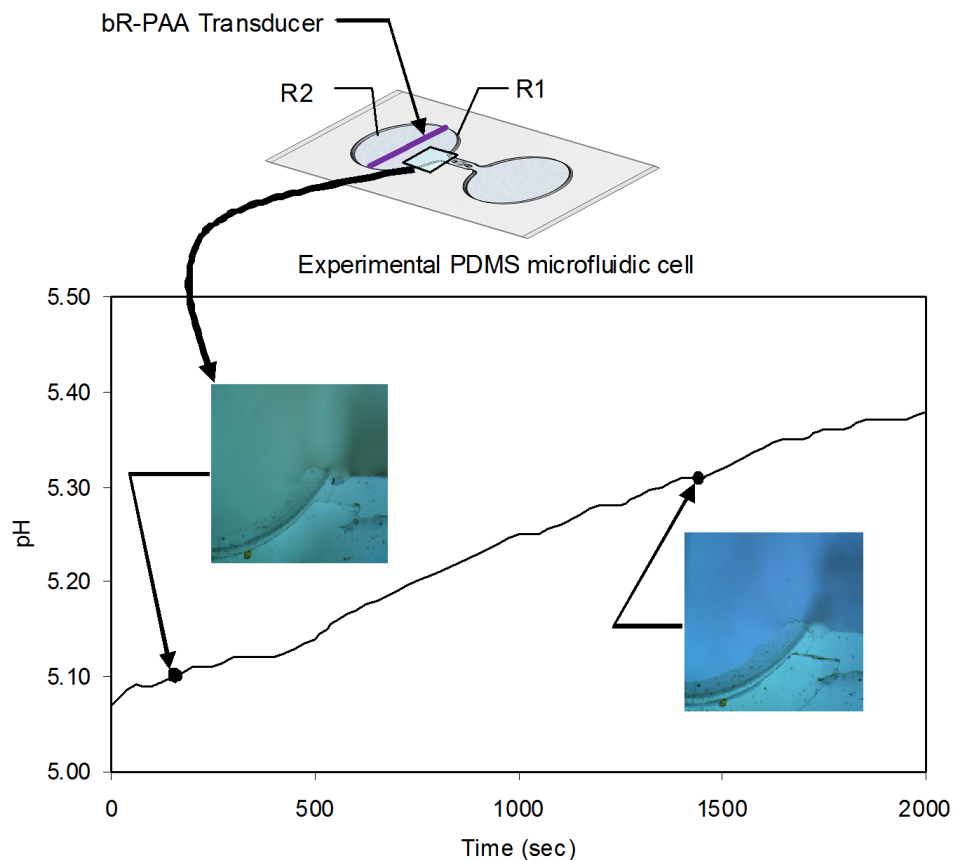


Figure 5.13 The change in pH of the target solution is sufficient to cause a phenolphthalein indicator dye to change colour. The optically driven proton pumps of the bR-PAA pH gradient generator cause the solution in R1 to transform from a light greenish blue (pH 5.10) to a darkened, more intense blue (pH 5.31).

Although details are beyond the scope of this thesis, the basic chemophotonic sensor is self-contained, operates in daylight conditions, and does not require an external power source or specialized instrumentation for monitoring response.

## 5.6 Concluding Remarks

The optically driven pH-gradient generating unit that exploits the photon activated bacteriorhodopsin (bR) molecular proton pumps in the purple membranes (PM) was described and characterized in this chapter. A self-assembled monolayer of oriented bR purple membranes was created on a biofunctionalized Au-coated porous anodic aluminum substrate surface using a biotin molecular recognition technique. The surface coverage of the substrate with the self assembled bR monolayer was quantified based on treating the bR purple membranes monolayer as a parallel plate capacitor and the photoelectric response of the monolayer. The density of the bR purple membranes coverage was determined to be  $2.33\text{ng}/\text{cm}^2$ . The biotin ensured that the extracellular sides of all PM patches were attached to the porous substrate enabling unidirectional and efficient transport of ions across the transducer surface.

Furthermore, the average pore diameter (100nm) of the PAA substrate was adequate to permit hydrogen ions to be effectively pumped across. Once assembled, the bR-PAA transducer was inserted into a polydimethylsiloxane (PDMS) device for experimental observation and performance verification. The experiments demonstrated that the transducer generated pH-gradients as high as 0.42 and absolute voltage differences as high as 25mV when illuminated by 18mW, 568nm light source. Additional tests showed that the  $\Delta\text{pH}$  over time was nonlinear with respect to light intensity and exposure time. The relationship between the solution's  $\Delta\text{pH}$  and transducer's light exposure was mathematically modeled and enabled the bR-PAA transducer's behavior to be predicted with reasonable accuracy. The change in pH of the target solution was sufficient to cause a phenolphthalein indicator dye to change color.

## CHAPTER 6

### SMART HYDROGEL MICROACTUATOR

#### 6.1 Introduction

Microactuators are critical component of member of microelectromechanical systems that can exchange energy with its surrounding. Moreover, the actuator receives nonmechanical energy and provides mechanical form of the energy. The category of micro-actuators includes piezoelectric, shape memory, magnetostrictive, electro, magnetorheological, and hydrogel actuators. Among these microactuators the hydrogel microactuators attracted the attention of microsystems and lab on a chip scientists and engineers because it provide large mechanical displacements, does not get stuck with microparticle obstacle as it swells around it. Moreover, it showed high sealing capability when used in microfluidic systems as microvalves.

#### 6.2 Hydrogel Microactuators

Smart hydrogels are fluid filled polymeric networks that can undergo in dramatic volume changes when triggered with external stimuli. The triggering stimuli can be a change in the surrounding temperature, pH, electric field, specific ion concentration, and light illumination. These stimuli are able to drive the volume phase transition of the smart hydrogels based on the chemical composition of the polymeric networks, and the ionic characteristics of the filling and surrounding solution. This unique ability to generate large actuation dynamics and specificity of the triggering mechanisms made the smart hydrogels preferable candidates for the core sensing and actuation transducers in the microsystem technologies in general (Richter *et al.*, 2008), and lab on a chip applications (Beebe *et al.*, 2000; Liu *et al.*, 2002).

Technically the smart hydrogel microactuators are the components that can process the non-mechanical stimuli such as pH-gradients, or ionic composition as input energy to drive electro-chemical transformations leading to the generation of mechanical work associated with volume phase transition of the hydrogel actuator. Among the different stimuli, pH-gradients are considered the fundamental input signal to the hydrogel transducer presented in this project, so that the theoretical and experimental studies are focused on the pH-sensitive hydrogels in general and in particular on the acrylic acid based hydrogel as it is the essential component of the introduced micro-actuator.

### 6.2.1 Physics and chemistry of the pH sensitive hydrogels

The pH-sensitive hydrogels structures from cross-linked polymer networks filled with liquid. The polymeric networks consist of neutral monomers plays the role of the network backbone and co-monomer ionisable pendant groups implanted on the network backbone (Peppas *et al.*, 2000; Van der Linden *et al.*, 2003). The network backbone can carry acidic or basic groups or both of them; the last hydrogel is called amphiphilic hydrogel (Richter *et al.*, 2008).

The acidic and basic groups are ionisable around their  $pK_a$  in the presence of the adequate ionic strength of the surrounding solution because the ionisation process is believed to be energy driven process that is triggered at  $pK_a$  of the ionisable groups. In the acidic groups such as the acrylic acid based hydrogel, the ionisation starts at  $pK_a$  and proceeds as pH goes in higher values (Figure 6.1), whereas, in the basic groups starts the ionisation process at  $pK_a$  and proceeds as pH goes in lower values (Van der Linden *et al.*, 2003). The ionisation process can also be defined as a charge separation process from the pendent group. This process consists of release of free hydrogen ions into the solution and ionising the pendent groups. Once the ionisable groups became charged and released hydrogen ions to the solution, counterions to the hydrogen ions are attracted to flow into inside the hydrogel networks to maintain the electroneutrality within hydrogel networks. The flow of counterions makes the charged networks able to repeal and moving apart from each other, and lead to the generation of osmotic pressure difference. The increase in the osmotic pressure, the charge density on the polymeric networks, the ionic strength

of the ionic solution and the elastic limits of the neutral backbone monomer are all factors contribute in the swelling process and in the final geometry of the hydrogel.

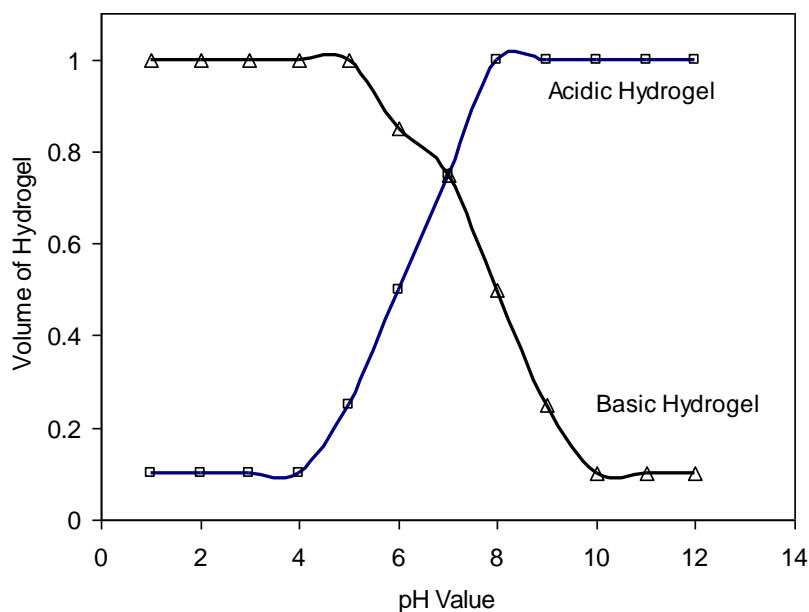


Figure 6.1 Volume transitions of acidic and basic hydrogels under pH gradient activation.

One of these factors, which is known by the ionic strength of the ionic solution, and chemically defined by the molar concentration, has dual-action on the volume transition process. The ionic strength must be kept high enough to allow the charged polymer networks maintain their electroneutrality providing salt to substitute the released hydrogen ions. If the ionic strength was not high enough the charged networks to maintain their electroneutrality will pickup the released hydrogen ions and return back to their uncharged phase. So that, it is very critical high to the level that can make the volume transition stable. On the other hand having the very high ionic strength increase the free ions density between the charged networks which leads to shielding the charged groups from being able to have repulsive forces enough to drive the volume swelling. So that it is highly recommended to study each hydrogel composition and select the suitable value of the ionic strength, because every chemical composition creates specific characteristics.

## 6.2.2 Synthesis techniques of hydrogels

Hydrogels are called chemical hydrogels when they are fabricated by cross-linking the backbone monomers with an external chemical cross-linker based on chemical reactions (Hoffman 2002), whereas they are called physical hydrogels when they are fabricated physical treatments without going in chemical reactions or chemical cross-linkers (Hassan *et al.*, 2000), Figure 6.2.

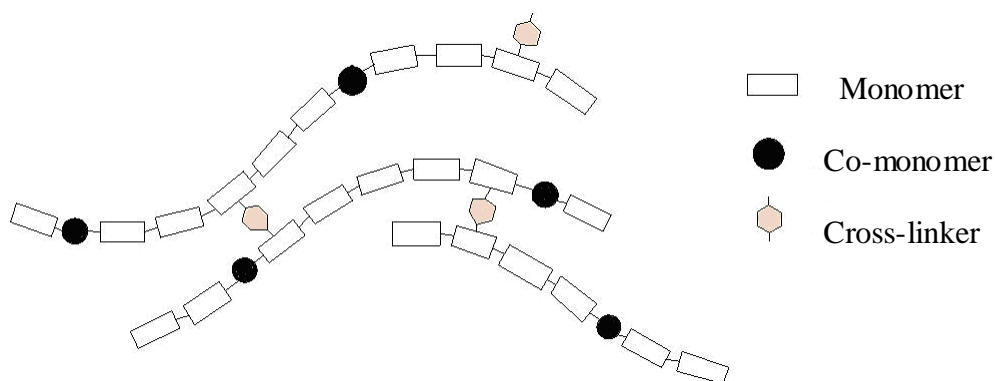


Figure 6.2 Schematic drawing showing the hydrogel network structure

The physical hydrogels are synthesized by forming monomers entanglements without using cross-linking agents. These entanglements are formed by exposing the hydrogel monomers to repeatable cycles of freeze and thaw treatments. The freezing part of the first cycle can be 12 hours and the thaw from 2 to 4 hours, then for the other cycles 4 hours freezing and 2 hours thawing (Al-Arife *et al.*, 2006). The freezing incubation was conducted at  $-20^{\circ}\text{C}$  and the thaw incubation was at  $23^{\circ}\text{C}$ . This physical treatment procedure allowed the pH sensitive monomers to keep their pH sensitivity (Al-Arife *et al.*, 2006); however other procedures with differences in the incubation times provided responsive hydrogels (Hassan *et al.*, 2000).

The following section provides a detailed description of the fabrication procedure of the hydrogel actuator and microfluidic chip. In Section 6.3 an experimental investigation of the phase transition dynamics of the acrylic acid based hydrogel is presented. The results and discussion are presented in Section 6.4, whereas the concluded remarks are presented in Section 6.5.

### 6.3 pH-Sensitive Hydrogel Microvalve

The construction of the light-driven microvalve from ionic hydrogels and photoresponsive bR proton pumps and involves several fabrication stages. The first stage is to create a pH-sensitive hydrogel by using a chemical cross-linker forming an “acidic” acrylic acid implanted on 2-hydroxyethyl methacrylate forming HEMA-AA hydrogel. The “acidic” hydrogel is required to undergo in phase transition when pH reaches pKa of the chargeable pendant groups supply protons (H<sup>+</sup>) and as the protons are released it will swell creating displacement and actuation force. The hydrogel microactuator is designed and fabricated to show its actuation affect in microchannel.

#### 6.3.1 Fabrication of pH-sensitive hydrogel

In this research, the microactuator shell is a chemically cross-linked pH sensitive hydrogel fabricated by using crosslinker, initiator, accelerator, backbone monomers and pH-sensitive monomers. The backbone monomer 2-hydroxyethyl methacrylate (HEMA) is purified by vacuum distillation. The vacuum distillation system is operated at temperatures less than 80°C to avoid the pre-polymerization. Acrylic acid (AA), the pH-sensitive monomer, is also purified by vacuum distillation. The vacuum distillation system is operated at temperatures less than 70°C to avoid the pre-polymerization. Ethylene glycol dimethacrylate, the cross linker, is directly used without further purification. The photoinhibitor (Irgacure 651) and the PDMS kit (Sylgard 184) were used without modification following the manufacturer’s instructions.

The mass of materials used to the ionic gel for this study are: 2-hydroxyethyl methacrylate (0.5024g), Acrylic acid (0.095g), ethylene glycol dimethacrylate (0.0195g), and Irgacure 651(0.013g). The pH-sensitive hydrogel materials are mixed carefully, and poured into the PDMS mold stencil produced by the method described in Section 6.3.2. The mold has diameter of 150μm and height of 100μm. A complete polymerization was achieved in 120s using Karl Suss MJB3 Mask Aligner at 12.5mW/cm<sup>2</sup>, and a light source at 365nm.



### 6.3.2 Fabrication of the microfluidic chip

The polydimethylsiloxane (PDMS) microfluidic chip that contains the hydrogel valve is first created using a SU-8 micromold. The key steps involved fabricating the test chip (Figure 6.3) involve: creating a photomask, spin coating SU-8 photoresist, polymerizing the SU-8 mold, and stamping the mold with PDMS to cast the final part in PDMS. Micromolds created from thick photoresists, such as SU-8, enable micro-features with high resolutions to be produced without the need for wet etching. Chemical etching on glass substrates is an expensive process that requires the use of environmentally harmful chemicals such as hydrofluoric acid and nitric acid (Abgrall *et al.*, 2007; Mourzina *et al.*, 2005).

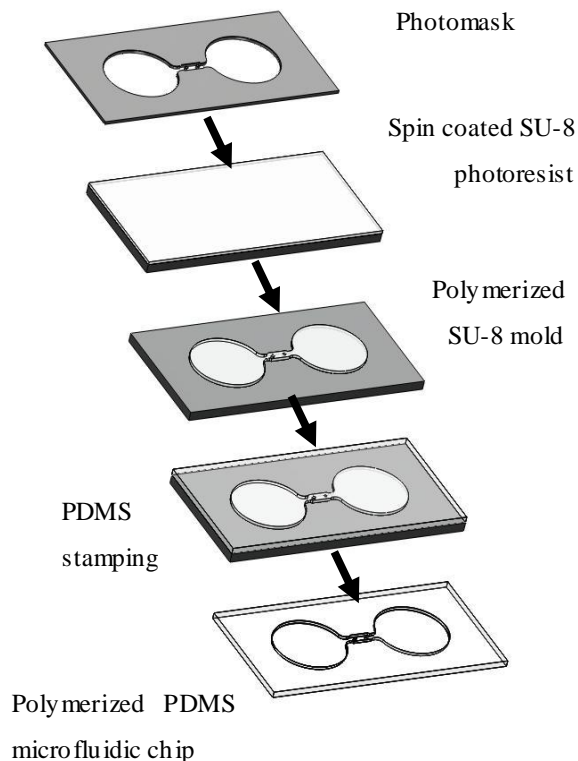


Figure 6.3 Steps in micromolding a PDMS microfluidic chip. (This Figure is to similar 5.2)

For this application, the SU-8 mold for the microfluidic device is created by initially soaking a glass substrate in 20% HCl for two hours and then rinsing it with de-ionized water. Once the glass substrate is dried on a 200°C hot plate for at least 15min it is coated with a thin film of the negative photoresist SU-8 2050. A film thickness of 100µm is achieved by spinning the coated substrate at 500rpm for 5s and then at 1700rpm for 30s. The formed photoresist film is then baked at 65°C on a hotplate for 5min, followed by further heating at 95°C for 30min. The process of baking and cooling the photoresist must be gradual to avoid creating large temperature gradients across the film which cause local stresses that influence surface roughness and introduce cracks. Thermal stresses can also cause the premature separation of the mold from the substrate. Based on experiments it is recommended that the temperature be ramped up in 2-3°C/min increments.

Once completed, the photoresist is exposed to light for 36s. This time exposure is provided in three doses of 12s each, and 1min rests between doses to avoid overheating. The photoresist coated substrate is baked again for 5min at 65°C and 15min at 95°C. The photoresist is then developed in a SU-8 developer, rinsed with isopropanol for 10s, and dried with compressed nitrogen. Finally, the formed micro mold was hard baked on the hot plate at 200°C for 20min. This last step in the process anneals the mold and prevents surface cracks from forming. The polymer replicated part is produced from the SU-8 micromold using a PDMS molding process. To complete this step a Sylgard 184 (Dow Corning) kit is mixed and de-gassed using a vacuum desiccator. The PDMS mixture is then poured on the SU-8 mold in a Petri dish, and exposed to a vacuum in order to remove air bubbles trapped at the interface of SU-8 and PDMS. The polymerization process is accelerated by applying homogeneous heating in an incubator at 80°C for 120 minutes. The formed PDMS microchannel, Figure 6.3, is cooled to room temperature, and soaked in acetone for 30min to reduce the adhesion between SU-8 mold and PDMS structure. The PDMS is then gently peeled off in acetone. This last step is very important, especially for designs that have very small features. The PDMS microchannel is treated with oxygen plasma in STS Reactive Ion Etch System to make the channel surface hydrophilic. Once this step has been completed the device is placed in de-ionized water.

## 6.4 Response of the pH-sensitive Hydrogel Microvalve

The role of the pH-sensitive valve is to control the flow by opening and closing the microchannel based on ionic changes to the transporting fluid. In this initial study the swelling characteristics of the 150 $\mu\text{m}$  diameter (HEMA-AA) pH-sensitive hydrogel microvalve were investigated. The valve was inserted in a 200 $\mu\text{m}$  wide PDMS microchannel between two 50 $\mu\text{m}$  diameter aligning anchors. The channel was filled with 50mM phosphate buffer at pH 3 and then covered with a glass cover slip. The valve absorbed part of the surrounding solution until it was stabilized at a diameter of 155 $\mu\text{m}$ . A 50mM phosphate buffer at pH 10 was then provided. The volumetric change to the pH-sensitive hydrogel microvalve at pH 3 and pH 10, respectively, was observed (Figures 6.4 and 6.5).

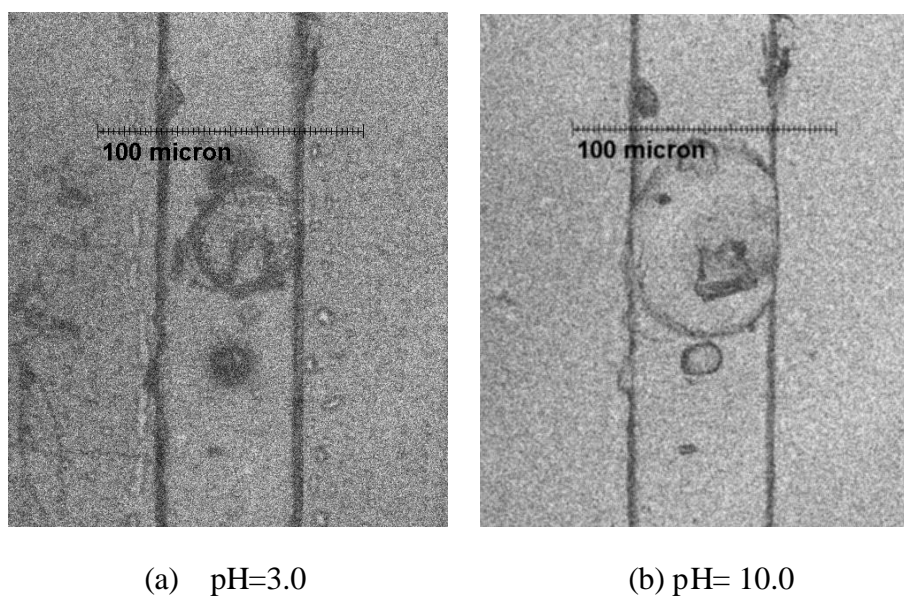


Figure 6.4 pH-sensitive (HEMA-AA) microvalve at pH 3 and pH 10, respectively (Nanofabrication Facility at the University of Western Ontario).

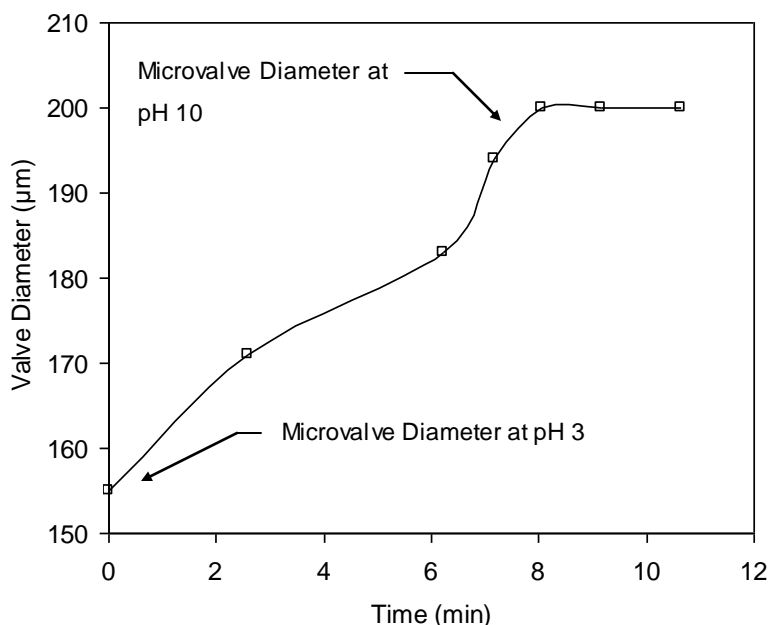


Figure 6.5 Swelling of 155µm (HEMA-AA) pH sensitive microvalve.

## 6.5 Results and Discussion

Basic volume transition monitoring with pH changes tests show that the HEMA-AA gel with the used molar concentrations can undergo in a dramatic volume transient. The tests started at pH 3.0, which lower than the phase transition point of the acrylic acid chargeable groups. The phase transition point is  $pK_a$  and evaluated to be at pH 4.7. At the de-swelling phase, the HEMA-AA had a diameter of 155 µm. Once pH of the solution is changed by replacing the low pH solution with another solution with pH 10.0 the hydrogel plug started the volume transition process until it blocked the microchannel in 10 minutes.

The HEMA-AA pH responsive microvalve tests were conducted in a polydimethylsiloxane (PDMS). The PDMS material is selected because of it is optical clear which allow providing light beams to the light responsive chip. Moreover its stretchability makes it very good base for multi component systems. The test media is made from 200mM KCl, adjusted at pH 3.0 in the first part of the test and then adjusted at pH 10.0. The pH adjustments were carried out using concentrated HCl and NaOH.

## 6.6 Concluding Remarks

Environmentally sensitive HEMA-AA is used as the microactuator shell because it experiences a sudden change in volume when the pH of the surrounding solution is raised above the phase transition point pKa.

The pH change from below the pKa of the acrylic acid chargeable groups to above it induces the volume phase transition swelling/deswelling in the polymer network. The fabrication of the PDMS microfluidic chip, and HEMA-AA hydrogel valve, were described in detail. The HEMA-AA gel microvalve was shown to close a 200 $\mu$ m microchannel as the pH of the surrounding solution increased from 3 to 10. The change in volume blocked an initial 45 $\mu$ m opening in the channel neutral state and triggers the swelling of the gel. One research challenge that needs to be resolved is accurately inserting the hybrid gel structure in the microchannel without affecting the gel dimensions. Other issues include controlling the pressure in the channels when the system is sealed.

## CHAPTER 7

# LIGHT DRIVEN HYDROGEL MICROACTUATOR

### 7.1 Introduction

Light sensitive hydrogels are often driven by one of three approaches. The first approach is to exploit molecules that can undergo volume changes when exposed to specific wavelengths of light. Ishihara *et al* (Ishihara *et al.*, 1984) investigated the swelling properties of 2-Hydroxyethyl methacrylate with azobenzene molecules as the side groups. The azobenzene molecule is a UV sensitive molecule that can make a 180° rotation around a carbon double bond. The rotation of the azobenzene group around the carbon double bond induces structural rearrangement. The maximum volume change that was observed with this structural rearrangement was 14% in 6 hours at 25°C. An alternative approach exploits light ionized molecules in a neutral hydrogel network. In this context, Ishikawa and Kitamura (Ishikawa *et al.*, 1994) used polyacrylamide microgels that have triphenylmethane leuco cyanide as the light ionisable molecule. UV light ionizes this molecule inducing repulsive forces that drive the hydrogel to swell. It was reported that the photo-dissociation of this light sensitive chromophore occurs in less than 60 seconds. The equilibrium time for an 11µm particle is about 1 hour, while for a 180 µm particle it takes more than 55 hours.

Utilizing the swelling and de-swelling properties of temperature responsive hydrogels is the third approach. These temperature responsive hydrogels are polymer networks that have N-isopropylacrylamide as the backbone monomer. This monomer has a transition temperature of around 32°C. Suzuki and Tanaka (Suzuki *et al.*, 1990) utilized heating power of a light beam raise the temperature of the material. The synthesized hydrogel contained N-isopropylacrylamide as the main constitute and trisodium salt of copper chlorophyllin as a light sensitive chromophore. Discontinuous volume transition was observed around 31.5°C. The diameter of the sample shrank from

about 240 $\mu\text{m}$  to about 100 $\mu\text{m}$  in response to a temperature increase from 25 $^{\circ}\text{C}$  to 40 $^{\circ}\text{C}$ . Mamada *et al* (Mamada *et al.*, 1990) investigated the response of a N-isopropylacrylamide gel with the photosensitive molecule bis(4-(dimethylamino)phenyl)(4-vinylphenyl) methyleluocyanide as a side group. Juodkazis *et al* (Juodkazis *et al.*, 2000) studied the effect of laser radiation on the temperature responsive hydrogel N-isopropylacrylamide. The experiments confirmed that radiation forces can alter the phase transition process by shifting back the volume transition temperature in the range of 10 $^{\circ}\text{C}$ . Sershen *et al* (Sershen *et al.*, 2005) incorporated optical absorption particles to drive the temperature responsive hydrogel poly[N-isopropylacrylamide-co-acrylamide]. The optical absorbing particles that were used are gold-colloid nanocomposites hydrogel that shrink when illuminated under green light and gold nano-shell hydrogel that shrink in response to near IR light. Both hydrogel composites have fast responses and can reach final state in 5s when fabricated in micron scale.

A novel micro-actuator activated by a monolayer photo-electric film that controls the expansion and shrinkage of a pH sensitive polymer gel is introduced. The activating photo-electric monolayer properties and the fabrication process have been presented in Chapter 3, and the photoelectric and photoelectrochemical responses and characterization have been presented in chapters four, and five respectively. The photo-electric and photo-electro-chemical responses have been considered as the input signal to the absolute optically driven microactuator. In this chapter the developed bR based monolayer is integrated with the pH-sensitive hydrogel microactuator presented in chapter six for constructing the absolute optically driven microactuator. The actuator structure is designed and fabricated to be operated in a common electro-chemical working zone between the bR array and the hydrogel actuator to keep all of the system components working without degrading response of each other. This approach has been studied on the base of a multi-stage theoretical and experimental tests. These tests include testing the fabrication of bR architecture, the photo-electric response, photo-electro-chemical response, and volume transitions processes. The stage-by-stage procedure of studying and characterizing the actuator performance has enabled designing the proper pH-sensitive hydrogel of the actuator.

The following section introduces the actuator working mechanism and the signal pathway and transformations. Section 7.3 shows the fabrication procedure and sets the working conditions. In Section 7.4, detailed characterization of the responses including the photo-voltage and photo-current responses and the volume phase transition have been presented. A case study for exploiting the generated volume changes in controlling the microchannels opening has been provided in this section. Section 7.5 discusses the experimental observations including the photo-voltaic, photo-current, and the volume transition responses. The Section 7.6 presents the concluding remarks.

## 7.2 Photo-Responsive Hydrogel Microactuator

A light driven micro-actuator activated by an ultra-thin organic photo-electric film that controls the expansion and shrinkage of a pH sensitive HEMA-AA hydrogel actuator is described in this chapter. The self-assembled monolayer of oriented bacteriorhodopsin (bR) purple membrane patches are immobilized on a porous bio-functionalized gold (Au) coated substrate using a biotin molecular labeling and recognition technique. When exposed to visible light, each bR molecule in the monolayer acts as a simple proton pump which transports hydrogen ions from the cytoplasmic to the extracellular side through a transmembrane ion channel that connects both sides of the membrane. Figure 7.1 schematically shows the actuator structure.

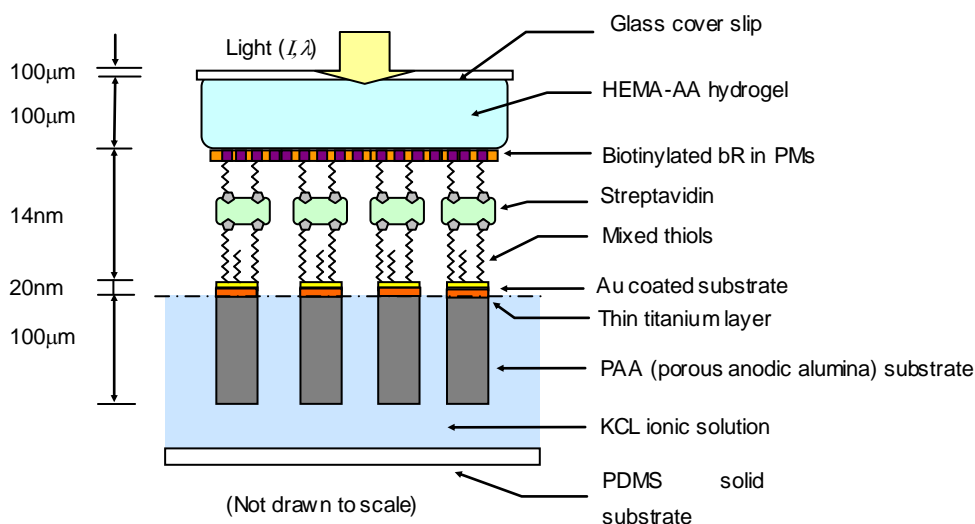


Figure 7.1 Schematic drawing of the bR activated hydrogel structure.



The flow of ions by the photon activated bR pumps through the membrane changes the pH value of the ionic solution that surrounds the gel microactuator. The active groups of the polymeric network remain uncharged until pH reaches the  $pK_a$  where each chargeable group on the hydrogel release proton into the surrounding solution and becomes charged. Charging the active groups are considered as the triggering signal for generating the osmotic pressure of the volume changes of the hydrogel; more details are provided in sub-Section 6.1. Figure 7.2 shows a simplified drawing of the ions flow through the hydrogel.

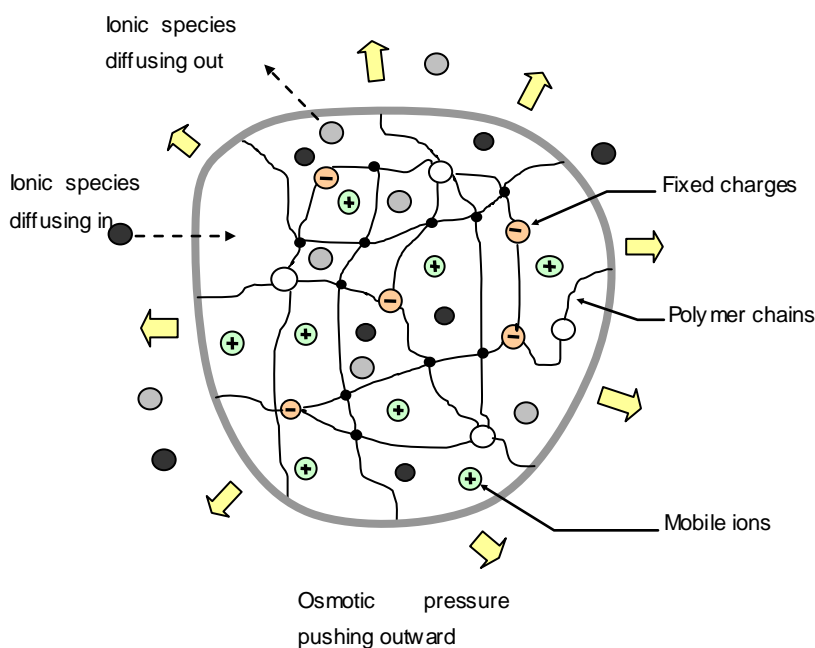


Figure 7.2 Schematic drawing of the ions flow through the activated hydrogel.

### 7.3 Fabrication of bR Activated Hydrogel Microactuator

The construction of the light-driven micro-actuator from ionic hydrogels and photo-responsive bR proton pumps involves several fabrication stages. The first stage is to create a pH-sensitive hydrogel by using a chemical cross-linker procedure forming an “acidic” HEMA-AA hydrogel. The “acidic” hydrogel senses the decrease in hydrogen ions concentration and undergoes an electric phase transition at its  $pK_a$ . This phase

transition triggers the volume transition process. The volume transition is the actuation displacement provider.

The second stage is to immobilize a thin layer of properly oriented bR purple membrane patches on a relatively “stiff” porous substrate. Consistent orientation of the PM patches on the electrode surface is necessary for efficient photon to ion flow and charge separation. If the PM patches adsorbed on the same electrode are a mixture of cytoplasmic and extracellular sides the photoelectric response will be significantly weakened. For the micro-actuator to function properly, it is also necessary that the protons be able to move unimpeded from the KCL ionic solution to HEMA-AA hydrogel. To achieve this, the thin bR layer must be constructed on a porous substrate that doesn't deflect under hydrostatic pressure but does permit significant ion diffusion. Details about the fabrication of the pH-sensitive hydrogel and bR proton pump layer are provided below.

### **7.3.1 Fabrication of the HEMA-AA hydrogel**

The micro-actuator shell is a chemically cross-linked pH sensitive hydrogel fabricated by using cross-linker, initiator, accelerator, backbone monomers and pH-sensitive monomers. Concentrations of the hydrogel components determine its swelling/deswelling characteristics. The backbone monomer 2-hydroxyethyl methacrylate (HEMA) is purified by vacuum distillation. The vacuum distillation system is operated at temperatures less than 80°C to avoid the pre-polymerization. Acrylic acid (AA), the pH-sensitive monomer, is also purified by vacuum distillation at temperature less than 70°C prior to use. Ethylene glycol dimethacrylate, the cross linker, is directly used without further purification. The photoinhibitor (Irgacure 651) and the PDMS kit (Sylgard 184) were used without modification following the manufacturer's instructions. The mass of materials used to the ionic gel for this study are: 2-hydroxyethyl methacrylate (0.5024g), Acrylic acid (0.095g), ethylene glycol dimethacrylate (0.0195g), and Irgacure 651 (0.013g). The pH-sensitive hydrogel materials are mixed carefully, and poured into the PDMS mold stencil produced by the method described in Section 5.3.2 The mold has diameter of 75 $\mu$ m and height of 100 $\mu$ m. A complete polymerization was achieved in 120s using Karl Suss MJB3 Mask Aligner at 12.5mW/cm<sup>2</sup>, and a light source at 365nm.

### 7.3.2 Fabrication of the bR functionalized porous substrate

The swelling and deswelling of the hydrogel is the result of protons being transported through a structurally “stiff” porous substrate. A relatively thick substrate is needed to prevent unwanted deflection under the hydrogel pressure. Unfortunately, the thickness of the porous substrate will also effect the time it takes the ions to diffuse out of the gel. The longer the diffusion time the slower the micro-actuation response. The response time is also effected by the porosity and size of individual pores. Porosity affects the rate of diffusion into and out-of the hydrogel structure. Although large pores are preferred, the diameter must be small enough not to allow the gel to protrude, or ooze, into the ionic solution. Based on percent porosity (20%) and average pore diameter (100 nm), a 100  $\mu\text{m}$  thick porous anodic alumina substrate was selected for this application.

The fabrication of the bR monolayer begins by coating a porous anodic alumina (PAA) substrate with a thin 3nm layer of titanium and gold (Au) to a thickness of 17nm. The titanium provides a permanent adhesive link between PAA substrate and the Au layer. Gold (Au) surfaces are characterized with their high affinity for thiol adsorption thereby enabling permanent bonds to be formed between the HS terminal of the thiols and the Au surface. A functionalized Au-coated porous substrate is shown in Figure 7.3, the deposition of the titanium and gold layers was performed with using electron-beam evaporation system at the University of Western Ontario’s Nanofabrication facility. In this work the anodic alumina substrate was first coated with titanium layer that ranged from 3nm at rate of 0.1 nm/s, then coated with Gold layer of 17nm at rate of 0.3nm/s.

An important factor in building a bio-functionalized Au coated substrate is the surface characteristics of the gold layer. The deposition method described above can produce Au-coated surfaces as smooth as 0-4 nm maximum surface roughness. Once the Au nanolayer has been deposited on the porous substrate, the substrate is bio-functionalized with a monolayer of biotinylated thiols. These thiols work as the building block for adsorbing the biotinylated bR by mediating the sterptavidin proteins. An atomic force microscope (AFM) is used to characterize the bio-functionalized layer, Figure 7.4.

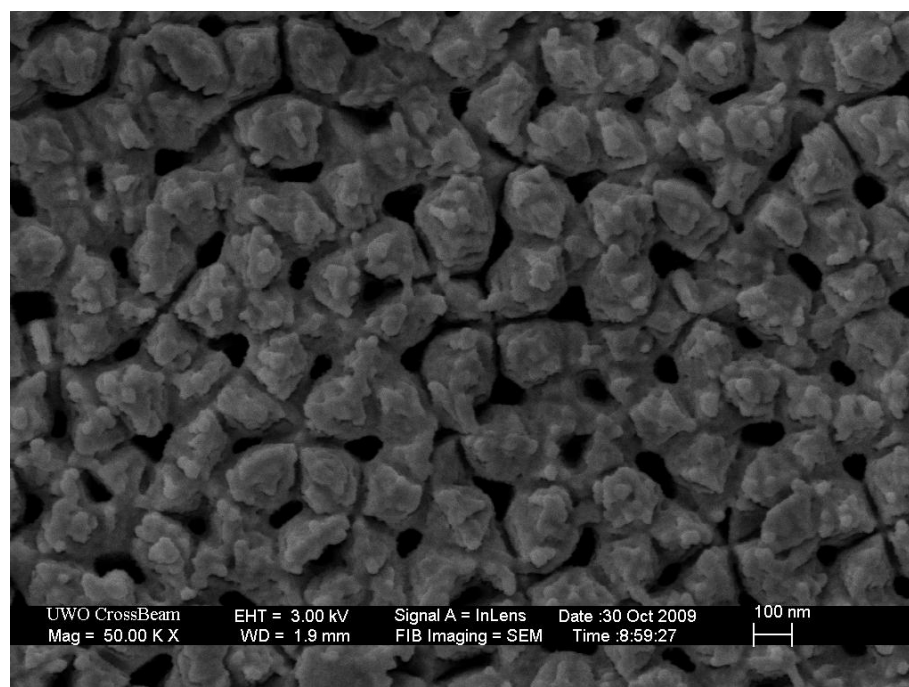


Figure 7.3 SEM photograph of the Au-coated PAA substrate.

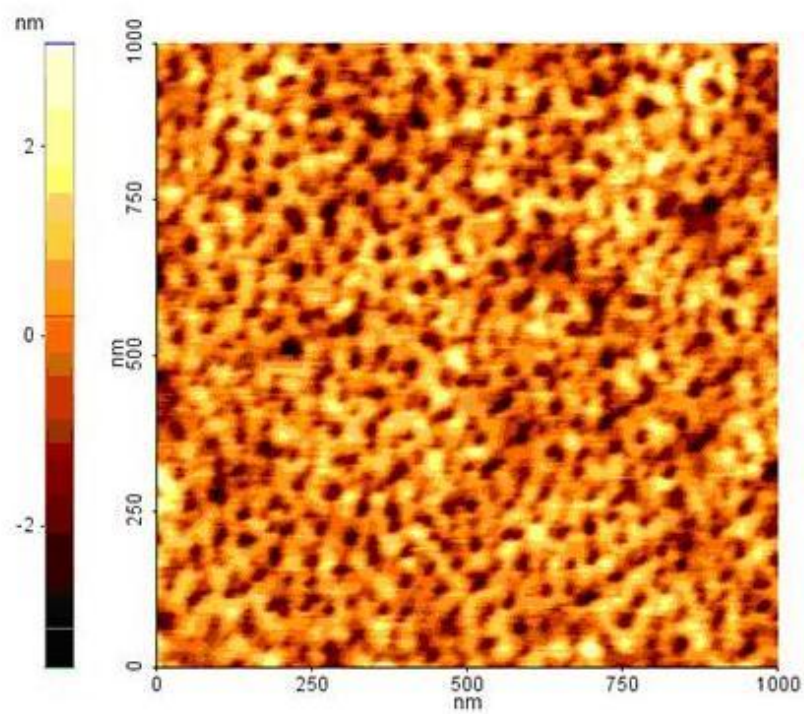


Figure 7.4 AFM photograph of bio-functionalized Au-coated substrate showing surface topology.

The next step is to use the biotin labeling technique to orient the bR purple membranes (PMs) in the same direction. This is necessary to immobilize the PM on the porous substrate and ensure the efficiency of the proton pumps. Biotin labeling is highly effective and produces a very thin PM layer of less than 13nm. Biotin labeling of the bR purple membranes is simply recognizing the extracellular side and making a permanent bond between Lysine-129 and Biotin-XX. The Biotin-XX is often called biotin ester. For this research, the Biotin-XX, SSE was acquired from Invitrogen ([www.invitrogen.com](http://www.invitrogen.com)). The biotinylated and hydroxyl-terminated thiols were purchased from nanoScience Instruments ([www.nanoscience.com](http://www.nanoscience.com)). Streptavidin was obtained from Sigma-Aldrich.

The biotin labeling and bonding procedure used to self-assemble the bR on the Au substrate was based on the method described by Henderson *et al.*, (Henderson *et al.*, 1978) and involves adding 100 $\mu$ l of 20mg/ml biotin ester in dimethyl formamide to 2ml of 1.9mg/ml PMs suspended in 0.1M sodium bicarbonate at pH 8.5. An orbit shaker was used to mix the solution for 2 hours at 20°C. The mixture was then centrifuged and re-suspended in 0.1M sodium bicarbonate at pH 8.5. This step was repeated three times and then left for approximately 12 hours to remove weakly coupled biotin to the hydroxyl groups of the PMs. The resulted biotin-protein suspension was dialyzed against two changes of phosphate buffer saline (PBS) at pH 7.4. The resultant biotinylated bR proteins were then suspended in PBS at a pH of 7.4.

The Au coated substrate was incubated in 45 mM mixture of biotin terminated thiol and the hydroxyl terminated thiol dissolved in ethanol for 14 days at room temperature. The mass ratio between the biotin-thiol, and hydroxyl-thiol was 1:4. The final step involved washing the prepared substrate with ethanol, milliQ water, and phosphate buffer saline (PBS) at pH 7.4.

## **7.4 Microactuator Response**

The final response of the bR activated hydrogel micro-actuator is the resultant response of the interaction between the photo-electro-chemical potential of the pH-gradient that is generated by bR with the pH sensitive hydrogel. The pH-sensitive hydrogel receive and

process the pH-gradient as an input signal for triggering chargeable groups of polymeric network. Once the polymeric network becomes charged, it builds an osmotic pressure. The osmotic pressure is considered as the driving force of the swelling process of the pH-sensitive hydrogel. These transformations of the powering signal from optical to electro-chemical to the mechanical form of the power as an actuator output are considered in characterizing the actuator response. The first part of the response has been studied based on the photo-electric response whereas the second part is studied based on the volume changes as these changes are considered to be the output response of the microactuator.

#### **7.4.1 Photoelectrochemical characteristics of the microactuator**

Once assembled on the Au coated PAA substrate the photoelectrochemical response characteristics of the self-assembled bR monolayer were measured under fixed light wavelength and intensity. For these measurements the cell was created by filling the PDMS reservoirs with 200mM KCl thin bR film between its Au-PAA substrate and a platinum wire was connected to each side of the reservoir. The platinum wire was used based on its electro-chemical stability. An 18mW, 568nm light source was used in the experiments because the peak photo-excitation of bacteriorhodopsin occurs at this wavelength. The voltage differences were measured using an Agilent 34420A Nano-volt/micro-Ohm meter. No additional signal processing or amplification was performed in an effort minimize distortions to the experimental readings.

The bR photo-electro-chemical cell is exposed to a continuous light beams. The light source is an 18-mW 568-nm Melles Griot Argon Ion laser with a mechanical shutter. Under dark conditions with no external illumination, the bR thin film exhibits no measurable response. When light first strike the photo-electric part of the device, there is a relatively fast photo-voltage of 2 mV has been generated, then continuous growth of the photo-voltage towards an accumulated voltage difference of 4mV (Figure 7.5).

The photo-cell is then tested under different conditions where it is connected to an external resistance of 1.0 k $\Omega$  to record the voltage and the current at these conditions. Connecting the cell to an external resistance enables calculating the internal resistance and the current of the circuit. The recorded measurements of the photo-voltage in the presence of the external resistance showed smaller values and less voltage difference

build-up compared with the cell's response without including the external resistance. This response is expected, because including the external resistance increases the overall resistance and therefore reduces the allowed current to flow in the cell. Once the photo-voltage is calculated, it is included in the basic voltage difference, resistance to current equation to calculate the real photo-current. The photo-current is usually calculated from the measured photo-voltage (Ahmadi *et al.*, 2011). Some of the measuring multi-meters have already this option so that the resistance can be selected internally, whereas the other multi-meters necessitate including a defined external resistance to measure the photo-current. The recorded photocurrent shows a consistent build-up when the cell is exposed to light beams, Figure 7.6. This response reflects the optical activity of the bR proton pumps. The generated photocurrent is characterized with its negative sign which arises from the nature of the current as it is a current of positive charges (Dolfi *et al.*, 2002; Liu *et al.*, 1988).

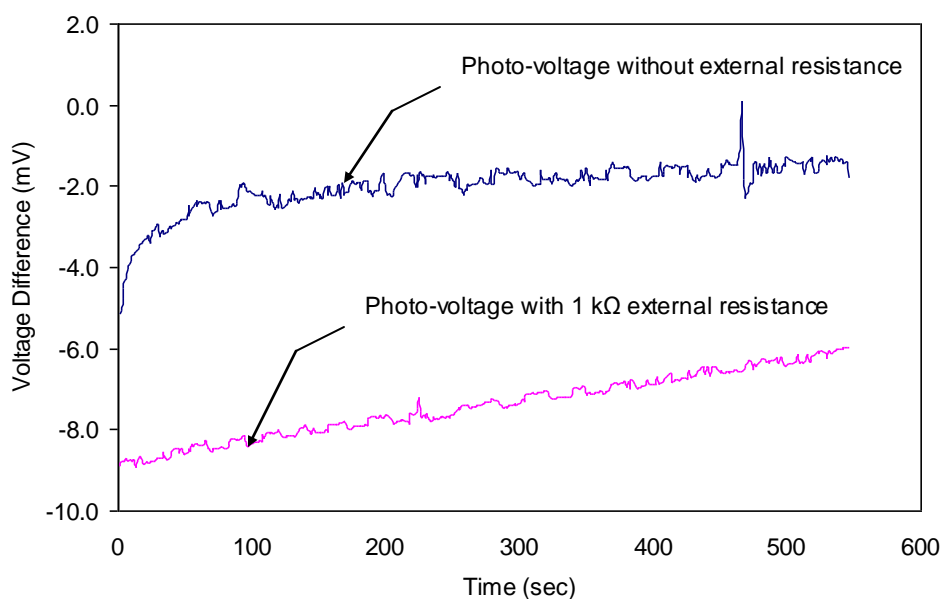


Figure 7.5 Measured voltage difference across the bR layer on a  $0.096 \text{ cm}^2$  substrate under continuous light exposure.

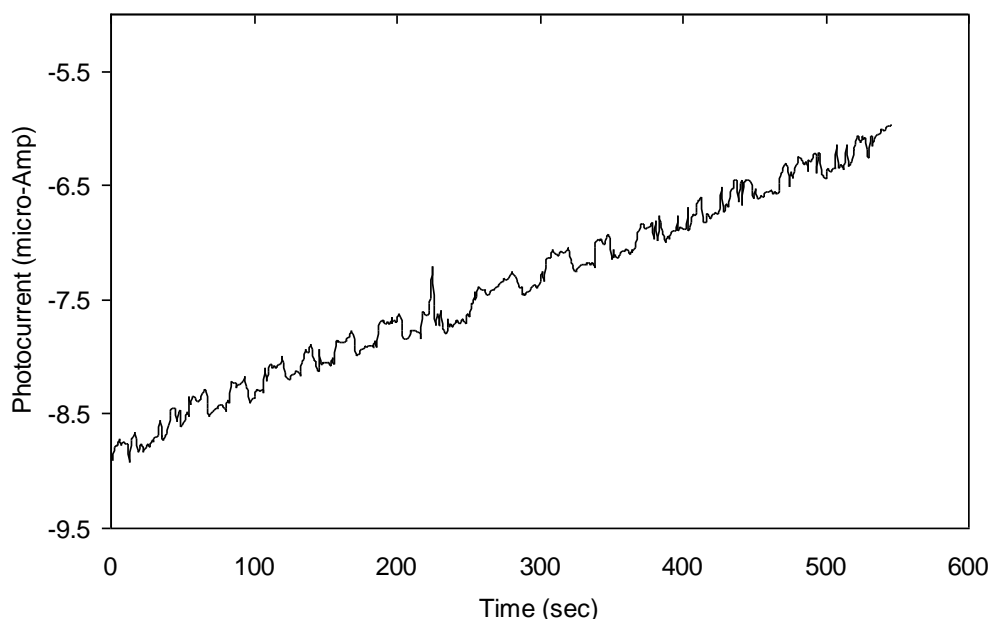
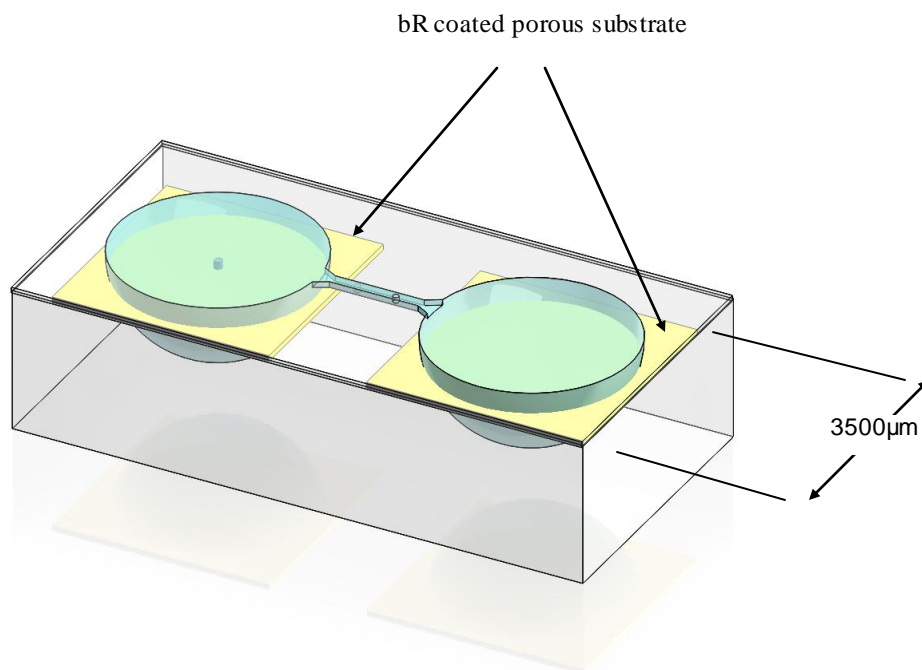


Figure 7.6 Recorded photocurrent based on the measured voltage difference across the bR layer on a  $0.096 \text{ cm}^2$  substrate under continuous light exposure.

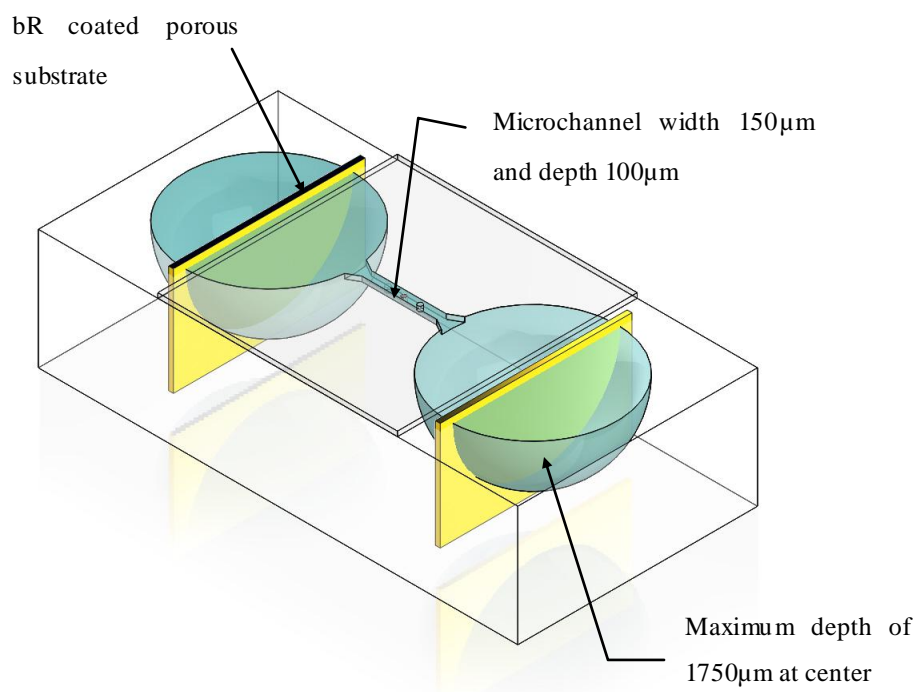
#### 7.4.2 Swelling characteristics of the microactuator

The functional performance of the presented bR driven HEMA-AA hydrogel structure was evaluated by observing the geometrical changes under light exposure. An 18 mW and 568 nm light source was used to perform the experiments. A PDMS microfluidic chip, and cylindrical hydrogel were integrated with the bR coated substrate. The hydrogel diameter of  $70 \mu\text{m}$  and length of  $100 \mu\text{m}$ , whereas the microfluidic chip has the same dimensions of that are used in Section 5.3.4. The experiments were performed in two configurations. In the first configuration the bR coated substrate is inserted parallel to the top surface of the chip, whereas in the second configuration it was inserted perpendicular to the top surface. Figure 7.7 describes both of the configurations. Having two configurations allows making more than one experiment. The configuration (a) allows having direct contact between the hydrogel and the bR coated substrate, which might reduce the time required for the ions migration to the microchannel.





(a) Configuration with bR substrate parallel to microchannel



(b) Configuration with bR substrate perpendicular to the channel

Figure 7.7 Schematic drawing of the test chip in two configurations (a), and (b)

The swelling characteristics of the hydrogel actuator are investigated in first configuration (a), and the hydrogel actuator was placed in contact with the bR coated substrate. In this experiment the hydrogel was allowed to swell without structural constraints. The chip was filled with an ionic solution of KCl with an ionic strength of 200mM and at pH of 4.5. The pKa of the acrylic acid based hydrogel is 4.7. The chip is covered with 100 $\mu$ m thick microscope cover slip to seal it against the natural evaporation. Figure 7.8 shows a photograph of the test setup.

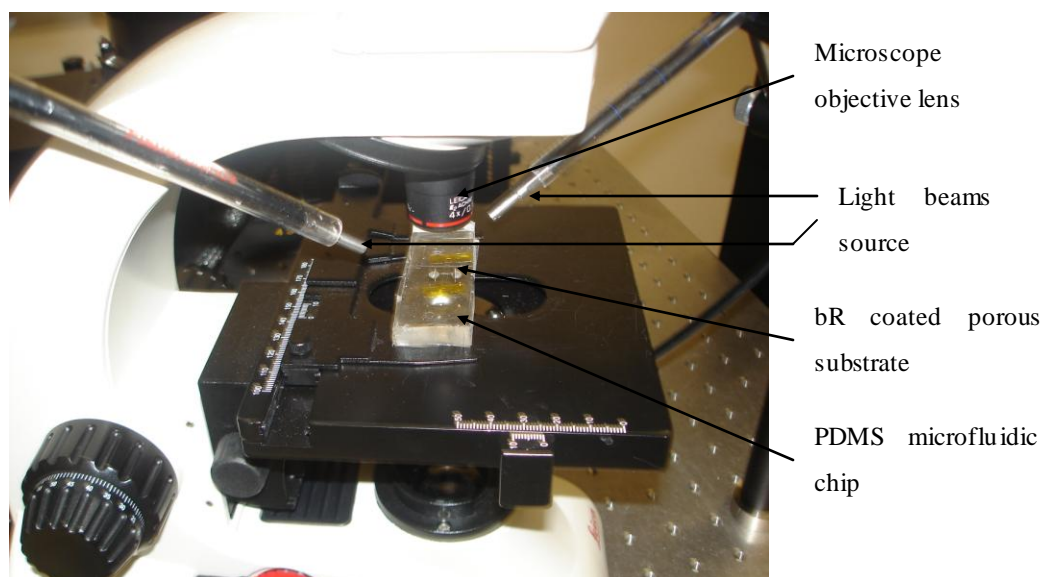


Figure 7.8 Photograph of the test setup.

Once the actuator was assembled, the light beam was provided to the bR coated substrate with an optical fiber. Within the first five minutes a change in the hydrogel dimensions was observed. These changes were noticed in the diameter and length of the hydrogel. These changes showed the volume dynamics based on these measurements. The actuator showed increase of 23% in its diameter and 22% in its length, and the volume swelling of more than 80% of its original volume in less than 85 minutes. Figure 7.10 shows a photograph of the micro-actuator before and after the swelling, the Figures 7.11, 7.12, and 7.13 provide the numerical measurements of the swelling process. The

recorded swelling characteristics show that the volume changes process is a nonlinear process.

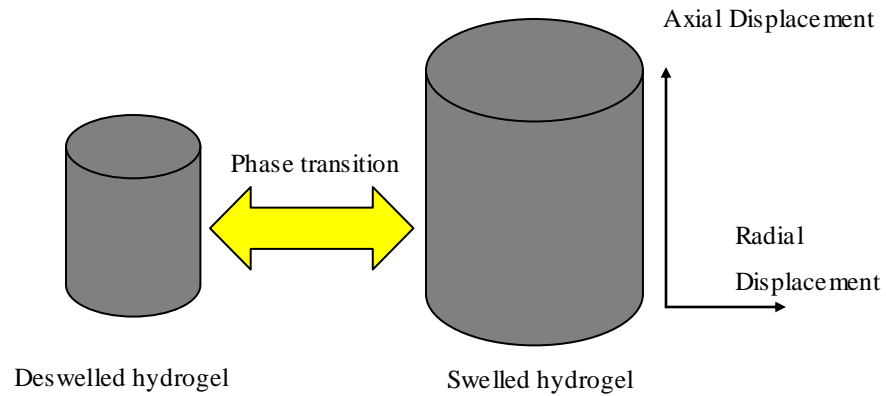


Figure 7.9 Schematic drawing of the (a) deswelled hydrogel, and (b) swelled hydrogel valve.

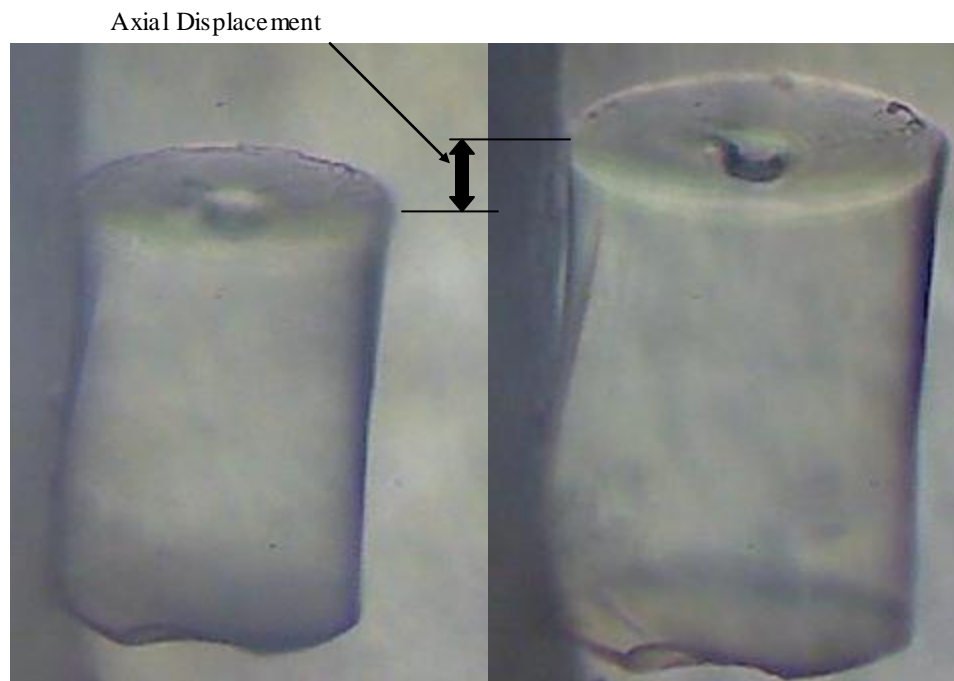


Figure 7.10 Photograph of the (a) deswelled hydrogel and (b) swelled hydrogel valve. The photographs are taken in the same scale.

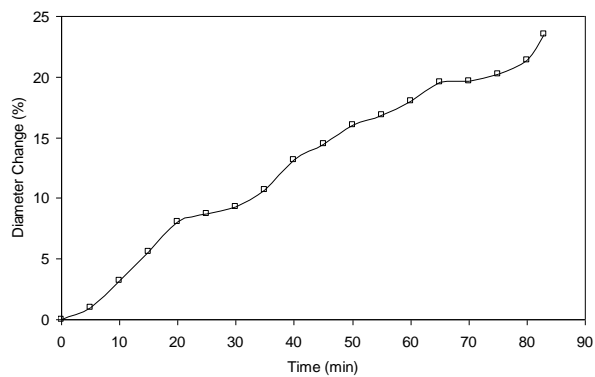


Figure 7.11 Change in diameter of the HEMA-AA hydrogel actuator over time.

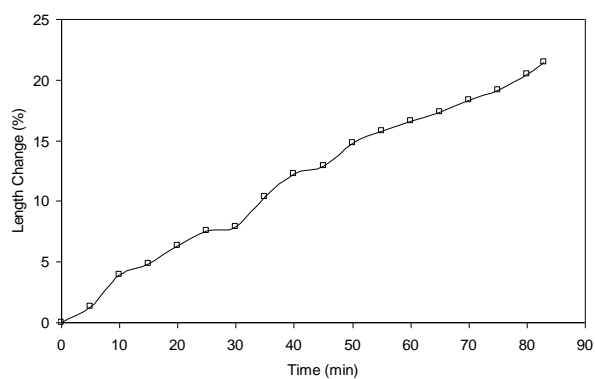


Figure 7.12 Change in length of the HEMA-AA hydrogel actuator over time.

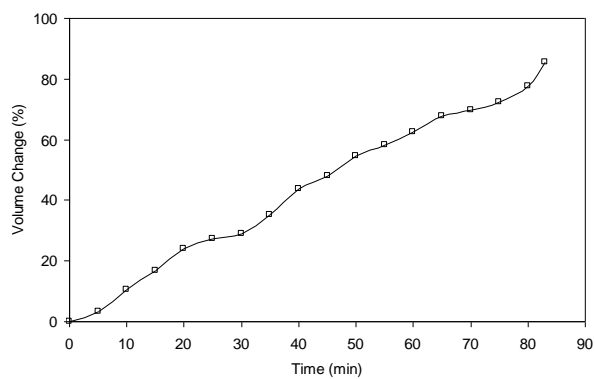


Figure 7.13 Change in volume of the HEMA-AA hydrogel actuator.

### 7.4.3 Response reversibility of the hydrogel microactuator

The HEMA-AA hydrogel actuator is tested for the swelling reversibility in a reversible pH gradient generating microfluidic chip, where the bR coated chips were inserted in opposite directions to generate the increase and decrease in the pH by switching the light beam from one the other bR coated chip. The hydrogel actuator was inserted in the connecting channel between the reservoirs. The hydrogel actuator inserted in the microchannel; the chip was filled with the KCl ionic solution with an ionic strength of 200mM and pH of 4.5. Figure 7.14 shows a photograph of the actuator in the microchannel.

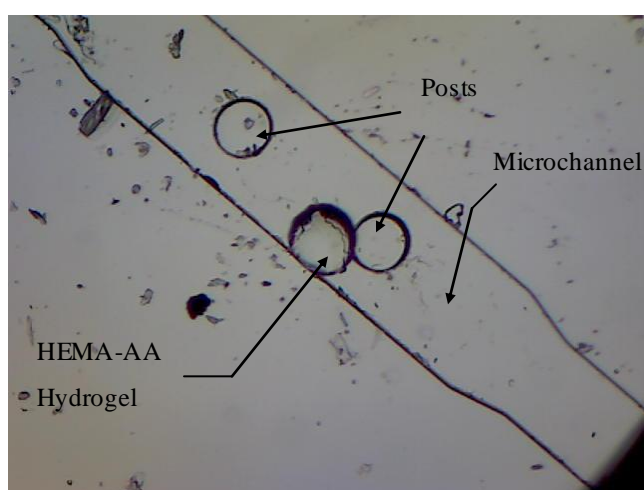


Figure 7.14 Photograph of the actuator in the microfluidic channel.

A light source was provided to the bR coated chip with a flexible optical fiber. The optical fiber enabled the light beam to be directed with an angle that was close to perpendicular to the bR coated surface. The closer orientation is to the perpendicular angle, the higher the amount of optical energy provided to bR proton pumps as the bR retinal located in the trans-membrane channel that require receiving the light beams in the channel to initiate the photocycle. Once the bR coated chip illuminated with light beam of 9 mW at 568 nm, changes in the diameter and therefore the cross-sectional area were observed. The area was increased by 30% in approximately ten minutes. At that point the light beam switched to the opposite bR coated chip to induce a decrease in the pH. The hydrogel actuator continued swelling for less than one minute and then remained without

measurable volume changes for approximately one minute, and then it started the shrinkage process until it reached its original volume in approximately twelve minutes. Figures 7.15 and 7.16 show the swelling-deswelling process. The actuator showed a hysteretic swelling, where the deswelling process took not exactly the same path of the swelling process. This behavior is expected because the driven force of the swelling process is the repulsive forces between the charged polymer network monomers and the associated osmotic pressure, whereas the deswelling process is driven by the fluidic flow out of the hydrogel due to neutralizing the polymeric network.

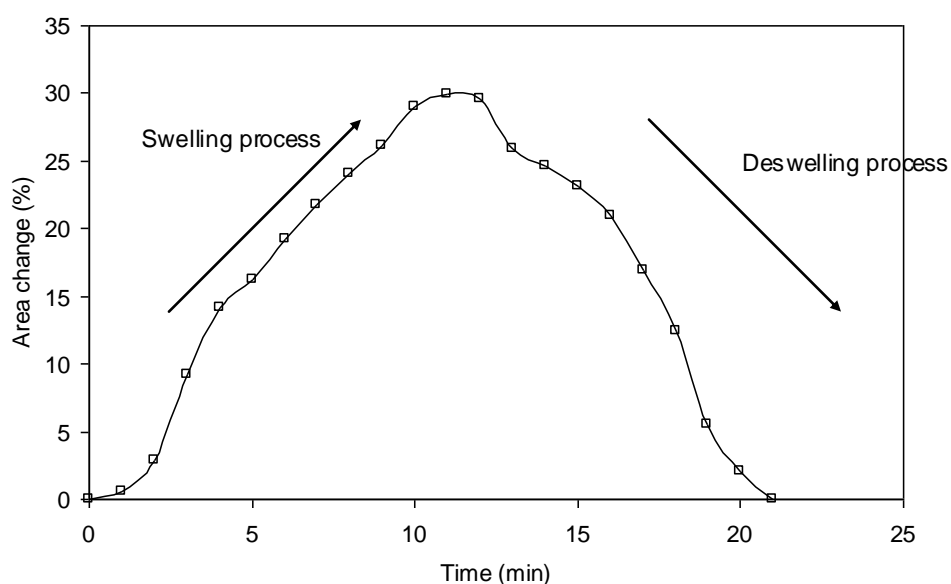


Figure 7.15 Change in microactuator cross-sectional area.

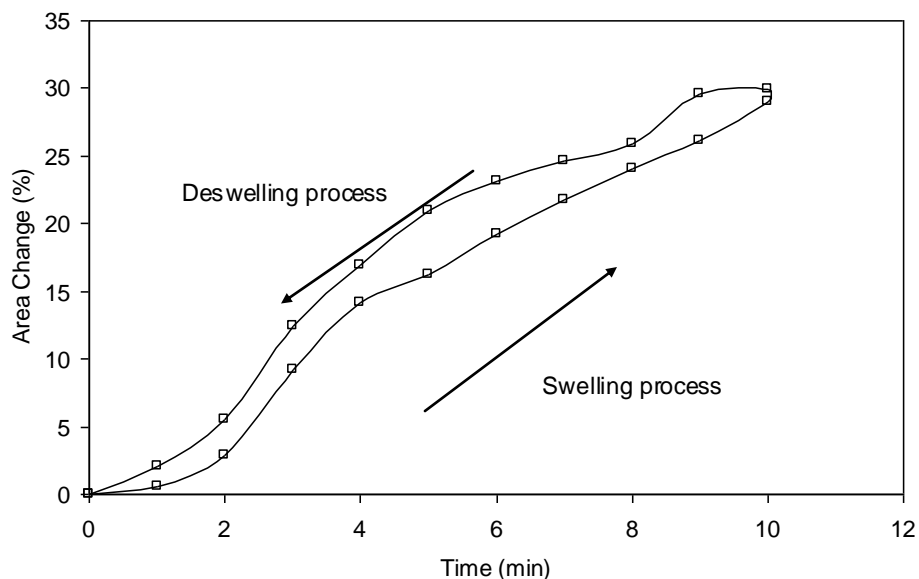


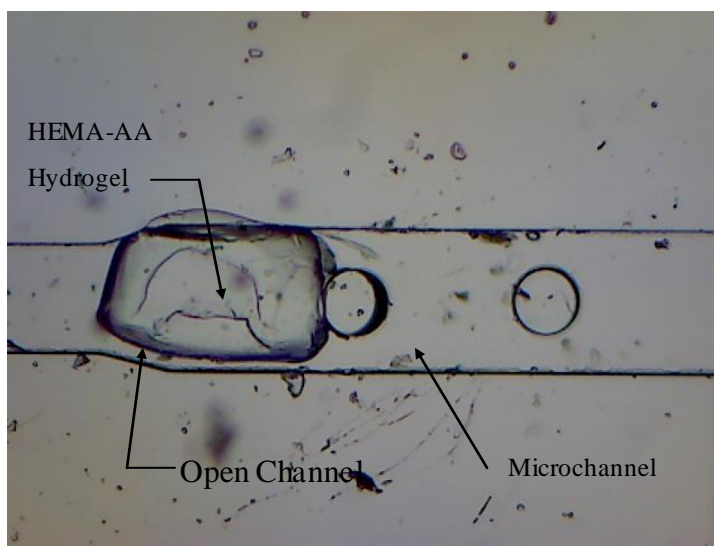
Figure 7.16 The reversibility of the microactuator response in the microfluidic channel.

#### 7.4.4 Microfluidic valve activated by bR based pH-gradient generator

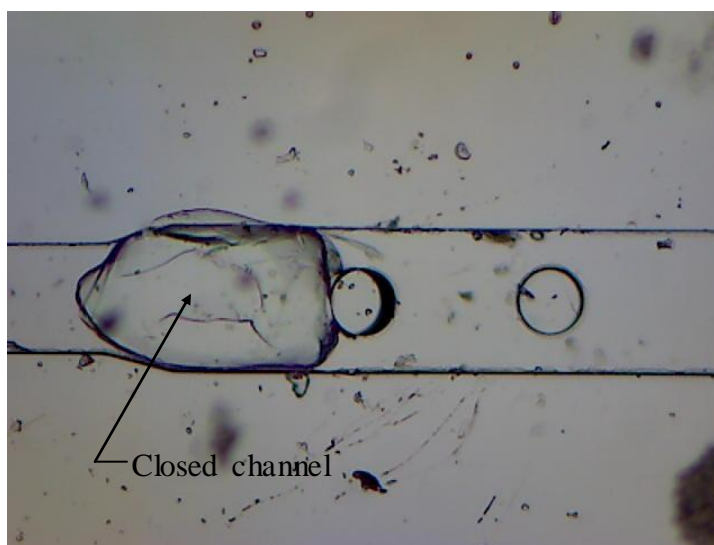
The swelling and shrinking of the smart hydrogels under environmental stimuli has been used to regulate the flow of liquids in a variety of microfluidic systems by introducing them as active microfluidic valves (Liu *et al.*, 2002; Baldi *et al.*, 2003). The hydrogel based microfluidic valves provide relatively large displacements and can seal complex geometries. However, most of the published work focused on using the temperature sensitive hydrogels and the pH sensitive hydrogels as microfluidic valves (Richter *et al.*, 2003; Liu *et al.*, 2002; Baldi *et al.*, 2003). In the temperature sensitive hydrogel micro-valves, the microfluidic chip must be kept at specific temperature to make the micro-valve functioning and the temperature of the surrounding fluid is controlled by electric resistance connected to the chip and operated wirely.

On the other hand, the pH sensitive hydrogel micro-valves are driven by replacing the working ionic solution by another solution each actuating or switching time. However the fluid replacement necessitates accessing the chip physically, which is not considered as the best option from the micro-contamination point of view, whereas, the presented hydrogel micro-actuator can be driven remotely with the light beams with the same solution. Moreover the presented hydrogel microactuator can be operated at a wide range

of temperatures. Figure 7.17 shows a photograph of the micro-valve in the microfluidic channel in the open and close positions.



(a)



(b)

Figure 7.17 Photographs of the actuator in the microfluidic channel in configuration (b) in the (a) deswelled phase and (b) swelled phase.



The micro-valve hydrogel was inserted in a microchannel at complex geometry location, and then the light beam was provided to the bR coated substrate with an optical fiber. After the first five minutes a change in the hydrogel dimensions started to be observed, and the microchannel opening of  $8\mu\text{m}$  started becoming smaller to be around  $7\mu\text{m}$  and continued the swelling process until it blocked the channel in 40 minutes. Figure 7.18 shows the swelling characteristics of the micro-valve.

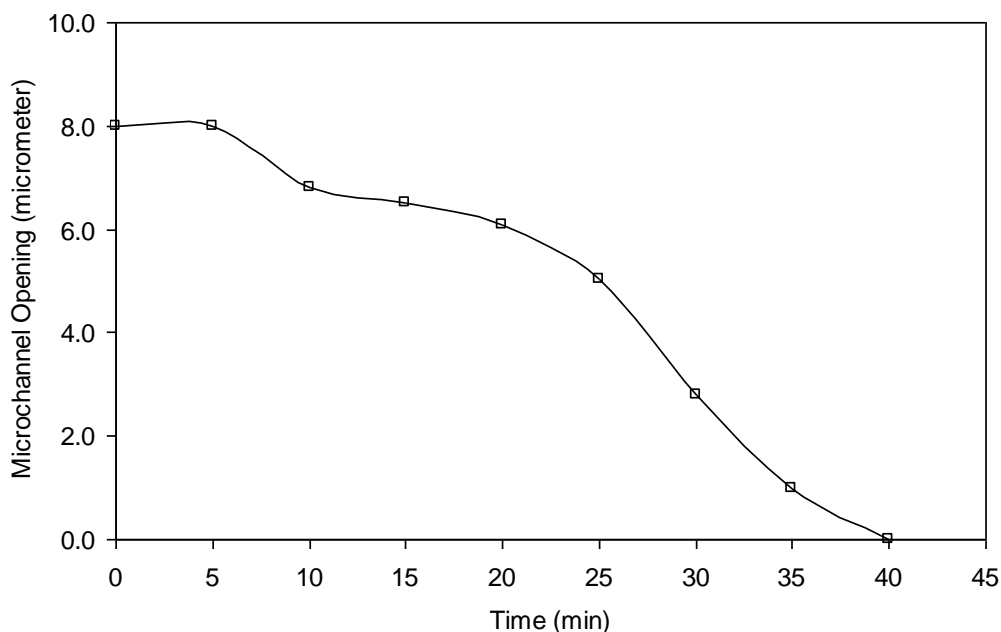


Figure 7.18 Change in microchannel opening.

## 7.5 Concluding Remarks

The design and fabrication of a microvalve activated by a bR monolayer that controls the expansion and contraction of a pH sensitive polymer gel was described. Environmentally sensitive HEMA-AA is used as the micro-actuator shell because it exhibits large change in volume when the pH of the surrounding solution is raised above the phase transition point  $pK_a$ . An ultrathin organic film constructed from light sensitive bR protein in purple membranes was then integrated with the gel to externally control the volumetric changes of the shell. When exposed to visible light beam, the bR purple membranes act as a

proton pump that transports  $H^+$  ions from the acidic gel to the surrounding KCL ionic solution. The movement of ions creates a pH gradient that induces swelling/deswelling in the polymer network. The fabrication process of the of the HEMA-AA hydrogel valve is described, on the other hand the fabrication process of the bR based monolayer is already described in Section 3.4, and the fabrication process of the PDMS microfluidic chip is already described in Section 6.3.2. The assembly technique and the used ionic solution are described.

Experimental investigations were performed in two stages. In the first stage, the generated photo-voltage and photo-current by the bR monolayer were investigated as they are the input signal to the hydrogel. On the other hand the swelling characteristics were extensively studied, including the volume swelling, swelling reversibility, and a case study on applying the presented actuator to work as a microfluidic valve. The actuator showed a swelling of around 80%. It also showed a reversible response with hysteresis. From the applicability point of view, the was used as a micro-valve in microfluidic chips, the actuator showed capability to swell in the micro-channel until it blocked an opening of  $8.0\mu m$  in micro-channel and good sealing characteristics as it was able to seal complex geometry. In general, the dynamic response of the presented optically activated hydrogel microactuator is characterized with its relatively slow behavior which may be useful for time-sensitive drug delivery systems and other applications that require slow actuators for reducing the inertia effect on the system response.

## CHAPTER 8

### CONCLUSIONS

#### 8.1 Thesis Summary

This thesis presented a novel optically driven microactuator by integrating monolayer of self-assembled bacteriorhodopsin proton pumps with pH-sensitive hydrogel. Bacteriorhodopsin is a robust biologically synthesized proton pump that reserves its pumping functionality and its photo-chromic characteristics when properly immobilized into an artificial system. On the other hand, the field of hydrogel based microactuation is a fast expanding branch of technology particularly in the microfluidics. Theoretically, the bacteriorhodopsin and one class of the hydrogels have a common electro-chemical working zone where each one of them can function within it. This zone is determined by ionic strength and pH of the working solution. In order to function properly, each bR proton pump requires a certain concentration of the free hydrogen ions in the ionic solution. The concentration of the hydrogen ions in the ionic solutions can be measured by the pH of the solution. On the other hand the pH-sensitive hydrogel undergoes in a phase transition when the molar concentration of the free hydrogen ions within it reaches the  $pK_a$  degree of the chargeable groups of the hydrogel. The research presented in this thesis describes artificial microsystem based on the molecular level labelling, organizing, and adsorption. The work is then extended to design the pH-sensitive hydrogels to function at specific pH zone. Finally, the basic concepts are used to create a microfluidic valve that can function in specific ionic environment. This process has produced a new class of optically driven microactuators that respond to the optical signal wavelength.

The characteristics and features of bR proton pumps are described in Chapter 2. The crystalline structure of bR provides high degree of chemical and thermal stability, and allows it to function in different conditions from the native biological environment. The bacteriorhodopsin protein has the potential to be used in wide range of applications,

as it exhibits remarkably high photo-electric and photo-chromic properties. The photo-electric response of bR is able to be detected the optical signals without using signal amplification circuitry when it is properly immobilized in the device. To exploit the photo-electric and photo-chromic properties and capabilities of bR, it must be grown properly in the bacterial living cells, then carefully isolated, and then properly immobilized in the system. In Chapter 3, the production of bR in the laboratory was described. The used growth protocols, isolation and purification of bR in purple membranes were able to generate approximately 500 mg from 10 liters process. Full details are provided in Chapter 3.

This chapter also discussed the immobilization techniques, and introduced a unique method of fabricating bR monolayer structure based on molecular labelling, recognition, and self-assembly technique. The method of constructing self-assembled bR monolayer on a solid substrate is described.

Employing the self-assembled bR monolayer in photonic applications requires an extensive characterization. Chapter 4 described in details the fabrication method for generating bR based monolayer. The monolayer characteristics, features and responses were extensively analysed. Atomic force microscopy analysis and scanning electron microscopy were applied to characterize the monolayer distribution and topology. The recorded measurements demonstrated the fabrication of bR based monolayer with the total architecture thickness of 12.33 nm. These features are essential requirements in fabricating nano-scale devices. The photo-electric response of the dry bR monolayer was investigated in this chapter, whereas the aqueous phase is studied in Chapter 5. In the dry bR monolayer each bR molecule releases only one charge so that this investigation provides the real photo-electric behaviour needed for optical system design. The experimental investigation demonstrated that the generated photo-voltage was as high as  $0.54\text{mV}/(\text{mW}\cdot\text{cm}^2)$ , when the cell exposed to 18mW light beam at 568 nm. This photo-electric response was recorded without using signal amplification or processing.

Chapter 5 presented a novel methodology to generate pH-gradients using a monolayer bR protein. This concept was demonstrated by fabricating a transducer that generates pH gradients when it receives light beams in the visible band. The bR chip is

the critical part of the system that is able to regulate the concentration of the hydrogen free ions in different locations of the ionic solution on the chip. This technical challenge is overcome by building the bR monolayer structure on a porous substrate. The pore size and distribution of the substrate was selected to be covered by the purple membranes and to allow the pumped hydrogen ions to pass through the substrate. The substrate was bio-functionalized by the biotinylated thiols monolayer and then coated with the self-assembled bR monolayer. A polydimethylsiloxane (PDMS) based microfluidic chip was fabricated to contain the bR coated chip and the ionic solution. The pH gradient generator was tested and it showed a gradient generation as high as 0.42. The initial experiments demonstrated that the transducer generated pH gradients as high as 0.42 and absolute voltage differences as high as 25 mV when illuminated by 18 mW, 568 nm light source. In addition to the experimental characterization, the pH gradient generator was mathematically characterized by developing a mathematical model based on the bR activity, structure, ionic properties of the chip, and the input light characteristics. The numerical results showed agreement with the experimental work.

Chapter 6 described the theoretical background and the working mechanism of the pH-sensitive hydrogels. The fabrication technique of the 2-hydroxyethyl methacrylate-Acrylic acid (HEMA-AA) pH-sensitive hydrogel is described. The HEMA-AA was fabricated to be functioning at specific pH so that it can be integrated with the pH-gradient generator. The pH sensitive hydrogel was characterized.

In Chapter 7, the pH gradient generator was integrated with the HEMA-AA hydrogel in order to make a novel optically driven micro-actuator. The HEMA-AA was fabricated in two different molds. The first one was made in a cylindrical form to quantify the swelling dynamics, and the other one is made in tapered form to characterize the swelling performance in micro channels and the capability of taking the shape of the channels when it swells. The cylindrical hydrogel actuator exhibited a swelling up to 80% of its original volume, and the micro valve showed the capability to close 8  $\mu\text{m}$  opening in micro-channel and good sealing capability as it took the shape of the shape of the micro-channels when it was in the swollen phase. The reversibility of the swelling dynamics was also characterized by testing a cylindrical hydrogel actuator. The actuator response showed hysteretic reversible swelling.

## 8.2 Thesis Contribution

The major contribution of this dissertation is developing, characterizing and modeling the photo-electro-chemical properties of the bR based pH-gradient generator and integrating the developed generator for making novel optically driven micro-actuator. However the design, fabrication, and testing the developed system components have included number of technical developments including the making successful technique for growing the *Halobacterium salinarum* in the laboratory, and making the suitable ionic solution for the pH gradient generator and the hydrogel.

The *Halobacterium salinarum* was grown in the laboratory; the bR was extracted and purified; the pH gradient generator was fabricated and tested. The model was formulated and validated with the experimental work; and the optically driven micro-actuator was fabricated. The major contributions of this thesis are classified and presented in the following subsections.

### 8.2.1 Production of bacteriorhodopsin

The thesis presented a methodology for producing the bacteriorhodopsin in the laboratories. The principle factor that was taken as a target point in making the growth media and setting the environmental conditions is to control in aeration of the media so that the oxygen level becomes very low. Reducing the oxygen supply to the living cells which is considered as a source of energy affects their life activities. Once the growth conditions are set, light beams are provided with light source in the visible band. The presence of the light source motivates the bacterial cells to synthesis the bR protein for utilizing the light beams so that, they compensate the lack in the oxygen level. On the other hand the growth media are prepared with high level of nutrition so that the cells grow and their mass increase. When the cell grows it needs more oxygen for the living activities so that they make more bR when they receive light beams. Summary of the growth media protocols and compositions in details are provided in Chapter 3.

### 8.2.2 The development of bR self-assembled monolayer

The bR protein is a directional acting proton pump found in the purple membranes of *Halobacterium salinarum* living cells. Each purple membrane consists of bR protein and lipid arranged in two dimensional hexagonal crystalline arrays. The molar ratio of the lipid to bR is 10:1. This structure enabled to work in artificial system and even in harsh chemical and thermal environments. However from the perspective of MEMS and microfluidic system design, all of these light-responsive devices require the bR to be properly immobilized on the surface of an electrode in order for the PM to act as a directional proton pump because the resultant response arising from two bR purple membranes with opposite orientation is zero. Consistent orientation of the PM patches on the surface is, therefore, necessary for efficient photon to ion flow and charge separation.

To properly exploit the bR functionality in an engineered system, it is necessary, therefore, to control how the bR proton pumps are adsorbed onto the substrate. Orientation specificity can be achieved by using either the antigen–antibody immobilization method, the genetically engineered bR protein, or the biotin labeling technique. Although the antigen–antibody technique is very lengthy because it is necessary to synthesize antigens, monoclonal antibodies, and bi-antibodies and using genetically modified bR protein might not be very convenient to designers without knowing the detailed characteristics of the generated product. In contrast, the use of biotinylation technique to adsorb bR monolayer on Au surface, which is introduced in this research, target only one reactive residue that is located at the extracellular side of bR, and it can be accessed at a specific pH, making biotin labeling a highly repeatable and reproducible process at the molecular level.

The fabrication process for building the self-assembled monolayer of bR can be divided into three major steps including: biotin labeling of the extracellular side of the bR protein, bio-functionalizing the substrate with biotinylated thiols, and assembling the biotinylated thiols with the functionalized substrate using the streptavidin protein. All these steps are performed separately and in well set time frame as the processes are time and environment sensitive.

Even though the biotin labeling of bR was reported in Henderson *et al.*, (Henderson *et al.*, 1978), and the monolayer adsorption was reported in Chen *et al.*, (Chen *et al.*, 2003). The structure that was made on the black lipid which is not stable to be integrated in MEMS and microfluidic systems because the lipid was not permanently linked to the solid substrate. Whereas, the contribution of presented technique is linking the bR to the solid substrate permanently with the following architecture: bR-Biotin-Streptavidin-Biotin-Thiol-Au. This structure enabled having permanent, ultra thin bR based monolayer of thickness of 12.33 nm, with all bR protein directed to pump the hydrogen ions in the same direction.

### **8.2.3 Fabrication of the optically driven pH-gradient generator**

The pH gradient generators became an essential component of several technological processes such as mass transport control for filtration, microdialysis, extraction, and gas-liquid exchange in micro-systems. The so far reported pH gradient generators focus on using electric power in different configurations to induce ions gradient, and thereby it leads to generating the pH gradients.

This thesis presented a low-power optically driven pH gradient generator based on the self-assembled bR monolayer. The presented generator provided an alternative noninvasive mechanism for modifying the target solution's pH without inducing strong electric fields near the solution or exposing the solution to high-intensity illumination and heat. The microscale planar transducer converts an optical signal into a flow of hydrogen ions from a reservoir to a target solution. The pH gradient generator exploits the molecular proton pumps found in the purple membranes (PM) of wild-type bR. The transducer structure is an ultrathin layer of oriented PM patches self-assembled on an Au-coated porous anodic alumina (PAA) substrate. A biotin labeling and streptavidin molecular recognition technique is used to attach uniformly oriented PM patches to the porous substrate and ensure the efficient transport of ions across the transducer surface. The photo-induced proton pumps embedded in the bio-functionalized porous substrate produce a flow of ions that generate a measurable  $\Delta\text{pH}$  proportional to the active surface area and light intensity.



The performance of the introduced pH gradient generator is mathematically formulated and studied by developing a mathematical model of the relationship between the illumination characteristics and target solution's  $\Delta\text{pH}$ . The mathematical model was formulated based on the purple membrane structure, bR activity, and the working ionic solution. Furthermore, an experimental work is presented to demonstrate how the photon responsive transducer generates a sufficient  $\Delta\text{pH}$  to cause a phenolphthalein indicator dye to change color.

#### **8.2.4 Fabrication of the optically driven microactuator**

Light-driven microactuators have advantages over conventional micro-electro-mechanical (MEMS) designs because they are activated by streams of photons instead of applied electrical currents and voltages. The light driven systems are free from the negative effects of current losses, electrical resistive heat dissipation, and friction forces of the mechanical systems that can greatly diminish the performance and efficiency of conventional MEMS devices.

This thesis presented a novel microactuator activated by a thin photo-electric layer that controls the expansion and shrinkage of a pH sensitive polymer hydrogel. An environmentally sensitive ionic hydrogel is used as the actuator shell because this networked polymer undergoes abrupt volumetric changes when the pH of the surrounding medium increases slightly above the phase transition point  $pK_a$ . Then an osmotic pressure builds-up due to the *association*, *dissociation* and *binding* of the various ions to the chains will cause the hydrogel material to swell and deswell producing a usable mechanical actuation work.

The actuator is formed by integrating two transducers the bR based pH gradient generator with the pH-sensitive hydrogel in suitable ionic conditions. The first transducer which is introduced in this thesis receives the light beams, and then processes them in the bR proton pumps and generating pH gradient. The resulted pH gradient from the first transducer is received by the pH-sensitive hydrogel containing hydroxyethyl methacrylate- acrylic acid (HEMA-AA) and processed by chargeable polymer networks to build osmotic pressure and then volume changes. These volume changes are used as actuation displacements. Successful fabrication technique and prototype design are

demonstrated. The actuator was also introduced as micro-fluidic valve. The experimental testing showed a successful actuation for closing a micro-fluidic channel.

### **8.3 Limitations and Recommendations for Future Work**

The current work has produced novel micro-actuation based on three new major steps: structuring permanent bR based photo-electric monolayer on solid substrate; integrating the developed bR based monolayer with a porous substrate, micro-fluidic chip and ionic solution for generating the optical driven pH gradient generator; and integrating the developed pH gradient generator with suitable pH sensitive hydrogel for constructing the optical driven micro-actuator. However there are number of limitations are noticed and proposed fields of research are recommended.

#### **8.3.1 Purple membranes distribution on the substrate**

The bR based photo-electric monolayer was able to generate photo-voltaic response without using amplification circuitry. The response was as high as  $0.54\text{mV}/(\text{mW}\cdot\text{cm}^2)$ . However when the system was studied under the scanning electron microscopy (SEM), it was noticed that the surface coverage was not an ideal coverage, as there were gaps between the purple membranes. In our understanding filling these gaps with bR might raise the photo-electric response to higher values. Overcoming this challenge will be only achieved by knowing the real reason for this sporadic distribution. From the nature of the bR in its purple membrane it is highly suggested that, the electrostatic nature is the key factor in studying this phenomenon. From the biophysics of bR, each bR proton pump like other proteins carries net electric charge which can be influenced by pH of the surrounding solution. So that it is recommended to study how to control the protein's net charge without affecting the adsorption characteristics.

#### **8.3.2 Optimizing the generated pH-gradient**

The presented pH gradient generating transducer was able to generate pH gradient when triggered with optical signal. The transducer output was high enough to change color of dye, and drive pH sensitive hydrogel for micro-actuation. However from the engineering

point of view, optimizing the design parameters and the operation conditions enhance the device output. So that it is recommended to optimize the constituting components of the device including: including the substrate pore size, area of the substrate, micro-fluidic chip reservoirs and channels dimensions, and the ionic solution strength.

### **8.3.3 Swelling dynamics of the microactuator hydrogel**

The presented optically driven micro-actuator exhibited large volume increase of 80%, capability to close micro-channels when used as a micro-fluidic valve. However the time frame of the actuator is relatively slow, where the 80% swelling was a result of the volume phase transition in approximately 83 minutes. Based on the published literature, it is well known that as the size of the hydrogel becomes larger the swelling dynamics becomes much slower. So that it was highly recommended to replace the larger hydrogel actuator by an array of smaller hydrogel actuators. Moreover, Richter *et al.*, recommended grinding the hydrogel into very fine particles and enclose them by a membrane to act faster (Richter *et al.*, 2003). The hydrogel dimensions can be sized to the targeted swelling dynamics.

## **8.4 Final Thought**

The presented results demonstrated the promise of using light in activating hydrogel microactuators and applying it in microfluidic valves. However improving the swelling dynamics is recommended through optimizing the design and operation parameters.

## BIBLIOGRAPHY

- Abgrall, P. Gue, A.M. (2007). Lab-on-chip technologies: making a microfluidic network and coupling it into a complete microsystem - a review. *J. Micromech. Microeng.* 17: R15-R49.
- Ahmadi, M, Yeow, J.T.W. (2011). Fabrication and characterization of a radiation sensor based on bacteriorhodopsin. *Biosensors and Bioelectronics* 26: 2171–2176.
- Al-Arife, K.M., Knopf, G.K. (2010). Photoresponsive hydrogel microvalve activated by bacteriorhodopsin proton pumps. *Proc. SPIE* 7646: 11-1–11-12.
- Al-Arife, K., Knopf G.K., Bassi, A. S. (2010). bR based light activated proton pumps for a chemophotonic toxin sensor. In: *The 2010 International Chemical Congress of Pacific Basin Societies (Pacifichem)*. Honolulu, Hawaii
- Al-Arife, K. M., Knopf, G. K., Bassi, A. S. (2011). Photoelectric monolayers based on self -assembled and oriented purple membrane patches. *IEEE/ASME J MEMS*, 20(4): 800-810.
- Al-Arife, K., Knopf, G.K., Bassi, A.S. (2006). Photo-responsive hydrogel for controlling flow on a microfluidic chip. *Proc. SPIE* 6343, 63432R-1.
- Alexiev, U., Marti, T., Heyn, M. P., Khorana, H. G., Scherrer, P. (1994). Surface charge of bacteriorhodopsin detected with covalently bound pH indicators at selected extracellular and cytoplasmic sites. *Biochemistry*, 33: 298-306.
- Baldi, A., Gu, Y., Loftness, P.E., Siegel, R.A. Ziaie, B. (2003). A hydrogel-actuated environmentally sensitive microvalve for active flow control. *J. Microelectromech. Syst* 12: 613-621.
- Batterbury, M., Bowling, B., Murphy, C. (2009). *Ophthalmology an illustrated colour text*. Edinburgh: Churchill livingstone Elsevier.
- Baylor, D. A., Lamb, T. D., Yau, K. W. (1979). Response of retinal rods to single photons. *J. Physiology*. 288: 613–634.
- Beebe, D., Moore, J., Bauer, J., Yu, Q., Liu, R., Devadoss, C., Jo, B. (2000). Functional hydrogel structures for autonomous flow control inside microfluidic channels. *Nature* 404(6): 588-590.
- Bhattacharya, S., Datta, A., Berg, J. M., Gangopadhyay, S. (2005). Studies on surface wettability of poly(dimethyl) siloxane (PDMS) and Glass Under Oxygen-Plasma

- Treatment and Correlation With Bond Strength. *IEEE/ASME J MEMS*, 14(3): 590-597.
- Birge, R. R., Gillespie, N. B., Izaguirre, E. W., Kusnetzow, A., Lawrence, A. F., Singh, D., Song, Q. W., Schmidt, E., Stuart, J. A., Seetharaman, S., Wise, K. J. (1999). Biomolecular electronics: Protein-based associative processors and volumetric memories. *J. Phys. Chem. B*. 103: 10746–10766.
- Blaurock, A. E., Stoeckenius, W. (1971). Structure of the purple membrane. *Nat. New Biol.* 233: 152–154.
- Bräuchle, C., Hampp, N., Oesterhelt, D. (1991). Optical applications of bacteriorhodopsin and its mutated variants. *Advanced Materials*. 3(9): 420–428.
- Cao, Y., Varo, G., Chang, M., Ni, B., Needleman, R., Lanyi, J.K. (1991). Water is required for proton transfer from aspartate-96 to the bacteriorhodopsin Schiff base. *Biochemistry*, 30: 10972-10979.
- Casuso, I., Fumagalli, L., Gomila, G. (2007). Nondestructive thickness measurement of biological layers at the nanoscale by simultaneous topography and capacitance imaging. *Appl. Phys. Lett.* 91: 063111-1-063111-3.
- Chen, D., Lu, Y., Sui, S., Xu, B., Hu, K. 2003. Oriented assembly of purple membrane on solid support mediated by molecular recognition. *J. Phys. Chem. B*, 107(15): 3598–3605.
- Cheng, X., Gurkan, U. A., Dehen, C. J., Tate, M. P., Hillhouse, H. W., Simpson G. J., Akkus, O. (2008). An electrochemical fabrication process for the assembly of anisotropically oriented collagen bundles. *Biomaterials* 29:3278–3288
- Choi, H. G., Jung, W. C., Min, J., Lee, W. H., Choi, J. W. (2001) Color image detection by biomolecular photodetector using bacteriorhodopsin-based complex LB films. *Biosensors & Bioelectronics*. 16: 925–935.
- Chung, S. E., Kim, J., Min, S., Kim, N. L., Sunghoon Kwon, S. (2010) Optofluidic in-situ fabrication of magnetic actuators in microfluidic channels. *Lasers and Electro-Optics (CLEO) and Quantum Electronics and Laser Science Conf. (QELS)*. JWA62
- Cullin, D. W., Vsevolodov, N. N., Dyukova, T. V., (1995). Holographic properties of triton X-100-treated bacteriorhodopsin embedded in gelatin films. *BioSystems*. 35(2–3): 141–144.
- Dancshazy, Z., Groma, G. I., Oesterhelt, D., Tittor, J. (1986). The photochemical cycle of bacteriorhodopsin has no refractory period. *FEBS LETT.* 196(2): 198–202.
- Dér, A., Hargittai, P., Simon, J. (1985). Time-resolved photoelectric and absorption signals from oriented purple membranes immobilized in gel. *J. Biochem. Biophys. Methods*. 10(5–6): 259–300.

- Dolfi, A., Aloisi, G., Rolando Guidelli, R. (2002). Photoelectric response of purple membrane fragments adsorbed on a lipid monolayer supported by mercury and characterization of the resulting interphase. *Bioelectrochemistry* 57: 155–166.
- Domachuk, P., Omenetto, F. G., Eggleton, B. J., Cronin-Golomb, M. (2007) Optofluidic sensing and actuation with optical tweezers. *J. Opt. A: Pure Appl. Opt.* 9: S129–S133.
- Edman, K., Nollert, P., Royant, A., Belrhall, H., Pebay-Peyoula, E., Hajdu, J., Neutze, R., Landau, E. M. (1999). High-resolution X-ray structure of an early intermediate in the bacteriorhodopsin photocycle. *Nature*. 401: 822–826.
- Eroglu, I., Aydemir, A., Turker, L., Yucel, M. (1994). Photoresponse of bacteriorhodopsin immobilized in polyacrylamide gel membranes. *J. Membr. Sci.* 86:171-179.
- Fainman, Y., Lee, L. P., Psaltis, D., Yang, C. (2010) *Optofluidics Fundamentals, Devices, and Applications*. New York; Chicago: McGraw-Hill.
- Ferrand, M., Dianoux, A. J., Petry, W., Zaccai, G. (1993). Thermal motions and function of bacteriorhodopsin in purple membranes: Effects of temperature and hydration studied by neutron scattering. *Proc. Nat. Acad. Sci. U.S.A.*, 90: 9668-9672.
- Forrester, J., Dick, A., McMenemy, P., Lee, W. (1996). *The eye basic sciences in practice*. London: WB Saunders Company Ltd.
- Frydrych, M., Silfsten, P., Parkkinen, S., Parkkinen, J., Jaaskelainen, T. (2000). Color sensitive retina based on bacteriorhodopsin. *Biosystems*. 54(3): 131–140.
- Gai, F., Hasson, K. C., McDonald, C., Anfinrud, P. A. (1998). Chemical dynamics in proteins: The photoisomerization of retinal in bacteriorhodopsin. *Science*. 279: 1886–1891.
- Ganea, C., Gergely, C., Ludmann, K., Varo, G. (1997). The role of water in the extracellular half channel of bacteriorhodopsin,” *Biophys. J.*, 73: 2718-2725.
- Gast, A. P., Robertson, C. R., Wang, S., and Yatsilla, M. T. (1999). Two-dimensional streptavidin crystals: macropatterns and micro-organization. *Biomol. Eng.*, 16: 21–27.
- Gau, J., Lan, E.H., Dunn, B., Ho, C., Woo, J. (2001). A MEMS based amperometric detector for E. Coli bacteria using self-assembled monolayers. *Biosens. Bioelectron.*, 16(9-12): 745–755.
- Gervais, L., Gel, M., Allain, B., Tolba, M., Brovko, L., Zourob, M., Mandeville, R., Griffiths, M., S. Evoy, S. (2007). Immobilization of biotinylated bacteriophages on biosensor surfaces. *Sens. Actuators B, Chem.* 125(2): 615–621.

- Groma, G.I., Kelemen, L., Kulcsár, Á, Lakatos, M., G. Váró, G. (2001). Photocycle of dried acid purple form of bacteriorhodopsin. *Biophys. J.*, 81: 3432-3441.
- Hamp, N. (2000). Bacteriorhodopsin as a photochromic retinal protein for optical memories. *Chemical Reviews*. 100: 1755-1776.
- Haronian, D., Lewis, A. (1992). Microfabricating bacteriorhodopsin films for imaging and computing. *Appl. Phys. Lett.*. 61(18): 2237-2239.
- Hassan, C.M., Peppas, N.A. (2000). Structure and applications of poly(vinyl alcohol) hydrogels produced by conventional crosslinking or by freezing/thawing methods. *Advances in Polymer Science* 153: 37-65.
- Hassan, C.M., Peppas, N.A. (2000). Structure and Morphology of Freeze/Thawed PVA Hydrogels. *Macromolecules* 33: 2472-2479
- He, J.A., Samuelson, L., Li, L., Kumar, J., Tripathy, K. (1999). Bacteriorhodopsin thin film assemblies: immobilization, properties, and applications. *Adv. Mater.*, 11: 435-446.
- Henderson, R., Baldwin, J. M., Ceska, T. A., Zemlin, F., Beckmann, E., Downing, K. H. (1990). Model for the structure of bacteriorhodopsin based on high-resolution electron cryomicroscopy. *J. Mol. Biol.* 213: 899-929.
- Henderson, R., Unwin, P. N. T. (1975) Three-dimensional model of purple membrane obtained by electron microscopy. *Nature* 257: 28 - 32.
- Henderson, R., December 2007. MRC Laboratory of Molecular Biology, Hills Road, Cambridge, UK, Private communication.
- Henderson, R., Stubb, J., Whytock, S., 1978. Specific labelling of the protein and lipid on the extracellular surface of purple membrane. *J. Mol. Biol.*, 123, 259-274.
- Heng, X., Reynolds, K. W., Cui, X., Erickson, D., Psaltis, D., Yang, C. (2006) Optofluidic Microscope and its Applications in Biology. *Proc. of SPIE*. 1: 6088 608816-1-6088 608816-9.
- Herber, S., Olthuis, W., Piet Bergveld, P. (2003). A swelling hydrogel-based PCO<sub>2</sub> sensor. *Sensors and Actuators B* 91: 378-382.
- Hoffman, A. (2002). Hydrogels for biomedical applications. *Advanced Drug Delivery Reviews* 43: 3-12
- Hong, F. T. (1999). Interfacial photochemistry of retinal proteins. *Progress in Surface Science*. 62: 1-237.

- Hong, F. (2007). Photoelectric biosensors: fundamentals and innovative designs. In *Smart Biosensor Technology*, G. K. Knopf and A. S. Bassi, Ed., Boca Raton FL: CRC Press. 385-435.
- Horn, C., Steinem, C. (2005). Photocurrents generated by bacteriorhodopsin adsorbed on nano-black lipid membranes. *Biophys. J.* 89: 1046–1054.
- Imanishi, Y., Lodowski, K. H., Koutalos, Y. (2007). Two-Photon Microscopy: Shedding Light on the Chemistry of Vision. *Biochemistry* 46: 9674-9684.
- Ishihara, K., Hamada, N., Kato, S., Shinohara, I. (1984). Photoinduced swelling control of amphiphilic azoaromatic polymer membrane. *Journal of Polymer Science* 22: 121-128.
- Ishikawa, M., Kitamura, N. (1994). Photoinduced volume change of polyacrylamide microgels; micrometer size effects and kinetic analysis. *Microchemistry, Spectroscopy and Chemistry in Small Domains* edited by H. Masuhara, Elsevier, 373-386.
- Jeffries, G. D. M., Edgar, J. S., Zhao, Y., Shelby, J. P., Fong, C., Chiu, D. T. (2007) Using Polarization Shaped Optical Vortex Traps for Single-Cell Nanosurgery. *Nano Lett.* 2: 415–420.
- Juodkazis, S., Mukal, N., Wakaki, R., Yamaguchi, A., Matsuo, S., Misawa, H. (2000). Reversible phase transition gels induced by radiation forces. *Nature* 408: 178-181.
- Korenstein, R., Hess, B. (1977). Hydration effects on cis-trans isomerization of bacteriorhodopsin. *FEBS Lett.*, 82: 7-11.
- Kossek, S. (2009). Nanoscience instruments, Phoenix, AZ, Private communication June-2009.
- Kovacs, G. (1998). *Micromachined Transducers Sourcebook*. Boston, MA: McGraw-Hill.
- Koyama, K., Yamaguchi, N., Miyasaka, T. (1994). Antibody-mediated bacteriorhodopsin orientation for molecular device architectures. *Science*, 265(5173): 762–765.
- Kuhlbrandt, W. (2000). Bacteriorhodopsin - the movie. *Nature*, 406: 569-570.
- Lanyi, J. K. (1993). Proton translocation mechanism and energetics in the light-driven pump bacteriorhodopsin. *Biochim. Biophys. Acta.* 1183: 241–261.
- Lanyi, J. K. (1998). Understanding structure and function in the light-driven proton pump bacteriorhodopsin. *J. Struct. Biol.* 124: 164–178.



- Lee, H., Ho, D., Kuo, K., Montemagno, C. D. (2006). Vectorial insertion of bacteriorhodopsin for directed orientation assays in various polymeric biomembranes. *Polymer* 47:2935–2941.
- Lemke, H. D., Oesterhelt, D. (1981). Lysine 216 is a binding site of the retinyl moiety in bacteriorhodopsin. *FEBS LETT.* 128(2): 255–260.
- Lensu, L., Frydrych, M., Parkkinen, J., Parkkinen, S., Jaaskelainen, T. (2004). Photoelectric properties of bacteriorhodopsin analogs for color-sensitive optoelectronic devices. *Opt. Mater.* 27: 57-62.
- Libertino, S., Fichera, M., Arrigo, G. D., Mantia, A. La, Ricceri, D. (2003). Characterization and patterning of bacteriorhodopsin films on Si-based materials. *Synthetic Metals.* 138: 71–74.
- Liu, R. H., Yu, Q., Beebe, D. (2002). Fabrication and characterization of hydrogel-based microvalves. *J. Microelectromech. Syst.* 11: 45-53.
- Liu, S. Y. (1990). Light-induced currents from oriented purple membrane I. Correlation of the microsecond component (B2) with the L-M photocycle transition. *Biophys. J.* 57: 943–950.
- Liu, S., Ebrey, T. (1988). Photocurrent measurements of the purple membrane oriented in polyacrylamide gel. *Biophys. J.* 57: 155– 166.
- Luo, X., Berlin, D. L., Betz, J., Payne, G. F., Bentley, W. E., Rubloff, G. W. (2010). In situ generation of pH gradients in microfluidic devices for biofabrication of freestanding, semi-permeable chitosan membranes. *Lab Chip* 10:59–65
- Luo, Q., Mutlu, S., Gianchandani, Y. B., Svec, F., Jean M. J. Fréchet, J. M. J. (2003) Monolithic valves for microfluidic chips based on thermoresponsive polymer gels *Electrophoresis.* 24: 3694–3702.
- Maeda, A., Iwasa, T., Yoshizawa, T. (1977). Isomeric composition of retinal chromophore in dark-adapted bacteriorhodopsin. *J. Biochem.* 82(6): 1599–1604.
- Malmivuo, J., Plonsey, R. (1995). *Bioelectromagnetism.* Oxford: Oxford University Press.
- Mamada A., Tanaka, T., Kungwachakun, D., Irie, M. (1990). Photoinduced phase transition gels. *Macromolecules* 23, 1517-1519 (1990).
- Martin, C. H., Chen, Z. P., Birge, R. R. (1997). Towards a bacteriorhodopsin-silicon neuromorphic photosensor. *In Proc. Pacific Symp. Biocomput.* 268–279. Hawaii, USA.

- Marx, K. A. (2007). Toward understanding the intelligent properties of biological macromolecules-implications for their design into biosensors. In *Smart Biosensor Technology*, G. K. Knopf and A. S. Bassi, Ed., Boca Raton FL: CRC Press. 3-81.
- May, E. L., Hillier, A. C. (2005). Rapid and reversible generation of microscale pH gradient using surface electric fields. *Anal. Chem.* 77:6487-6493.
- Miyasaka, T., Koyama, K. (1993). Image sensing and processing by a bacteriorhodopsin-based artificial photodetector. *Applied Optics.* 32(31): 6371–6379.
- Mohd-Yasin, F., Nagel, D.J., Korman, C.E. (2010). Noise in MEMS. *Meas. Sci. Technol.* 21: 012001- 012022.
- Monat, C., Domachuk, P., Eggleton, B. J. (2007) Integrated optofluidics: A new river of light. *Nature Photonics.* 1: 106-114.
- Mourzina, Y., Steffen, A. and Offenhausser, A. (2005). The evaporated metal masks for chemical glass etching for BioMEMS. *Microsyst. Technol.* 11: 135–140.
- Murata, K., Fujii, Y., Enomoto, N., Hata, M., Hoshino, T., Tsuda, M. (2000). A study on the mechanism of the proton transport in bacteriorhodopsin: The importance of the water molecule. *Biophys. J.* 79: 982–991.
- Mutlu, S., Yu, C., Svec, F., Mastrangelo, C. H., Fréchet, J. M. J., Gianchandani, Y. B., (2003) A Thermally responsive polymer microvalve without mechanical parts photo-patterned in a parylene channel. *Proc. Transducers* 1:802-805.
- Ort, D. R., Parson, W. W. (1978). Flash-induced volume changes of bacteriorhodopsin-containing membrane fragments and their relationship to proton movements and absorbance transients. *J. Biol. Chem.* 253:6158-6164.
- Ort, D. R., Parson, W. W. (1979). Enthalpy changes during the photochemical cycle of bacteriorhodopsin. *Biophys. J.* 25:355-364.
- Oesterhelt, D., Stoeckenius, W. (1971). Rhodopsin-like protein from the purple membrane of *Halobacterium halobium*. *Nature new biology* 233: 149-152.
- Pabst, T. M., Carta, G. (2008). Separation of protein charge variants with induced pH gradients using anion exchange chromatographic columns. *Biotechnol. Prog.* 24:1096-1106.
- Pepe, I. M., Nicolini, C. (1996). Invited review: Langmuir-Blodgett films of photosensitive proteins. *J. Photochem. Photobiol. B: Biology.* 33: 191–200.
- Peppas, N.A., Huang, Y., Torres-Lugo, M., Ward, J.H., Zhang, J. (2000). Physicochemical foundations and structural design of hydrogels in medicine and biology. *Annu. Rev. Biomed. Eng.* 2: 9-29.

- Psaltis, D., Quake, S. R., Yang, C. (2006) Developing optofluidic technology through the fusion of microfluidics and optics. *Nature*. 442: 381-386.
- Ratner, B. (2007). A paradigm shift: biomaterials that heal. *Polym Int* 56:1183–1185.
- Ren, Q., Zhao, Y., Han, L., Zhao, H. (2006). A nanomechanical device based on light-driven proton pumps. *Nanotechnology*, 17(6): 1778– 1785.
- Renner, T. Hampp, N. (1993). Bacteriorhodopsin-films for dynamic time average interferometry. *Opt. Commun.* 96: 142–149.
- Richter, A., Kuckling, D., Howitz, S., Gehring, T., Arndt, K. (2003). Electronically controllable microvalves based on smart hydrogels: magnitudes and potential applications. *J. Microelectromech. Syst.* 12: 748- 753
- Richter, A., Paschew, G., Klatt, S., Lienig, J., Arndt, K., Hans-Jürgen P. Adler, H. P. (2008). Review on hydrogel-based pH sensors and microsensors. *Sensors* 8: 561-581.
- Rosenauer, M., Vellekoop, M. J. (2008). Optofluidic Elements for On-Chip Sample Analysis. *Proc. of GMe Forum* 149-153.
- Roy, S., Prasad, M., Topolancik, J., Vollmer, F. (2010). All-optical switching with bacteriorhodopsin protein coated microcavities and its application to low power computing circuits. *J. Appl. Phys.*, 107: 053115-053124.
- Saga, Y., Watanabe, T., Koyama, K., Miyasaka, T. (1999). Mechanism of photocurrent generation from bacteriorhodopsin on gold electrodes. *J. Phys. Chem. B.* 103: 234–238.
- Schranz, M., Noll, F., Hampp, N. (2007). Oriented purple membrane monolayers covalently attached to gold by multiple thiole linkages analyzed by single molecule force spectroscopy. *Langmuir*, 23(22): 11 134–11 138.
- Sershen, S. R., Ng, M., Halas, N. J., Beebe, D. J., West, J. L. (2005). Independent Optical Control of Microfluidic Valves Formed from Optomechanically Responsive Nanocomposite Hydrogels *Adv. Mater* 17, 1366-1368.
- Sharmar, P., Roy, S. (2004). All-optical biomolecular parallel logic gates with bacteriorhodopsin. *IEEE Trans. on Nanobioscience.* 3(2): 129–136.
- Shen, Y., Safinya, C. R., Liang, K., Ruppert, A., Rothschild, K. (1993). Stabilization of the membrane-protein bacteriorhodopsin to 140 °C in 2-dimensional films. *Nature*. 366(39): 48–50.
- Stayton, P.S., Nelson, K.E., McDevitt, T.C. Edwards, T., Castner, D.G., Shimoboji, T., Ding, Z., Hoffman, A. (1999). Streptavidin assemblies that communicate. in *Protein*

*Architecture: Interfacing Molecular Assemblies and Immobilization Biotechnology*, Lvov, Y., Moehwald, H., Eds. New York: Marcel Dekker. 287–309.

- Subramaniam, S., Henderson, R. (2000). Molecular mechanism of vectorial proton translocation by bacteriorhodopsin. *Nature*, 406: 653-657.
- Sumper, M., Reitmeier, H., Oesterhelt, D. (1976). Biosynthesis of the purple membrane of halobacteria. *Angew. Chem., Int. Ed.*, 15, 187-194.
- Suzuki, A., Tanaka, T. (1990). Phase transition in polymer gels induced by visible light," *Nature* 346, 345-347.
- Suzurikawa, J., Nakao, M., Kanzaki, R., Takahashi, H. (2010). Microscale pH gradient generation by electrolysis on a light-addressable planar electrode. *Sens. Actuators B* 149: 205–211.
- Tajkhorshid, E., Baudry, J., Schulten, K., Suhai, S. (2000). Molecular dynamics study of the nature and origin of retinal's twisted structure in bacteriorhodopsin. *Biophysical Journal* 78: 683–693.
- Takei, H., Lewis, A., Chen, G. P., Nebenzahl, I. (1991). Implementing receptive fields with excitatory and inhibitory optoelectrical responses of bacteriorhodopsin films. *Applied Optics*. 30(4): 500–509.
- Talghader, J.J. (2004). Thermal and mechanical phenomena in micromechanical optics. *J. Phys. D: Appl. Phys.* 37: R109–R122
- Van der Linden, H., Herber, S., Olthuis, W., Bergveld, P. (2003) Stimulus-sensitive hydrogels and their applications in chemical (micro) analysis. *Analyst*, 128: 325–331.
- Váró, G., Keszthelyi, L. (1983). Photoelectric signals from dried oriented purple membranes of *Halobacterium halobium*. *Biophys. J.*, 43: 47-51.
- Varo, G., Lanyi, J.K., (1991). Thermodynamics and energy coupling in the bacteriorhodopsin photocycle. *Biochemistry*, 30: 5016-5022.
- Vsevolodov, N. (1998). *Biomolecular Electronics: An Introduction via Photosensitive Proteins*. Herndon, Virginia: Birkhauser Publishing, ch. 3.
- Voet, D., Voet, J. G., Pratt, C. W. (2006). *Fundamentals of Biochemistry Life at the Molecular Level*. Hoboken, NJ, John Wiley & Sons, Inc.
- Wang, W.W. (2006). Bioelectronic photocell and flexible photoreceptor array based on bacteriorhodopsin film. PhD dissertation, The University of Western Ontario, Dept. Mech. Mat. Eng.

- Wang, W., Knopf, G. K., Bassi, A. S. (2004). Biological transducers based on bacteriorhodopsin for smart biosensor applications. *Proc. IEEE International Conf. on MEMS, NANO and Smart Systems*, 243-248.
- Wang, W. W., Knopf, G. K., Bassi, A. S. (2005). Photoelectric properties of a detector based on dried bacteriorhodopsin film. *Biosensors & Bioelectronics*. 21: 1309–1319.
- Wang, W. W., Knopf, G. K., Bassi, A. S. (2006). Time and frequency response characteristics of bacteriorhodopsin-based photodetectors. *Opt. Eng.*, 45: 084001-1-084001-9.
- Wang, W.W., Knopf, G.K., Bassi, A.S. (2007). Protein-based photoreceptor array on flexible plastic substrates. in *Smart Biosensor Technology*, G. K. Knopf and A. S. Bassi, Ed., Boca Raton FL: CRC Press, 461-502.
- Walczak, K. A., Cheam, D. D, Lueking, D., Bergstrom, P. L., Friedrich, C. (2008). Electronic Characteristics of Bacteriorhodopsin. *Proc. of 8th IEEE Conference Nanotechnology*, 553-556.
- Xu, J. (2003). Bio-photosensors based on monolithic integration of light sensitive proteins with semiconductor devices and integrated circuits. PhD. dissertation, University of Michigan-Ann Arbor, Elect. Eng. Comp. Sc. Dept.
- Xu, J., Bhattacharya, P., Váró, G. (2004). Monolithically integrated bacteriorhodopsin/semiconductor opto-electronic integrated circuit for a bio-photoreceiver. *Biosensors & Bioelectronics*. 19: 885–892.
- Xu, J., Stickrath, A.B., Bhattacharya, P., Nees, J., Varo, G., Hillebrecht, J.R., Ren, L., Birge, R.R. (2003). Direct measurement of the photoelectric response time of bacteriorhodopsin via electro-optic sampling. *Biophys. J.*, 85: 1128-1134.
- Yamaguchi, N., Jinbo, Y., Arai, M., Koyama, K. (1993). Visualization of the morphology of purple membrane surfaces by monoclonal antibody techniques. *FEBS Letters*, 324: 287-292.
- Yang, J., Wang. G. (1998) Image edge detecting by using the bacteriorhodopsin-based artificial ganglion cell receptive field. *Thin Solid Films*. 324: 281–284.
- Zhang, L., Zeng, T., Cooper, K., Claus, R.O. (2003). High performance photovoltaic behavior of oriented purple membrane polymer composite films. *Biophys.* 84: 2502-2507.

## CURRICULUM VITAE

**Name**            **Khaled AL-ARIBE**

### Post-secondary Education

- 2012            Doctor of Philosophy (Ph.D.) in Mechanical Engineering,  
The University of Western Ontario, London, Ontario, Canada
- 1999            M.Sc. in Mechanical Engineering (University of Garyounis, Fall 1999)  
M.Sc. thesis title is “Vibrational Analysis of Flexible Cam Mechanisms.”
- 1992            B.Sc. in Mechanical Engineering (University of Garyounis)

### Awards and Scholarships

- 2005            Western Engineering Graduate Research Thesis Award, The University of  
Western Ontario
- 2006            Best paper award, at the conference on Optomechatronic Actuators and  
Maipulators II at Boston Massachusetts.

### Published Journal Papers

- Al-Arife, K.M., Knopf, G.K., Bassi, A.S. (2011). Photoelectric Monolayers Based on Self -Assembled and Oriented Purple Membrane Patches. *IEEE/ASME Journal of Microelectromechanical Systems*, vol. 20, No 4, pp. 800- 810.
- Al-Arife, K.M., Knopf, G.K., Bassi, A.S. (2011). Fabrication of an optically driven pH-gradient generator based on self-assembled proton pumps. *Journal of Microfluid Nanofluid* (DOI 10.1007/s10404-011-0876-4)

- AL-Arife, K.M., El-Sawy, M.M. (2002). Vibrational Analysis of Flexible Cam Mechanisms. *Al-Azhar University Engineering Journal*. Vol. 5, No. 4, Oct 2002 pp. 504-513

### **Book Chapters**

- Knopf, G.K. and Al-Arife, K.M. (2012). Light Driven Micro/Nano-fluidic Systems. *Optical Nano and Micro Actuator Technology*, G.K. Knopf and Y. Otani (Eds), CRC Press, to be submitted 2012.

### **Published Conference Proceedings Papers**

- Al-Arife, K. Knopf, G.K. (2010). Photoresponsive hydrogel microvalve activated by bacteriorhodopsin proton pumps. *Proc. SPIE 7646, 764611*, doi:10.1117
- Al-Arife, K., Knopf, G.K., Bassi, A.S. (2006). Reconfigurable microfluidic chip based on a light-sensitive hydrogel, *Proc. SPIE*, vol. **6374**, 63740E (2006); DOI:10.1117/12.686211
- Al-Arife, K., Knopf, G.K., Bassi, A.S. (2006). Photo-responsive hydrogel for controlling flow on a microfluidic chip. *Proc. SPIE*, vol. **6343**, 63432R (2006); DOI:10.1117/12.707765
- Al-Arife, K. Knopf, G.K. (2005). Neural network control of a MEMS torsion micro mirror. *Control Applications Conference, Proceedings of IEEE*, vol 28, Issue 31, pp. 737 – 742

### **Conference Presentations**

- Al-Arife, K.M., Knopf, G.K., Bassi, A.S. (2010). bR based light activated proton pumps for chemophotonic toxin sensor. *The 2010 Chemical Congress of Pacific Basin Societies (Pacficchem) Honolulu, Hawaii*

### **Full Time Work Experience**

- 1999 - 2003 Assistant Lecturer and Head of the Mechanical Workshops Section at the Higher Institute of the Electrical and Electronic Technology Benghazi-Libya.

Courses taught:

- Machine Design
- Mechanical Vibrations
- Mechanical Measurements
- Engineering Mathematics
- 1993 - 1999 Mechanical Engineer at North Benghazi Steam Power Station  
Benghazi-Libya

### **Part Time Work Experience**

- **2006 – 2008** Proctor with the department of services for students with disabilities at UWO
- **1999 - 2003** Part time Lecturer at the Mechanical Engineering Department, University of Garyounis Benghazi, Libya.

**Courses taught:**

- Dynamics of Machinery
- Mechanisms
- Strength of Materials
- Engineering Mechanics II
- **2001-2002** Part Time Lecturer at Mechanical Engineering Department University of Omar Al-Mukhtar, Libya.

**Courses taught:**

- Machine Design
- Theory of Machines